FINAL REPORT

Project Title: Development of Advanced Manufacturing Technologies for Low Cost Hydrogen Storage Vessels

Project Period: September 26, 2008 to September 30, 2014 [project ended on 3/31/14]

Date of Report: December 29, 2014 [program activities between 9/26/08 and 3/31/14]

Recipient: Quantum Fuel Systems Technologies Worldwide, Inc.

Award Number: DE-FG36-08GO18055

Working Partners: Boeing Research and Technology
Pacific Northwest National Laboratory (PNNL)
Lawrence Livermore National Laboratory (LLNL) [Phase I]

Cost-Sharing Partners: Boeing Research and Technology

Contact: Mark Leavitt (Quantum), (949) 399-4584; mleavitt@qtww.com
Karl M. Nelson (Boeing), (206) 544-2358; karl.m.nelson@boeing.com

DOE Managers: Jesse Adams, DOE Project Officer
Genevieve Wozniak, DOE Award Administrator
Nancy Garland, DOE Technology Development Manager

Table of Contents

Table of Figures

Table of Tables

1.0 Executive Summary

The U.S. Department of Energy (DOE) defined a need for low-cost gaseous hydrogen storage vessels at 700 bar to support cost goals aimed at 500,000 units per year. Existing filament winding processes produce a pressure vessel that is structurally inefficient, requiring more carbon fiber for manufacturing reasons, than would otherwise be necessary. Carbon fiber is the greatest cost driver in building a hydrogen pressure vessel.

The objective of this project is to develop new methods for manufacturing Type IV pressure vessels for hydrogen storage with the purpose of lowering the overall product cost through an innovative hybrid process of optimizing composite usage by combining traditional filament winding (FW) and advanced fiber placement (AFP) techniques.

A numbers of vessels were manufactured in this project. The latest vessel design passed all the critical tests on the hybrid design per European Commission (EC) 79-2009 standard except the extreme temperature cycle test. The tests passed include burst test, cycle test, accelerated stress rupture test and drop test. It was discovered the location where AFP and FW overlap for load transfer could be weakened during hydraulic cycling at 85°C.

To design a vessel that passed these tests, the in-house modeling software was updated to add capability to start and stop fiber layers to simulate the AFP process. The original in-house software was developed for filament winding only.

Alternative fiber was also investigated in this project, but the added mass impacted the vessel cost negatively due to the lower performance from the alternative fiber.

Overall the project was a success to show the hybrid design is a viable solution to reduce fiber usage, thus driving down the cost of fuel storage vessels. Based on DOE's baseline vessel size of 147.3L and 91kg, the 129L vessel (scaled to DOE baseline) in this project shows a 32% composite savings and 20% cost savings when comparing Vessel 15 hybrid design and the Quantum baseline all filament wound vessel.

Due to project timing, there was no additional time available to fine tune the design to improve the load transfer between AFP and FW. Further design modifications will likely help pass the extreme temperature cycle test, the remaining test that is critical to the hybrid design.

2.0 Background

The incumbent process uses a filament winding process, which does not have the benefit of placing *cut and adds* of material in precise locations, as does AFP machines. There have been considerable advances in precision composite material processing in the aerospace sector. By leveraging its advancements, innovative manufacturing technologies for high-pressure composite hydrogen storage vessels will integrate the most optimal features of high precision AFP and commercial FW, with the intent to significantly drive down costs. AFP utilizes a process where end caps were laid in order to build up the dome areas that require more material. These critical locations are located in the forward and aft domes where the fiber would otherwise be passed

back and forth end to end, creating excess in the center region of the vessel. For this reason, the hybrid process produces a more efficient and structurally optimized vessel.

The precision and flexibility of AFP technology could enable reduction of carbon fiber requirement by as much as 64% [1] due to elimination of waste through material placement at ideal locations and improved structural properties from:
(a) elimination of band overlaps,
(b) elimination of fiber distortions and
(c) placement of reinforcing fibers in ideal orientations.

Dry winding technique allows significant increase in "fiber volume fraction", which results in weight and cost savings. Traditional fiber placement techniques are relatively slow, and the elaborate equipment developed for aerospace applications are not amenable for commercial applications. By integrating precision AFP techniques from the aerospace industry with high-speed commercial FW, the Quantum team anticipates the potential to reduce carbon fiber usage will be achievable at a production rate that is suitable for the automotive industry.

The project team, consisting of Quantum Technologies (Quantum) as the prime, the Boeing Research and Technology division of the Boeing Company (Boeing) as the subcontractor, as well as Pacific Northwest National Lab (PNNL) and Lawrence Livermore National Lab (LLNL), will (a) analyze the current processes and state-of-the-art FW and AFP, including their ability to mass produce relatively small-diameter hydrogen storage vessels, (b) prepare economic and analytical models capable of evaluating FW and AFP processes including manufacturing process variables and their impact on mass savings, material cost savings, processing time, manufacturing energy consumption, labor as well as structural benefits, (c) develop a new hybrid process that integrates the relatively high speed of modern FW; the precision and flexibility of AFP and associate tooling that are designed to dramatically reduce material consumption, labor cost and therefore the overall cost of fabricating composite hydrogen storage vessels and (d) establish baseline parameters and demonstrate a product-scale 5kg, 700 bar (10,153 psi) composite vessel that meets the automotive industry performance criteria.

3.0 Quantum Report

3.1 Phase I

Phase I of this project focused on finding compatible materials that would work for the interface between traditional filament winding (FW) and advanced fiber placement (AFP) in the hybrid design. A decision was also made on how to split up where FW and AFP would be applied on the vessel. Two vessels were wound to demonstrate the hybrid vessel concept.

3.1.1 Different Manufacturing Processes

Two key manufacturing processes were employed in this project: traditional filament winding (FW) and advanced fiber placement (AFP). Quantum specializes in developing Type IV pressure vessels through a highly automated, precise and repeatable filament winding process.

However, there are some limitations with FW. First, FW is a continuous process; therefore, any fiber tow on the dome region has to pass through the cylinder region as well, even though it is not required from a stress analysis point of view. The result is a presence of parasitic fibers in the cylinder region, which decreases the weight, volumetric and cost efficiency of a composite vessel. In addition, the possibility of laying fiber tow in the desired orientation to reinforce the dome regions depends on the coefficient of friction and the local surface curvature greatly, which leads to numerous constraints on composite design and optimization.

One possible solution is AFP, which is an automated composite manufacturing process of heating and compacting bundled fibers with resin pre-impregnated (towpreg) on typically complex tooling mandrels. The advantage of using such a process is the efficiency of 'placing' fiber in specific locations. Significant improvements in cost and weight efficiencies can be gained by combining both FW and AFP processes.

A common material system to be used in both FW and AFP has to be agreed upon prior to commencing any significant work on other aspects of the project. It should be noted that intrinsically the resin systems are quite different because of the processes they represent. Usually the resin in the towpreg is required to have a long storage life; therefore, the towpreg is cured at a relatively high temperature (above 250 ºF or 120 ºC). Consequently, it is difficult to find an exact resin system that works for both FW and AFP.

3.1.2 Material Search and Compatibility Tests

Since the 5kg, 129L pressure vessel made by FW was used as the baseline model for this project, it was decided to use the same materials (fiber and resin) for the FW portion of the hybrid process. It's necessary to find materials that are similar to the baseline materials for use in the AFP process to achieve compatibility and similar cost.

In the AFP process, the fiber towpreg is always pushed between the machine heads about 1 inch away from where the fiber is placed. The tow is required to have a certain stiffness, so that it doesn't fold during the process. Therefore, besides the requirement on the thickness and width of the towpreg, it needs to possess a special tack and resin impregnation level. Almost all vendors in the United States who make towpreg were contacted, and their materials were investigated. These vendors include Advanced Composites Group (ACG), Newport Adhesives & Composites (Newport), TCR Composites (TCR) and Toray Composites America, Inc. (Toray).

The materials from Newport and TCR have a tack level too high, and it is too easy for the towpreg to fold in the AFP process. The material from ACG seemed to match all the requirements quite well. The curing temperature can be as low as 120 ºC, which is quite close but still lower than the high density polyethylene (HDPE) liner softening temperature. The resin has fairly low tackiness and has the appropriate stiffness in the AFP process. However, the material used in the testing was some leftover, and ACG would have to produce additions for this project. It is extremely expensive to set up the slit process to produce the small amount of towpreg we need for the research work. With no time to wait until another similar request for such material is made by another customer, the only choice left was the material from Toray,

consisting of T800 carbon fiber and highly toughened resin system, designated as "T800 towpreg". T800 towpreg satisfies AFP process requirement but has a much higher curing temperature of 176 – 180 ºC, which is higher than HDPE liner softening temperature (about 125 ºC). In addition, the highly toughened resin system may not have good communication with the material used in the FW process. Therefore, some testing needed to be performed to evaluate their compatibility for design work and to address the thermal issue.

Material panels with unidirectional (UD) fibers were made with baseline fiber and resin, as well as baseline fiber and resin hybridized with T800 towpreg. Baseline fiber and resin UD panels were made by filament winding the material on a flat steel plate. The hybrid material plate was made in a similar method, except that the T800 towpreg was laid down by hand on the peel ply first and then baseline fiber with resin was wound over. It was cured at 179 ºC for 2 hours to fully cure the T800 towpreg. The plate dimension and weight were measured. It was then cut into coupons for interlaminar shear strength test and fracture toughness test according to the corresponding ASTM standards.

Upon completion of testing, a statistical analysis was performed to compare the shear strength of composite coupons made of baseline fiber and resin and the shear strength of those made of baseline and T800 towpreg hybrid. From the statistical analysis, no difference was found between the two materials. Consequently no material compatibility issue due to interface shear between different materials was found.

The results from interlaminar shear strength test are used in the composite design lay-up to indicate the amount of overlap between baseline fiber and T800 towpreg required to effectively transfer the tensile stress through the interface shear.

On the thermal issue, the curing temperature of T800 towpreg, 176 – 180 ºC, specified by Toray, is higher than the HDPE liner softening temperature. Differential scanning calorimetry (DSC) was performed to determine the appropriate cure profile for T800 towpreg. Because Toray specifies 176 – 180 ºC cure temperature for 2 hours, the plan was to cure this material at a lower temperature with longer duration to compensate.

A series of DSC for T800 towpreg were run at different temperatures and durations to come up with the proper cure profile. The results indicated the AFP material can be properly cured at a temperature lower than the specified cure temperature with a prolonged time to prevent damaging the liner.

3.1.3 Composite Optimization in High-pressure Vessel through Combination of AFP and FW Processes

Quantum started the design work to maximize the composite performance for a given liner profile. The approach taken was through iso-tensile strain assuming zero in-plane shear stress [1-3], as well as through strength maximization according to Tsai-Hill criteria. The latter may offer some discrepancies, which are mostly determined by material properties. The optimization work was the first step in bridging FW and AFP technologies. An abstract of the theoretical optimal vessel analysis follows.

3.1.3.1 Composite Optimization in the Dome Region

A series of calculations, derivations and integrations were made to develop an optimized composite model for the dome and cylinder regions, with only the final result provided in this report. Figure 1, shown below, illustrates a typical dome region with uniform internal pressure p loading the interior of the vessel and axial force T uniformly distributed along the contour of the shell cross-section r=r0. Nα and Nβ are defined as the meridional and parallel/circumferential shell stress resultant, respectively.

Once the dome profile is known (r, z' and z" at any point are given), and the stress state is known (pressure p and the combined axial stress), the stress resultant distribution Nα and Nβ can be calculated. The next step is to determine the optimum composite orientation under such stress resultants.

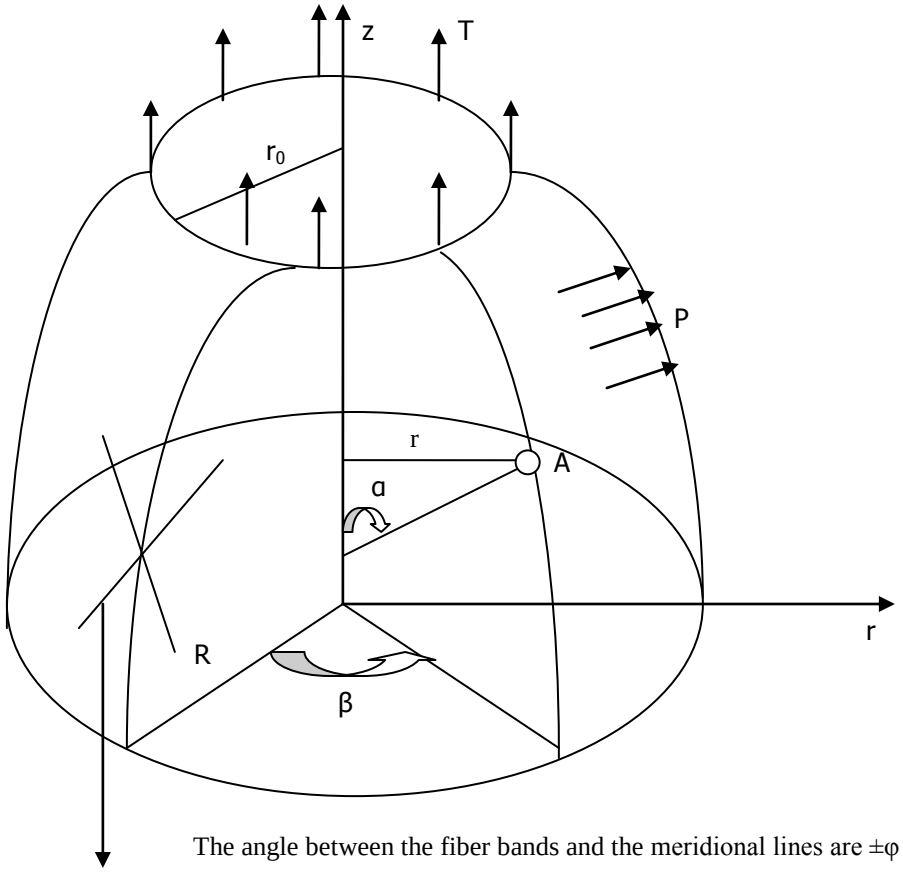

Figure 1. Axi-symmetrically loaded membrane shell of revolution

The fiber direction in the UD fiber composite band is designated as direction 1, and that in the perpendicular direction as 2. The angle between direction 1 in the orthotropic composite band

and the meridional direction is represented as ±φ. Then the stresses in the principal material coordinates, σ1, σ2 and τ12, can be expressed in terms of Nα and Nβ as [1]

$$\sigma_1 = \frac{1}{2hC}\left\{(N_\alpha + N_\beta)[1+\frac{2G_{12}}{E_2}(1+\nu_{12})\tan^2 2\varphi] + \frac{N_\alpha - N_\beta}{\cos 2\varphi}\right\}$$
$$\sigma_2 = \frac{1}{2hC}\left\{(N_\alpha + N_\beta)[1+\frac{2G_{12}}{E_1}(1+\nu_{21})\tan^2 2\varphi] - \frac{N_\alpha - N_\beta}{\cos 2\varphi}\right\}$$
$$\tau_{12} = \frac{G_{12}\tan 2\varphi}{hC\cos 2\varphi}\left\{N_\beta(\frac{1+\nu_{21}}{E_1}\sin^2\varphi + \frac{1+\nu_{12}}{E_2}\cos^2\varphi] - N_\alpha(\frac{1+\nu_{21}}{E_1}\cos^2\varphi + \frac{1+\nu_{12}}{E_2}\sin^2\varphi]\right\} \quad (1)$$

It has been shown through extensive research [3] that the strength of fiber is fully utilized when the participating laminate individual layers are aligned according to the direction of the maximum principal stress, which implies that $\tau_{12} = 0$ or the strain is the same in the meridional and parallel directions.

The directions of the principal strain for pressure vessels are in the meridional and parallel directions [5-6]. So ideally the optimum orientation for the fiber band would be φ = 0º and 90º. The combination of 0º and 90 º is difficult to realize in the FW process because of the dimensional constraints from the polar boss, the friction of the wet fiber band, the constraints from the curvature on the dome surface, and the continuous nature of FW. Similarly, the dimensional constraints from the polar boss and the constraints from the curvature on the dome surface also pose difficulty to lay the fiber band in the 0º and 90º in the AFP process. Another choice for fiber orientation on the dome surface is ±φr and 0° < φr < 90°, shown in Figure 1.

The stress in the fiber direction is not a function of r under optimum conditions and the approximation of $n = \frac{E_2(1+\nu_{21})}{E_1(1+\nu_{12})} = 0$. Such a structure is termed an "Isotensoid" structure. Therefore, for the choice of ±φr and 0° < φr < 90° to be used, according to the stress condition, η^2 is calculated using $\eta^2 = r_0^{\,2} - \frac{2T}{p}r_0$. In addition, we need to have the fiber band remain on the geodesic line. In a pressure vessel, η^2 changes when the composite shell contacts the polar boss in the forward dome or in both domes if the vessel is symmetric.

3.1.3.2 Composite Optimization in the Cylinder Region

The principal stresses in the cylinder region are much simpler compared to the dome region and they are constant [4]:

$$N_\alpha = \frac{1}{2}pR,\ N_\beta = pR \quad (2)$$

The radius of curvature in the meridional direction is zero and that in the parallel direction is not a function of z. With similar derivations as above, the optimum fiber orientation for the same basic composite lamina used can be obtained as below

$$h = \frac{3pR}{2\overline{\sigma_1}} \tag{3}$$

$$\sum_{i=1}^{k} \overline{h_{\varphi_i}} (3\cos^2 \varphi_i - 1) = 0 \tag{4}$$

Where $\overline{\sigma_1}$ is the composite strength in direction 1; k is the number of total plies; $\overline{h_{\varphi_i}}$ is the ratio of the individual ply thickness over h, the optimal total structure thickness, such that $\sum_{i=1}^{k} \overline{h_i} = 1$. Immediately, there are several cases to satisfy these two equations theoretically.

1. $k = 2$, $\varphi_1 = 0^0$, $\varphi_2 = 90^0$, $\overline{h_{90}} = 2\overline{h_0}$
2. $k = 2$, $\varphi_1 = -\varphi_2 = 54.44^0$, $\overline{h_{54.44}} = \overline{h_{-54.44}}$
3. $k = 3$, $\varphi_1 = -\varphi_2 = \varphi$, $\overline{h_{\varphi_1}} = \overline{h_{\varphi_2}} = \overline{h_\varphi} / 2$, $\overline{h_{90}} / \overline{h_\varphi} = 3\cos^2 \varphi - 1$

3.1.4 Initial Plans for Composite Optimization

Since FW is a much faster process and has a lower cost than AFP, it lends itself to be the process of choice in the cylinder region. Conversely, AFP is preferred in the dome regions due to its efficiency advantage except for the polar boss spatial constraint where AFP cannot reach. The region immediately around the polar boss will require design and development efforts by both Quantum and Boeing.

From the three optimization choices for the cylinder region listed above, due to the existence of the polar boss and blind boss, it is difficult to realize 0° on either the dome or the cylinder region. Therefore, the first case cannot be considered. In the FW process, researchers [7] as well as our own experience demonstrate that the possibility of laying down any fiber band on the dome surface with the desired orientation depends on the surface curvature and radius in polar coordinate system at that specific location and coefficient of friction. The coefficient of friction depends greatly on resin viscosity, with a typical value of 1,000 to 2,000 cps with FW. Such low viscosity does not allow the fiber orientation or path to deviate too much from the geodesic path, which depends on the ratio between r at the dome region and R, the radius in the cylinder region.

In the second choice, the fiber bands running at ±54.44° at the cylinder region are only able to cover certain areas on the dome surface. Suppose that ±54.44° fiber bands can only reach a region on the dome in the FW process with a polar radius r1, and then the dome surface with a polar radius between r0 and r1 is not covered (r0 shown in Figure 1). It is desirable to cover this region with AFP. However, due to the spatial constraints from the polar boss, it is very difficult to lay any fiber bands on the dome region with a polar radius close to r0. Therefore the region with a polar radius close to r0 has to be reinforced and covered with fiber bands in FW process,

and these fiber bands have to run through the cylinder region as well so that they become parasitic since only ±54.44° fiber bands are enough to reinforce the cylinder region. The current pressure vessel has a relatively long cylinder region, and the parasitic fiber bands will decrease the weight and cost efficiency significantly. Therefore, the possibility of using the first two choices shown above was eliminated.

The third choice is a much more practical solution. The design will be simulated through finite element analysis (FEA) work, after which manufacturing trials will be made at both Quantum and Boeing. Based on the properties of the basic composite lamina used, and considering the spatial constraints in the AFP process, a design of fiber band orientation using the FW process will be made according to the third choice listed above. According to this design, fiber bands with $\pm\varphi$ relative to the vessel axial direction will be laid on the cylinder surface, and when these bands reach the dome surface, they should follow the geodesic line as much as possible. Furthermore, FW needs to be able to reinforce the region where AFP is not able to reach. It may be difficult to satisfy all these conditions, so a compromise may have to be made so that the minimum amount of material is used.

If r2 is designated as the limit of AFP process, then the AFP process will not be able to lay fiber bands in the region with polar radius between r0 and r2, which is supposed to be reinforced by the fiber bands laid in FW process. They will cover the entire dome region but they may not be able to reinforce the dome region with polar radius between r2 and R, where AFP process can be applied to fully secure the dome. These fiber bands will have orientation $\pm\varphi r$ relative to the meridional line. Quantum and Boeing will coordinate the work in order to determine the material used in AFP and measure the basic lamina properties, which will be used in the design.

Some complications can be anticipated in this project. First, the material choice used in AFP has to be made according to several constraints: the curing profile should be close to what is used in FW process, the curing temperature cannot be higher than the softening temperature of the HDPE liner, and the cost should be low since this project intends to reduce cost.

Second, the limit of the AFP process is still unknown, especially with respect to how much area in the dome the process can reach and whether it is possible to orient the fiber band in the desired direction at the given curvature. Trials will be required to understand this issue after the initial design. In addition, the fiber bands laid on the dome surface need to have certain overlapping zone in the cylinder region, so that the tensile stress on the fiber can be effectively transferred through shear. Furthermore, for a thick composite structure, it is difficult to translate the stress effectively from the inner layer to the outer layer. Fiber orientation optimization is another challenge because the radius of curvature changes when any layer of material is added on the surface. Finally, it is unknown how the deformation will look like when the vessel is pressurized since the deformation also changes the dome curvature, which will deviate the fiber orientation from the optimized condition.

Because of the spatial constraints from the polar boss and the constraints from the surface curvature, it is difficult to lay 0^o and 90^o fiber on the dome surface through FW or AFP, especially on the area close to the polar boss. However, a fabric with fiber bands running at 0^o

and 90º can be designed, which looks like a hat and can be 'worn' or draped on the dome surface directly to fit the liner curvature.

3.1.5 Liner Production

A 129L HDPE liner was provided to Boeing for their head development of the AFP process. The dome profile was designed according to one of the equations derived in the study: $\frac{z}{R} = \frac{k_2}{\sqrt{1-k_2}} F(k,\theta_1) + \sqrt{1-k_2} E(k,\theta_1)$. After the liner was made, the dome surface profile (the axial distance z versus polar radius) was measured using a coordinate measuring machine (CMM), along 0º, 90º, 180º and 270º, shown in Figure 2 below.

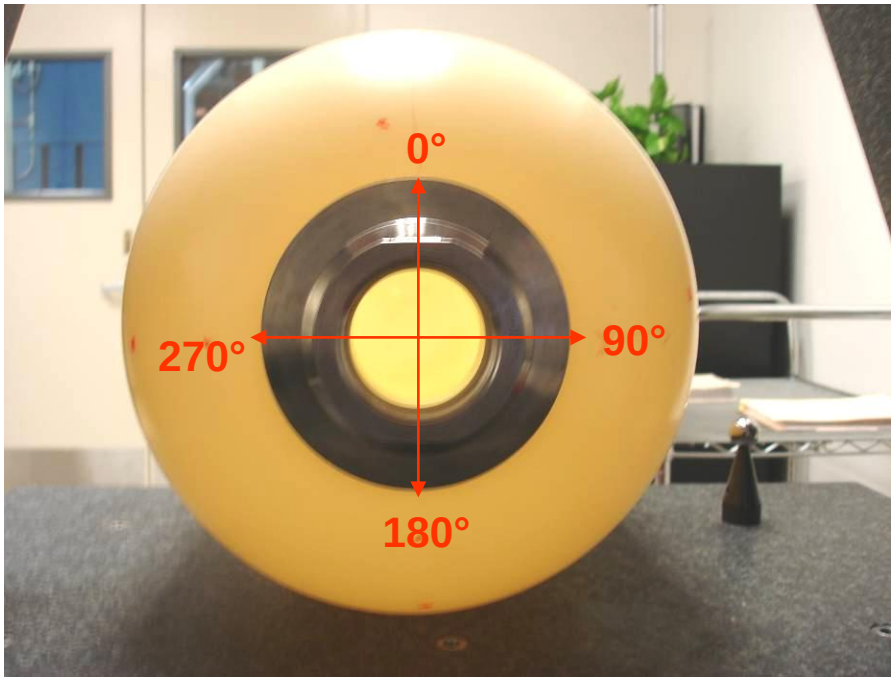

Figure 2. CMM measurement of dome surface profile

The measurement results from these four angles were averaged, and this data was used in later comparison studies. The results for the forward (the end that connects the polar boss) and aft (the closed end) domes were compared with the theoretical results calculated from the equation above. The resultant plot is shown below in Figure 3.

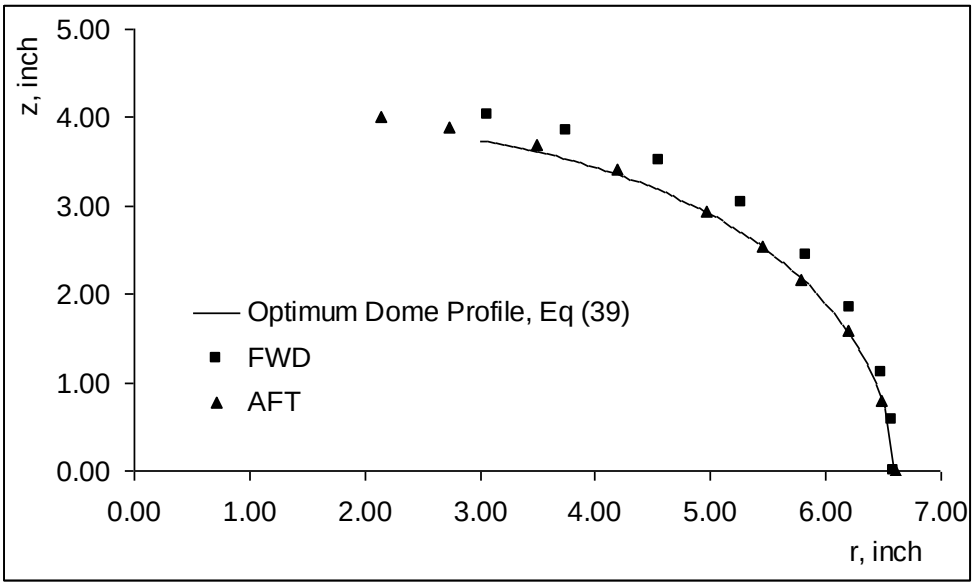

Figure 3. Plot of the theoretical and measured optimum dome profile

From Figure 3 above, the aft dome surface profile is almost an exact match to the theoretical design, but there is a slight difference between the forward dome surface and the designed shape. The difference may be explained by the plastic shrinkage after the molding process in the forward dome is much more significant due to the existence of the polar boss. Another reason may be that less data was taken for the forward dome surface measurements, which could amplify the measurement errors.

3.1.6 System Savings Target

The DOE target for system storage efficiency is based on the assumption of producing 500,000 units per year. A system considered here consists of a single 129L type IV H_2 tank (approximately 5 kg hydrogen capacity) with a solenoid valve, a set of high pressure and low pressure regulators, a mid stage valve (MSV), a receptacle with filter, all tubing and fittings for this system, a frame, a wire harness, a pressure sensor and a balance of parts (consisting mainly of fasteners etc). The end-user cost efficiency of such a system, based on the assumption of 500,000 units/year and that 1 kg of hydrogen is able to generate 33.3 kWh energy, is estimated to be $45.9/kWh, with a weight efficiency of 1.50 kWh/kg. The 10 kg of composite savings will improve the storage system weight efficiency approximately to 1.64 kWh/kg.

3.1.7 Composite Design

The liner profile mentioned above was used in the path generation for the AFP process to place the material in the desired locations. Quantum worked on the composite design using stress analysis and finite element modeling. The first design iteration was generated, assuming a towpreg width of 0.30 inch, which resulted in approximately 6 kg of materials which may be eliminated from the current 76 kg baseline all filament winding design. According to Boeing's updated information on their choice of T800 towpreg width, a second design iteration was generated, assuming a towpreg width of 0.50 inch, which resulted in approximately 10 kg of

materials which may be eliminated from the current design. According to composite lay-up designs, the non-continuous materials will be laid down in the AFP process first on the dome region locally as shown in Figure 4 below, and then FW is used to cover continuous composite material all over the vessel surface. The estimated amount of materials placed by AFP is 1.5 kg, and the rest (about 65 kg) is placed by FW.

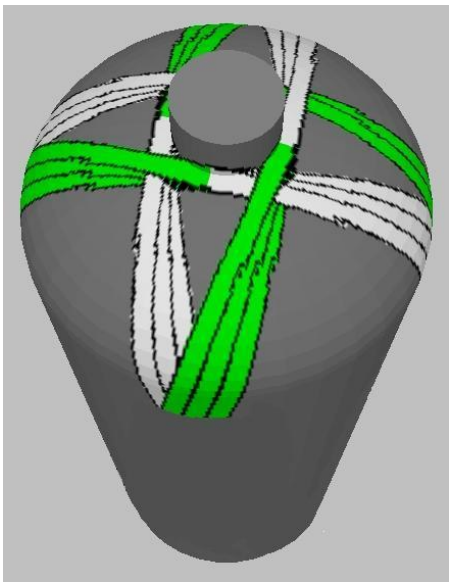

Figure 4. Local dome reinforcement

3.1.7.1 Vessel 1

On the first vessel, for design flexibility with AFP, 2-tows were used in parallel to each other, resulting in a bandwidth of 0.5 inch. This minimized the amount of difference of the fiber path length from the inside tow to the outside tow and the possibility of wrinkling the fibers as the fibers traveled along the spherical surface of the dome. This also requires many circuits to cover the dome as each circuit is only covering a band of 0.50 inches wide. The robot's path is driven by CGTech-VCP software adapted for a hybrid AFP/FW process.

The placement process is shown in Figure 5 to Figure 7 below. When the robot is laying down the material on the dome, a slight amount of heat is required to generate the right tackiness and soften the material to conform it to the curvature. The heat is generated from a heat gun. A little practice is required since too much heat pre-cures the material and produces possible delamination. The temperature on the dome surface is checked from time to time through an infrared (IR) detector to make sure it is well below the material cure temperature. As shown in Figure 5, the aft dome of the liner assembly is mounted on the so-called "Roller-support System", instead of being mounted on the rotation chuck, in order to increase the clearance between the robot head and supporting system, and decrease the polar opening as much as possible, since it is inferred from design that the smaller the polar opening the more material can be saved. The finished forward dome is shown in Figure 6. Since the forward dome is different from the aft dome, the composite design, mounting system and process development for both domes are different and have to be done separately, resulting in different final appearance. Figure 7 shows the material compaction force is from the rubber roller, approximately 80 psi. To

counter the compaction force of the rubber roller, about 5 psi of air pressure is inside the liner to make the liner surface sufficiently rigid.

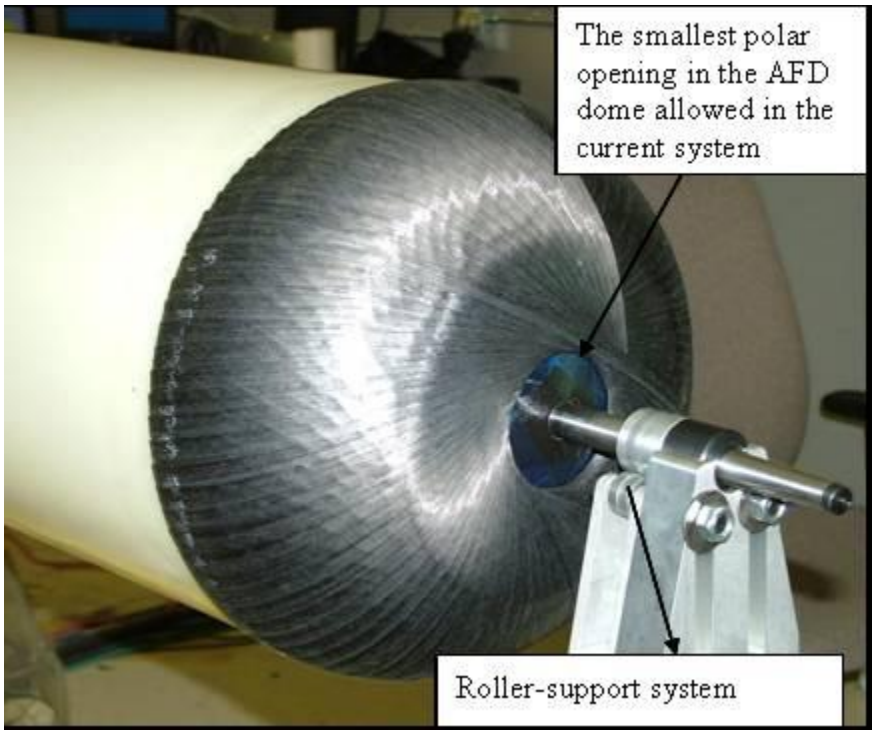

Figure 5. Finished aft dome

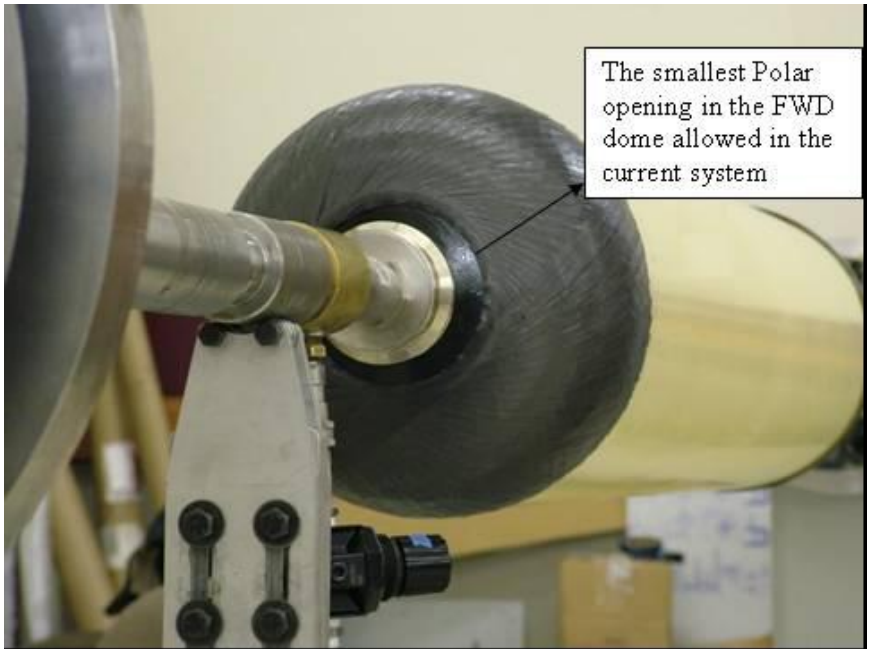

Figure 6. Finished forward dome

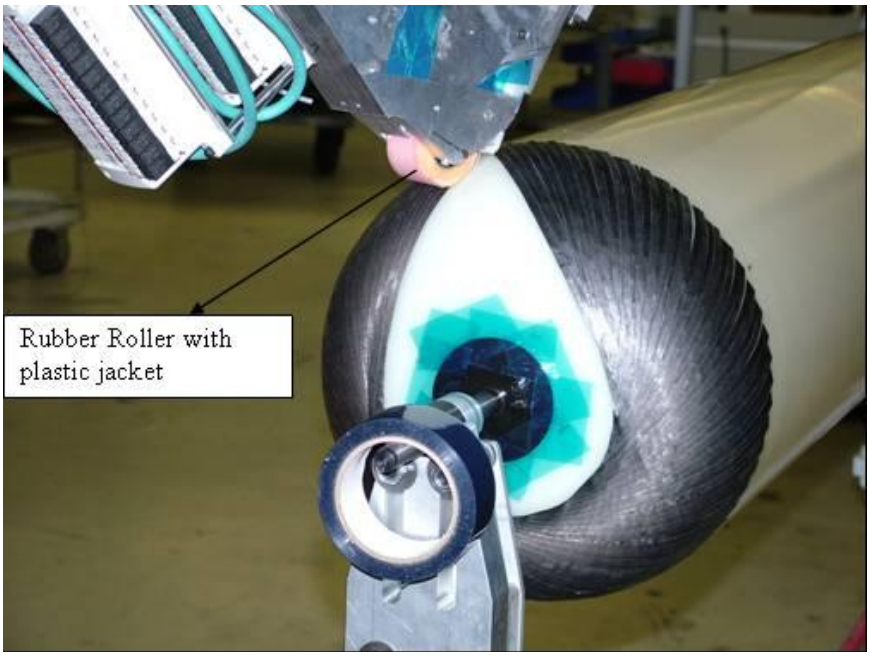

Figure 7. Material compaction from the rubber roller

Compared to FW, the AFP process is more flexible in terms of material usage, since it allows non-continuous material to be placed on the vessel surface, especially on the dome to reinforce the dome only without having to lay the parasitic material on the cylinder section. Therefore it helps to save material usage. However, there are also some disadvantages on the current system, which further improvements are needed. First, material with the right tackiness is needed so that it can be laid down, adhere to and conform to the surface underneath without heat. The heat from the heat gun introduces inconsistency to the process, making it more operator dependent. Second the compaction force from the rubber roller (shown in Figure 7) needs to be adjusted because too much force deforms the material underneath and produces small wrinkles, which were visible in the process. The wrinkles produce some unknown knock-down factors for the mechanical performance of the material in the vessel. However, insufficient force may not produce enough compaction for the material. In FW, wrinkles are absent since tension is applied constantly to pull the material straight. The tension in FW but absent in the AFP process also helps to pick up the slackness of the fiber tow. In addition, in the AFP process, the tow segment is being cut as laid down on the dome surface. The heat generated in the cutting process softens and toughens the material and makes the cutting more and more difficult, so that the cutting blade has to be cooled down before the process can be continued from time to time. Therefore, a cooling system for the cutting blade may be added in the line.

After the materials were laid on both domes according to the design, the whole liner assembly surface was covered by a plastic film and shipped from Boeing to Quantum. The FW process development followed in Quantum to finish winding the vessel for burst test. The burst test was performed according to European Commission (EC) 79-2009 standard. The final composite weight of this vessel was 65kg, which is 14.5% less heavy than the baseline vessel. The vessel passed the burst test at 23,771 psi (163.9 MPa), exceeding the minimum requirement of 22,843 psi (157.5 MPa) by 4%. After the test, composite design iterations and improvements in the AFP process capabilities continued to further optimize the design.

3.1.7.2 Vessel 2

On the second vessel, the band width was increased to 0.75 inches. This was done to reduce fiber placement and winding time by 33%. This decision was based on the results from the previous wind, showing no issues in fiber wrinkling with a 0.50 inch bandwidth. Additionally, on the first vessel, all AFP layers were on the inside of the composite structure against the liner. On the second wind, the AFP layers were distributed into two segments with FW layers between them. The initial AFP layers were against the liner. This was followed by FW layers consisting principally of circumferential winding in order to build up the thickness in the cylinder section equal to the AFP layers on the domes. The remaining AFP layers were then applied prior to placing the final FW layers on the vessel. The partitioning of the AFP layers was approximately 57% on the inner layer and the remaining 43% after the first FW layers.

The AFP process was conducted at Boeing, while the FW process was completed at Quantum. In order to minimize the time to manufacture this vessel and also minimize the need to ship the vessel between California and Washington states, a semi-rigid tooling was manufactured by Boeing using CMM data of the liner provided by Quantum. This style of tooling could also be used in production to allow independent processing of the AFP and FW layers. This independent processing is discussed in the financial models and allows significant reduction in manufacturing space, equipment and process time. However, cost saving on vessel is minimal as material costs are significantly higher than equipment or labor cost.

The forward and aft end caps were manufactured at Boeing using the semi rigid tooling as shown in Figure 8, and the end caps were then removed from the tooling and shipped to Quantum. To maintain the shape of the parts during shipment, the parts were packed in dry ice to increase the stiffness. Quantum placed the AFP end caps on the vessel and overwrapped with the first layers of FW material. An initial low temperature cure was conducted prior to shipping the partial wound vessel back to Boeing to ensure the FW layers would not be damaged during shipment. Upon arrival at Boeing, the second layer of AFP fibers were put on top of the FW layers. The vessel was then returned to Quantum for the final layers of FW over the previous layers.

Final composite weight on this latest design was 61.3 kg, which represented a reduction of 19.3% from the baseline vessel and 5.7% further reduction from Vessel 1.

Figure 8. Semi-rigid foam tooling

The vessel achieved a burst pressure of 18,666 psi (128.7 MPa), which is 82% of the burst pressure requirement. The tank ruptured at the edge of the AFP layer on the aft end of the vessel. From the appearance and location of the burst, it is hypothesized that the reason for the low burst pressure is due to an abrupt transition from the AFP section of the vessel to the FW region. The FEA model used to design this vessel did not model this interface accurately, but inspection of the helical layers on the burst vessel shows this location as the failure initiation point. Analysis of the helical layers away from the interface shows helical fiber strains well below the strains of the helical layers on the baseline vessel.

3.2 Phase II

With the positive results from Phase I, the project continued with Phase II to fine tune the design. In addition, to further lower the vessel cost, the use of alternative lower cost fibers on the outer layers of the pressure vessel where lower strength fibers may be used was investigated.

3.2.1 Stress Analyses Approach Revisited

Because Vessel 2 did not exceed the burst requirement unexpectedly, the approach on stress analyses was revisited to understand why the failure was not realized in the model. Stress analyses on Vessels 1 and 2 were based on three individual analyses: forward dome, aft dome and cylinder section. However, this analysis method failed to evaluate the stresses in the transition areas between the domes and the cylinder section. Instead, two integrated analyses are necessary. One is for the forward dome and the cylinder section, and the other is for the aft dome and the cylinder section.

On the forward dome, the patterns from AFP and FW are fed into the stress analysis model, but the material placed in the cylinder section by AFP is manually replaced with material of the

hoops. This simulates the actual situation, where hoops make up for the fiber that is missing between the domes wrapped by AFP. The same methodology also applies for the aft dome.

With this improved approach, stress analyses were performed on the AFP and FW patterns from Vessel 2. The results confirmed that maximum stress was observed at the transition areas between the domes and the cylinder section, which is consistent with the actual burst location. Consequently the AFP and FW patterns were modified to reduce stresses at the transitions to levels below those seen in the cylinder section of the vessel to achieve a mid-cylinder burst.

3.2.2 Vessel 3

In the AFP build process of Vessel 3, the layup mandrels (machined from foam) having the geometry of the liner and boss at each end were used as surfaces for AFP. This formed the tow-placed end caps in a stand-alone operation.

This set of APF end caps made by Boeing according to the modified patterns from stress analyses was installed on the liner. The liner with end caps was then installed onto a winding machine. FW patterns were laid down according to the design. All hoop layers went onto the liner smoothly. As soon as the first helical layer was laid down, the end caps wrinkled. The wrinkles were caused by air gaps between the AFP end caps and the liner. The tension from the FW carbon fiber compressed the AFP end caps toward the cylinder section, but the end caps were constrained from movement in the axial direction due to FW hoop layers already placed over the edge of the AFP end caps. This resulted in the wrinkles in the AFP end caps. The wrinkles made these end caps not usable.

On the second set of end caps received from Boeing, it was decided to use a FW low-angle helical to capture the end caps. The liner with end caps was placed on a winding machine. Heat was applied to the end caps using a heat gun. Once both end caps started to get softened and become pliable, a complete low-angle helical that closed around both forward and aft bosses was applied to hold the end caps tight. Then the helical was removed before laying down the first set of FW pattern. Once FW finished, the vessel was put on B-stage until the surface became tack free. The vessel was then shipped back to Boeing to complete the task of laying-up the next sequence of tows in this hybrid design. Quantum then finished the vessel with the final courses of filament wound material.

Vessel 3 achieved a burst pressure of 21,658 psi (149.3 MPa), which is 95% of the burst requirement. It improved over Vessel 2 by almost 3,000 psi. The failure location was at the aft end transition between AFP and FW.

Upon reviewing the stress analysis model, the failure location did show the highest strain. Since the burst pressure was 95% of the requirement on the standard, the plan was to lower the highest strain by approximately 7% to ensure the next vessel would pass the burst test.

The forward end of Vessel 3 was sent to Boeing for evaluation. The intent was to determine whether any non-destructive image technique such as ultrasound or computerized tomography (CT) scan could be used to evaluate the fiber lay-up quality of hybrid pressure vessels. Please

refer to Boeing's report section 4.2.2, "Post-Test Analysis of Vessel 3", for further details. The results from cross-section photomicrographs showed fiber waviness in the second AFP. However, this discovery was after the completion of burst test on Vessel 4.

3.2.3 Vessel 4

When designing Vessel 4, a number of improvements were incorporated to ensure passing the burst test criteria. First, the highest strain location of the vessel was moved to the cylinder section by adding localized hoops at the transitions between AFP and FW. As soon as the cylinder section was brought up even with the AFP end caps, these hoops were applied on both ends.

The addition of localized hoops required changes on some of the others layers to keep all helical strains below the highest hoop strain. Positively, these localized hoops helped to lower the peak strain evaluated in Vessel 3 by 7% without adding additional hoop or helical layers.

The last layers of FW after each application of AFP dome caps have been reordered to have a hoop as the outer layer instead of a helical. This was done to improve squeegeeing of the resin, keep tension in the last helical circuit and improve appearance.

Due to variation of plastic liner dimensions, the AFP end caps provided by Boeing were larger than the liner for Vessel 4. To make the domes conform to the liner, Quantum applied nine to ten circuits of a sacrificial helical layer to capture the end caps. Once captured, a heat gun was used to mildly heat up the end caps to make the fiber pliable and conform to the liner. The applied partial helical remained on the vessel. New foam tools will be made to ensure better fit between liner and end caps for future vessels.

With the addition of localized hoops, the total composite weight was 65.0 kg, equivalent to Vessel 1. The burst pressure reached a consistent 95% of minimum requirement or 21,719 psi (149.7 MPa), which is only about 50 psi above Vessel 3. The burst location was again at the aft end transition between AFP and FW. With similar failure locations, further investigation was necessary on the structure between AFP and FW.

A block of approximately 1-inch wide by 2-inch long from the aft end (failure location) of Vessel 4 was polished before inspected under a microscope. It was found that the second AFP was wavy on top of the FW surface. However, the first AFP did not show any sign of waviness because it was applied on the foam tool, which has a much more uniform surface in comparison to the FW surface. This observation is consistent with the results from cross-section photomicrographs performed by Boeing on Vessel 3. By the time results from Boeing on photomicrographs were available, Vessel 4 was already being wound.

For comparing the manufacturing differences between Vessel 1 and 4 designs, an approximately same-size block (1 inch by 2 inches) of composite from Vessel 1, which passed the burst test, was cut from the aft end. After polishing, inspection under the microscope revealed that the AFP had a small amount of waviness. This design only involved one time of FW after direct application of AFP onto the liner. The waviness was very likely caused by the AFP roller

deforming the liner slightly as it was laying down the fiber. Please refer to Boeing's section 4.2.3, "Characterization of Wrinkling in the Tow Placed Layers" for details.

It is believed the premature failure of Vessel 4 was due to fiber waviness from the second AFP, which was caused by the irregular surface of the FW layers. When a layer of fiber is wavy, it does not carry the portion of the load that those layers are designed to carry. This explains why Vessel 4 still failed the burst test at the aft end after decreasing the peak strain by 7 percent and relocating the highest strain location to the mid cylinder section. According to the lessons learned from the first four vessels, it is concluded that the first AFP should be manufactured on foam tools to prevent fiber waviness and second AFP should be eliminated to avoid laying down fiber on an irregular FW surface. This became the design direction for Vessel 5. It is similar to the manufacturing method of Vessel 1 with the exception that AFP will be applied on the foam tool instead of directly on the liner.

3.2.4 Alternative Fibers

Various alternative fibers were investigated to further lower the cost of manufacturing fuel storage vessels by utilizing lower tensile strength fibers on the outer layers of FW due to lower stresses in comparison to the inner layers. Possible alternative fibers included glass, basalt, Saffil, alumina, boron, and silicon carbide. However, all these fibers have been disqualified for consideration because the fibers either do not have the required tensile and/or modulus, are not available in continuous form or too expensive.

Without finding an alternative fiber that is cost effective for the application, the focus shifted back to searching for an alternative carbon fiber. Two different alternative fibers were down selected and evaluated. With the fiber specifications provided by the manufacturer, stress analyses were performed based on a design that the last 11 layers of FW would be replaced with alternative fiber.

Due to the different material properties of Alternative Fiber 1 (AF1), changes in the layup were required to stay within design parameters.

Results from investigating Alternative Fiber 2 (AF2) were quite different. Due to the lower tensile modulus of this fiber, the stress analysis model showed a number of layers with strain higher than the max hoop strain. The fiber was not able to carry the load from the inner layers. To bring down the strain, more fiber was needed, but it would defeat the purpose of using a lower-cost fiber. Although AF2 is $8/lb while AF1 is $9/lb, the savings quickly disappeared when a considerable amount of additional fiber was necessary to lower the strain. The added weight would work against the gravimetric goal as well. Due to these reasons, AF2 was not further pursued as an alternative fiber candidate.

Since the burst test result of Vessel 4 was not satisfactory, the vessel design with alternative fiber was on hold until a new design with baseline fiber was complete. However, there was a clear direction on what alternative fiber would be used for the next design from the investigation completed so far.

3.2.5 Vessel 5

Because Vessel 1 passed the burst test and its design only utilized one time of fiber placement to avoid fiber waviness (lesson learned from Vessels 3 and 4) and streamline manufacturing process (no multiple transfers between production cells for second AFP), it was decided to begin the design of Vessel 5 with Vessel 1 design as a starting point. This works well in a production atmosphere because the processes for AFP and FW can be in parallel and machine utilization can be maximized. The design of Vessel 5 was much improved from that of Vessel 1 in terms of fiber usage, stress distribution and strain values.

The difference in the manufacturing process on Vessel 5 was that the AFP layers were applied on the rigid foam tool instead of directly on the liner. The foam tool allowed better compaction by the AFP roller.

All available liners were used up for vessels built up to date; a new batch of liners were manufactured. Due to measurements on a liner in the previous batch provided by Quantum appeared to have discrepancy (the end caps for Vessel 4 were much oversized than the liner), a new liner from the latest batch was sent to Boeing for dome profile measurements. The foam tool for manufacturing the AFP end caps had to be re-machined as a result of the new measurements. Please refer to the Boeing section 4.2.4, "Reduction of Wrinkling Through Design Build Activities" for further details on liner measurements.

The AFP end caps built on the modified foam tools fit very well on the liner. In addition to the improved end caps, thermoformed shear protectors (placed between metal boss and fiber) were used. On previous vessels, flat shear protectors were used, but their flatness prevented the end caps from sitting flush with the metal bosses. In an all FW process, flat shear protectors would have worked fine because the fiber tension would pull in the shear protectors to conform to the bosses.

Upon completion of the vessel with FW, it was burst tested and achieved a burst pressure of 20,500 psi (141.3 MPa) or 90% of the minimum requirement, which was lower than that of Vessel 4 but had a fiber reduction of 10.6 kg or 16.3% lower than Vessel 4. The burst location was at the aft end blind boss (see Figure 9), which was different from the previous failure modes.

The composite pieces from the aft end revealed that the surfaces of the AFP layers detached from the FW layers were rather dry (see Figure 10), which is a sign of insufficient resin between the two layers. Prior to FW, the AFP end caps were not wetted out. The amount of resin on the end caps was depended on FW only, which could have contributed to this shear failure.

With failure at the blind boss, the vessel was propelled like a rocket during the burst test, destroying both ends of the vessel and losing its usage for any analysis work.

Figure 9. Vessel failure on the aft end

Figure 10. Composites from the aft end showing dryness between FW and AFP layers

3.2.6 Shearing Fracture Toughness Study

Due to repeated failures at the interface between AFP and FW, shearing fracture toughness (Giic) study was repeated to ensure the lower than desired curing temperature on AFP material does not jeopardize its integrity. In addition, there was interest to study a new material, BMS 8-168, which has a potential for better performance due to its curing temperature similar to that of the Quantum resin system.

Boeing offered to run this study. It was consisted of six different laminates for the interface combinations between the original AFP material – BMS 8-276, Quantum baseline fiber wet wind, and a new candidate – BMS 8-168.

Quantum supported this study by preparing the laminates that involved wet winding of baseline fiber. Fiber was wound on a flat panel. For the laminate with baseline-baseline interface, a crack starter film made of fluorinated ethylene propylene (FEP) was inserted in between the two layers of fibers at Quantum. For laminates between baseline fiber and another material, the films were inserted by Boeing. The prepared laminates were vacuum-bagged and shipped overnight to Boeing in dry ice. Please refer to the Boeing report section 4.2.5, "Process-Property Relationship for Tow Placement Candidates", for additional details.

3.2.7 Vessel 6

Due to the amount of damages on Vessel 5, Vessel 6 was built identically to Vessel 5 for failure analyses only. No burst test was performed on this vessel.

Upon completing Vessel 6, both forward and aft domes were cut from the vessel. Half of each dome was sent to Boeing for non-destructive inspection (NDI) with X-ray, CT scan and photomicrograph. More details on NDI of Vessel 6 are provided under Boeing's report section 4.2.6, "Evaluation of Vessel 6".

After polishing up half of the domes at Quantum, excessive voids were found in the aft end due to fiber bridging, as shown in Figure 11. The bridging was caused by incorrect assumption of the "necking factor" value used in the design input file. Necking factor is defined as the ratio of fiber width at the turn around next to the boss vs. bandwidth in the cylinder section.

Figure 11. Voids shown in the sectioned aft dome

To further understand the reason for separations between AFP and FW layers in Vessel 5, samples, measuring ½" wide by 2" long, which encompassed the transition between AFP and FW were cut out to perform short beam shear test. Out of four samples, two showed the failure was between a FW helical and a hoop, which is where a shear failure is expected. However, the

remaining two failed inside the group of FW hoops that were used to "fill" the cylinder section between the AFP end caps.

3.2.8 Vessel 7

With two promising results from the short beam shear test, it was believed that the bridging issue was causing separation and reduction of load translation between the FW layers. Effort was therefore spent to resolve the bridging issue, so that load could be distributed to the outer layers before the inner layers fail. In addition, Vessel 5 burst pressure was only 10% from the burst requirement, but the amount of fiber saved was 16.3% from Vessel 4. There was room to put back more fiber on the vessel and still meet the design goals.

One of the parameter on the design was adjusted to match the actual fiber build up at the boss vs. theoretical. After such modification, the models on both forward and aft ends showed multiple opportunities to improve bridging in the design. The excessive bridging locations were resolved by adjusting the fiber angles and polar openings. Due to these changes, local strains became excessive at the dome to cylinder section of the vessel. Lengths of some hoop layers were adjusted to reduce these stresses in the composite at the dome transitions. To ensure success, the last helical that captured both bosses was doubled to further lower the strains since Vessel 5 failure was at the aft end boss.

Prior to conducting burst test on Vessel 7, eight strain gages were attached on the aft end of the vessel to measure the strains vs. pressure between 0 psi and 1.5X service pressure (15,000 psi). In addition, Boeing has offered to measure vessel strain optically with digital image correlations – ARAMIS®. It essentially measured strains of the entire vessel by optically measuring displacement of the exterior surface. The vessel first had to be painted white to cover up the natural black color of carbon fiber. Then black dots were sprayed on top of the white paint. ARAMIS measures the displacement of these black dots to evaluate the strains, as shown in Figure 12. The vessel was pressurized 14 times between 0 to 15,000 psi to take pictures of all vessel surfaces (8 on the cylinder section, and 6 on the domes). Images generated from the measurements are shown in Figure 13. In each case, the physical strain gages were used to compare with the values measured by ARAMIS and showed good correlations.

Figure 12. ARAMIS measures the displacement of dots on vessels and evaluates the strains

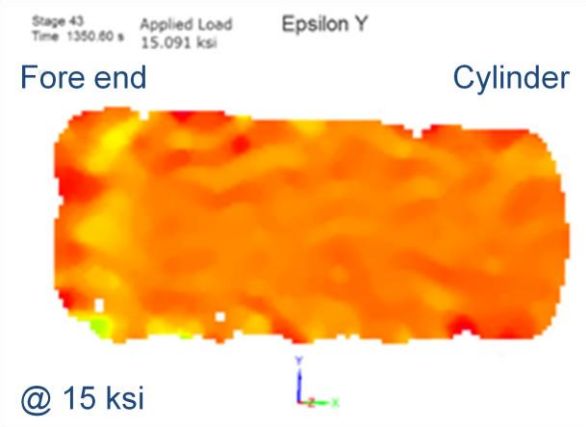

Figure 13. Result from ARAMIS system. The little difference in colors shows that the strains are uniform at 15,000 psi.

Vessel 7 passed burst test at 22,925 psi (158.1 MPa). The burst location was in mid cylinder (see Figure 14). The total weight savings on this vessel was 17.37kg, which is 22.9% savings from the baseline (all FW) vessel. In comparison to Vessel 1, additional 6.27 kg or 9.7% was saved.

Figure 14. Vessel 7 ruptured in mid cylinder, as predicted by the model.

3.2.9 Vessel 8 Build

Vessel 8 was built identically to Vessel 7 for the ambient cycle test. Out of the requirement of 15,000 cycles, it completed 13,500 cycles. This represents achieving 90% of the requirement.

3.3 Phase III

With Vessel 7 passing the burst test and Vessel 8 almost passing the ambient cycle test, the project continued into Phase III. The goal of this phase is continue lowering the vessel cost and to pass the remaining tests that are critical to the hybrid design per EC79 standard.

3.3.1 Vessel 8 Analysis

After cutting the forward dome off the vessel, it was found the liner was bonded to the composite at two different locations. One was close to the forward boss, and the other was along the entire circumference of the transition area between AFP and FW on the forward dome. The bonding was caused by curing the vessel at a temperature that was too close to the softening temperature of the liner material. On the vessels for ambient cycle tests in the future, a plastic film, which has a higher melting temperature than the vessel curing temperature, will be applied between the liner and composite to prevent bonding. Previous experience with this film provides confidence that this failure mode will not repeat in future vessels.

3.3.2 Vessel 9

Since the goal of this project is to reduce vessel cost, Vessel 9 will utilize the lower-cost fiber that was down-selected in Phase II. The identified lower-cost fiber (AF1) has lower strength, but its modulus is higher than that of the baseline fiber. The thought is that the outer layers do not experience as much load as the inner layers; therefore, there is no need to use the higher-strength baseline fiber on the outside. The goal is to replace as many outer layers of baseline fiber with AF1 without significantly increasing the number of layers while satisfying the burst requirement.

Because Vessel 7 passed the burst test requirement, its hoop and helical strain values from the analyses were used as guidelines on the Vessel 9 design. A significant number of layers were removed while satisfying the criteria in the FEA. Preliminary design showed more than 30% of the baseline fiber could be replaced with AF1. Further design improvements were done to minimize bending and maximize conformance to the liner shape at the forward and aft dome locations.

When the design was completed, both the hoop and helical strains were equal or less than those of Vessel 7. To maintain the strain values, two additional helical patterns were added before the final hoop. Although the vessel weight went up due to the additional helical patterns, the overall cost of the vessel decreased due to the price difference (at low volume, $13/lb for AF1 vs. $16/lb for baseline fiber). The difference represents more than an 18% savings. Please note that the alternative carbon fiber price increased significantly between Phase II and III ($9/lb vs. $13/lb) because carbon fiber price is strongly tied to oil price.

To accommodate the localized strains caused by the introduction of AF1, some layers of the forward AFP end cap and FW were modified. Out of the original 46 layers of baseline fiber, 17 layers were replaced with AF1. This equates to a 37 percent replacement. Two additional layers of AF1 were required to equalize the strain levels of Vessel 7. At the end, Vessel 9 had 29 layers of baseline fiber and 19 layers of AF1. Although an additional fiber had been introduced in the design, the resin system remained the same for the entire FW process.

In this design, peak helical strain was maintained on the inner layers, and peak hoop strain was maintained in the cylinder section. Stress analysis results predicted that the burst location would be in mid cylinder.

Vessel 9 was 760 psi (5.2 MPa) short of the burst requirement. This translates to achieving 97% of the minimum requirement Figure 15 shows the failure location was at the tangent between the cylinder section and aft dome. Since the result was very close to the requirement and the vessel was wound over two days (due to winding pattern development time), it was determined to build Vessel 10 in one day with design identical to Vessel 9.

Figure 15. The aft end cap failed at edge of AFP layers

3.3.3 Vessel 10

From experience, approximately 10% performance gain is possible when a vessel is wound in one day instead of two due to air curing overnight on the winding machine. However, Vessel 10 only improved by 305 psi (2.1 MPa) when compared to Vessel 9 performance. The improvement was negligible. Vessel 10 is still 355 psi (3.1 MPa) short of the minimum burst requirement, but the achieved pressure is 98% of the minimum requirement. The failure location was again at the tangent between the cylinder section and aft dome. The results indicated that it was not a manufacturing issue.

3.3.4 Vessel 11

The allowable strains of Vessel 9 and 10 designs were based on the values from Vessel 7, which passed the burst test successfully. Both Vessels 9 and 10 results showed that the design criteria used in the previous analyses were too aggressive. It was believed that the design criteria for using AF1 were not conservative enough to ensure successful test results. To test out the hypotheses, 12 layers of AF1 were replaced with baseline fiber. Although this design would make it heavier and more expensive than Vessel 7, it would verify whether the failure was caused by using the wrong material properties or other design issues.

Surprisingly the burst test result was even lower in Vessel 11 than those of Vessels 9 and 10. It only achieved 20,026 psi (138.1 MPa), achieving 88% of the minimum requirement, although the fiber strains from FEA were lower than those of Vessel 7. While the vessel was designed with the highest strain in the cylinder section, the burst location was again in the transition area between the cylinder section and aft dome. It showed the analysis method needs modifications to accommodate for the hybrid design.

3.3.5 Finite Element Model Generation Software Upgrade

Quantum's in-house computer program, KWind, is used to generate finite element models for vessel design and optimization. This program has been used for over a decade to design Quantum's pressure vessel products and is an effective design tool for filament wound structures.

KWind was originally written to generate an input file for FEA of composite pressure vessels fabricated using the filament winding process. This filament winding process lays down one composite ply at a time from a start point to an end point that generally lies on both the forward and aft domes. KWind does not allow plies to start and stop in the middle of the vessel.

Up to this point, models generated with KWind were hand-modified to account for different start and stop points in the middle of a layer. Accuracy would have been reduced from the model due to these modifications.

The source code for KWind was reviewed, and plans were made to upgrade the software. KWind was written in FORTRAN and contains outdated third party code for input forms and plotting. KWind also does not provide methods for other data calculations. Writing additional computer programs or moving the data into other computer formats and programs was required for additional analyses.

The FORTRAN source code is easily moved and converted into Visual Basic source code. Microsoft Excel contains Visual Basic and is often used to generate other data calculations and analysis methods on the data results obtained from the finite element programs. Visual Basic in Excel also does not require any third party software for forms and plots. Quantum also creates shop floor wind sheets using Excel. Thus the decision was made to use Microsoft Excel and Visual Basic for the next generation of KWind called mWind.

The basic subroutines of KWind were moved to Visual Basic and checked to ensure correct operation. Additional subroutines were written to interface these subroutines with Excel worksheets. The input of mWind was changed from an external file to several worksheets in the Excel workbook. Basic geometry is input on one worksheet. The material properties of the individual plies are input on another worksheet. The composite layup is input on a third worksheet, and the analysis loads are input using a different worksheet. These four worksheets replaced four forms on KWind. The worksheets also allow users to write equations for input values that are unavailable in KWind. The input subroutine of KWind was modified to read legacy KWind input files and populate the input worksheets in mWind.

KWind has several hard coded plots that are used during the input and model generation phases. These hard coded plots cannot be modified and are difficult to save. Since mWind is based in Excel, additional plots or modifications of plots are easily made and saved by the user.

KWind is based on building one composite layer on top of a previous layer at a time starting with the liner mandrel shape. This is the natural method of the filament winding process. mWind took a different approach by breaking the model into individual segments and building up each layer one segment at a time. This allows mWind to easily start and stop plies in the middle of a layer. This method also provides a natural definition of shell elements.

mWind starts by building a base model from the geometry, material properties, and composite layup information. The base model and loading conditions are used to write an input file for a 2D axisymmetric shell model, a 3D shell model, or the traditional 2D axisymmetric continuum model similar to KWind. mWind is capable of write shell models for two different finite element computer programs, Abaqus and ANSYS.

KWind contains a subroutine to read the results of finite element solution and calculate fiber strains for selected layers in the composite structure. mWind also has incorporated this subroutine to calculate and plot fiber strains. mWind also reads the base finite element results into Excel and allows users to create other calculations and plots using Excel commands and other user written subroutines. In addition, mWind has subroutines to read and store analysis results into an Excel worksheets without the base model information.

3.3.6 Vessel 12

Upon completion of the mWind program, it was used for designing Vessel 12. One of the major differences in this latest design was that the AFP end cap terminations were further into the cylinder section. This provided improvements on load transfer between AFP and FW, eliminating fiber strain spikes at the forward and aft end transitions between AFP and FW shown in the analysis results.

Both forward and aft AFP end cap designs were also modified to increase the number of layers from 10 to 12 to further strengthen the dome region. When designing the 12 layers, less fiber steering was introduced. Because of the increased number of layers in the end caps, the number of hoops between the dome caps also increased to bring the vessel surface even for completing the remaining FW portion.

With the FW portion of Vessel 12 design not significantly different from previous designs (thus short winding pattern development time), the build was completed in one day. After curing, burst test was subsequently performed, but it only reached 20,958 psi (144.5 MPa), meeting 92% of the minimum requirement. Failure location was on the aft end at the transition area between AFP and FW again. The aft end dome was detached from the rest of the vessel. This failure mode provided insight that the transition between AFP and FW was still not sufficient, although it had been lengthened for this latest design.

Further evaluation revealed the actual build was different from the design. With the analysis tool modified, Vessel 12 was built with the assumption that the maximum number of AF1 layers (Vessel 9) was incorporated in the design. Instead of only putting on five layers of AF1, 13 layers were applied. This mistake slipped pass un-noticed because the winding patterns were all identical in those 13 layers with the exception of the type of carbon fiber used. The tensile strength of AF1is not significantly lower than that of the baseline fiber. Even if only five layers of AF1 were applied, the vessel would still not able to make up the approximately 1,900 psi (13 MPa) deficit during burst test. 12 layers of partial helicals in the AFP dome caps might be too stiff as one entity for effective load transfer. In typical FW, helicals and hoops are distributed evenly throughout the layers.

In addition to making design changes to eliminate the chance of failing at the transition between AFP and FW, more hoops were applied between the AFP dome caps to bring the composite even before the first helical pattern. Vessel 12 was the first time that the calculated hoop thickness between end caps did not match the height of the end caps. An uneven surface provides a chance for bridging to occur when laying down the helical patterns.

The analysis results of Vessel 12 using mWind showed the fiber strains near the tangent line were low and the maximum fiber strain was in the first hoop layer near the mid section of the cylinder. Figure 16 shows the fiber strain results of Vessel 12 for the aft end.

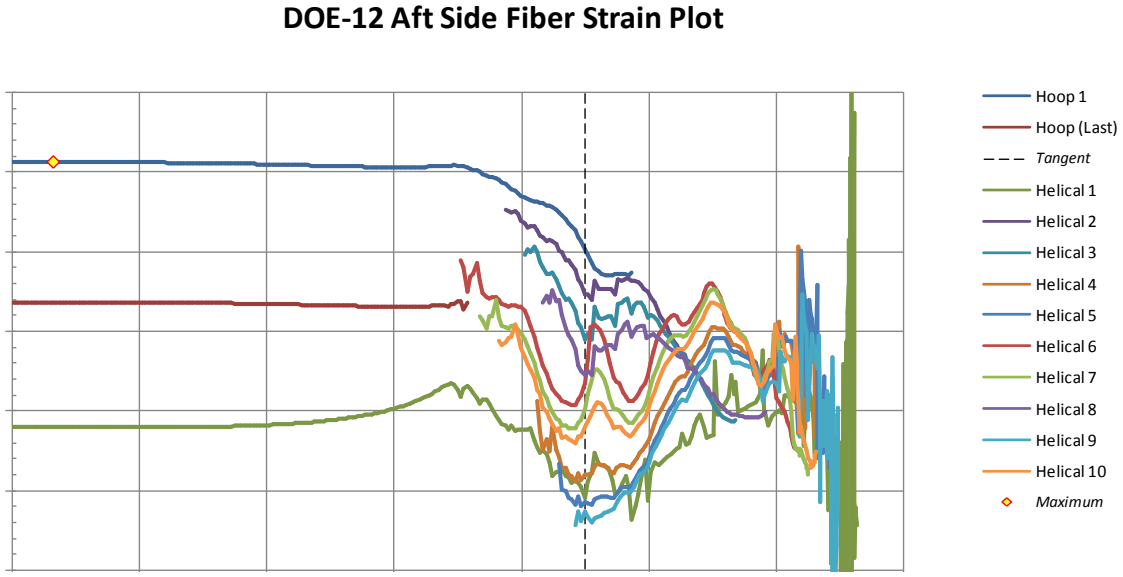

Figure 16. Vessel 12 aft end fiber strain results using mWind

During winding of Vessel 12, bridging was observed in the mid cylinder for the first full helical layer. A review of the finite element model showed that the first hoop layers did not fill the cylinder section enough to match the end cap maximum height in the cylinder section. Figure 17 shows the finite element model near the tangent line. This bridging likely caused Vessel 12 to not meet the required burst strength.

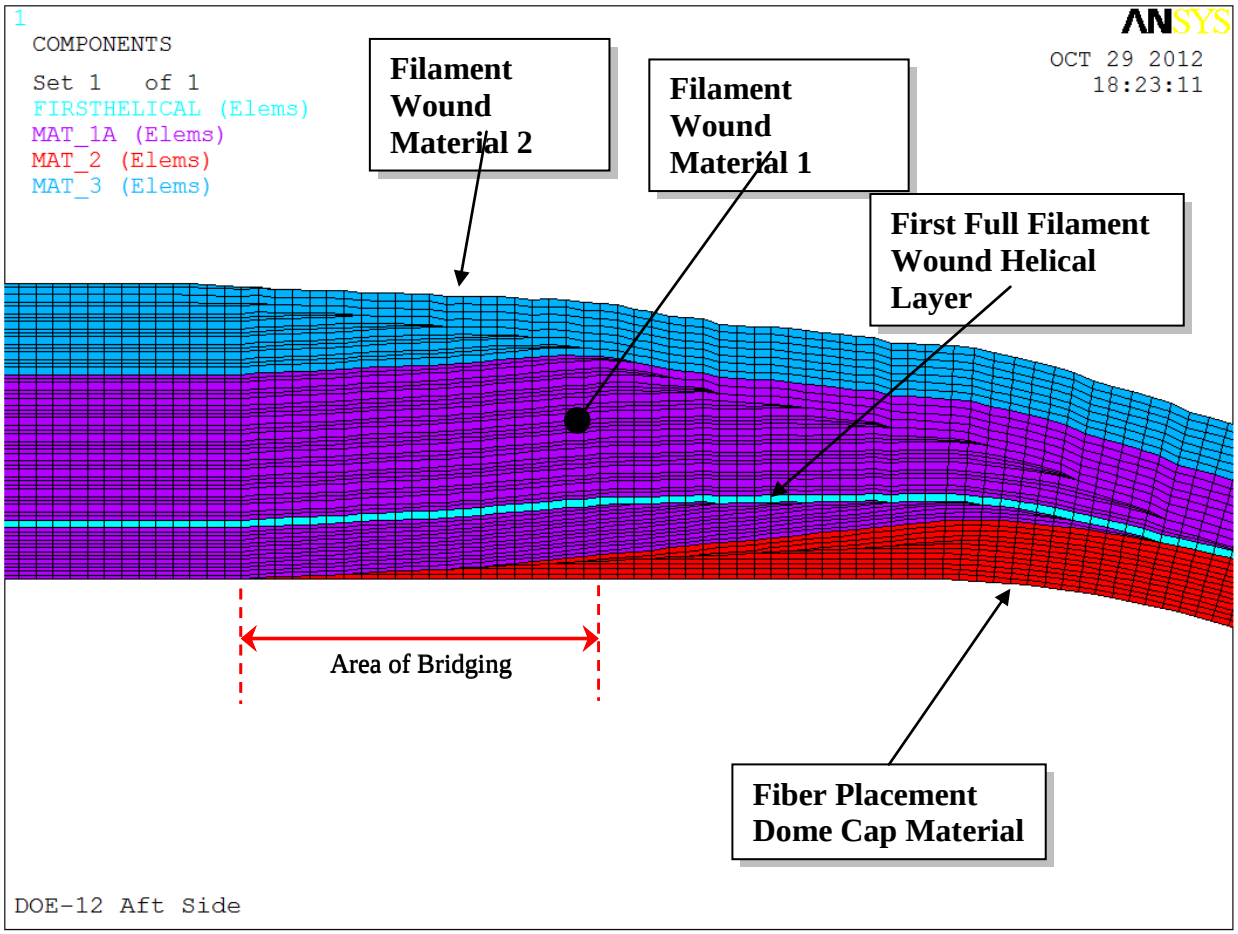

Figure 17. Vessel 12 finite element model for aft end near tangent location using mWind

The latest pricing information from carbon fiber suppliers show the baseline fiber is the most cost effective option in terms of performance per dollar. By using AF1, the vessel becomes heavier and more expensive. There is also labor cost involved to switch out baseline fiber for AF1 or any alternative fiber in the middle of a wind. For the remaining time of this project, no vessel will be built with AF1. The focus will be on designing a vessel to pass the burst test and continuing onto other tests per EC79 that are critical to evaluate the compatibility of resins and fibers used in a hybrid vessel, thus confirming the results from the flat panel studies done by Boeing.

3.3.7 mWind Software Update

Several updates to mWind have been completed since it was introduced. One updated feature was a new plotting procedure for the fiber strain plots. The previous version of mWind was very slow for the fiber strain plots of large models.

The first version of mWind plotted the fiber strain results for each layer and node in the model, which generated a very large amount of data to be plotted, most of it being non-data or null data. The null data required an additional amount of computer memory which over taxed the computer

program and made it non-functional. The plotting program was rewritten to eliminate the null data and reduce the amount of data storage requirements.

Additional features were also added to the plotting routine to reduce the amount of data plotted. The maximum fiber strain value of each layer is used to rank the layers. First, each individual layer is divided into one of two classes; hoop layers and helical layers. The hoop layer with the highest fiber strain and the one with the lowest fiber strain are plotted. This procedure essentially 'brackets' the hoop layers, and all other hoop layers are to be within this range of values.

For the helical layers, a parameter can be provided to mWind to plot the top "n" plies. Typically, the top 10 helical plies are plotted. This greatly reduces the amount of memory required to graph the fiber strain plots. Additionally, the user can manually select individual plies to be plotted.

There were some features not working correctly in mWind that were debugged and fixed to ensure the finite element model was generated correctly. Some of the bugs encountered were in the composite thickness in the dome and start and end points of non-continuous layers.

3.3.8 Review of Past Designs

An in-depth review of past designs was completed to assess any trends or commonality between each design. The one common result was that all fabricated pressure vessels that were burst tested failed in the aft dome at the cylinder to dome tangent line (at a minimum) except Vessel 1. Vessel 1's burst location was in mid cylinder with the helical fibers failing first, then the vessel split into two sections. Figure 18 shows a photo of Vessel 1 after the burst test.

Figure 18. Vessel 1 shown after burst test

Vessels 1 and 7 burst pressures exceeded the minimum required burst pressure of 22,843 psi, (157.5MPa) with Vessel 7 just barely passing the requirement. The results of all vessel built up to this point on this project are listed in Table 1 for reference.

Table 1. DOE vessel fabrication and testing results

Vessel #	Weight (kg)	Burst Pressure (psi)	Burst Pressure (MPa)	Burst Location	Notes
0	76	-	-	-	Baseline
Phase I					
1	64.9	23,771	164	Mid cylinder	Helical fiber rupture
2	Not Available	18,666	129	Aft	
Phase II					
3	67.1	21,658	149	Aft	
4	65.0	21,719	150	Aft	
5	54.4	20,500	141	Aft	
6	55.0	N/A	N/A	N/A	Same design as Vessel 5, Vessel cut for analysis
7	58.6	22,925	158	Mid cylinder and aft dome	Passed burst requirement
8	57.3	N/A	N/A	N/A	Cycle test, Cycled 13,500 times out of 15,000
Phase III					
9	59.6	22,083	152	Aft	With AF1, 2-day wind
10	59.4	22,388	154	Aft	Same design as Vessel 9, 1-day wind
11	59.6	20,026	138	Aft	Replaced some AF1 layers with baseline fiber
12	58.8	20,958	145	Aft	1st mWind design with AF1, fiber bridging observed
13	TBD	TBD	TBD	TBD	2nd mWind design without AF1

The design for Vessel 1 was misplaced; therefore, the design cannot be recreated to be checked in mWind. Vessel 7 was re-analyzed using mWind to build the finite element model and compared to the KWind model results.

Figure 19. KWind fiber strain results of Vessel 7 aft end. The high peaks at approximately 9.5 inches are modeling anomaly due to material replacement. and Figure 20 show the fiber strain results of the model generated using KWind for the aft and forward ends of the Vessel 7 design, respectively. They both show the highest fiber strains are in the cylinder section. Figure 21 shows the fiber strain results of the model generated using mWind. The maximum fiber strain is at a location near the tangent between the cylinder section and the aft dome. One factor that is believed to cause higher fiber strains in mWind is because it has the ability to start and stop layers in the middle of the model and does not require any post model generation modifications. mWind is more accurate in predicting vessel performance because of the additional pre-processing features that KWind lacks.

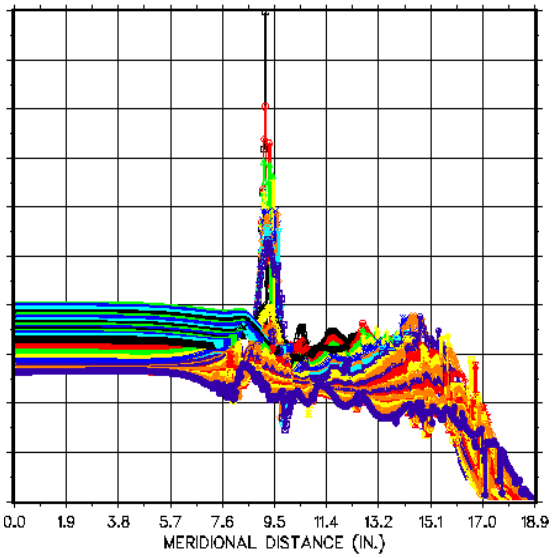

Figure 19. KWind fiber strain results of Vessel 7 aft end. The high peaks at approximately 9.5 inches are modeling anomaly due to material replacement.

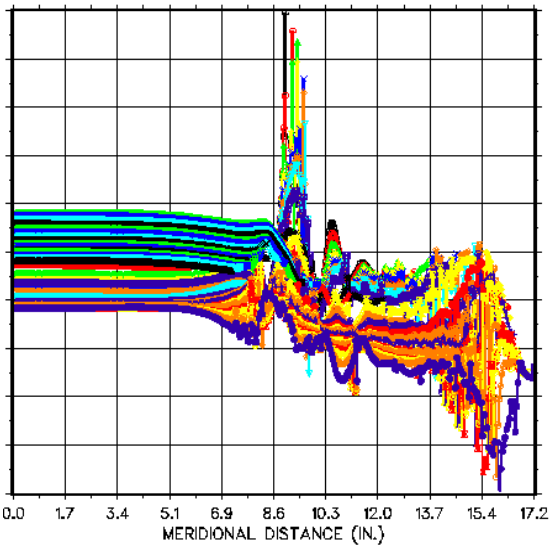

Figure 20. KWind fiber strain results of Vessel 7 forward end. The high peaks at approximately 9.5 inches are modeling anomaly due to material replacement.

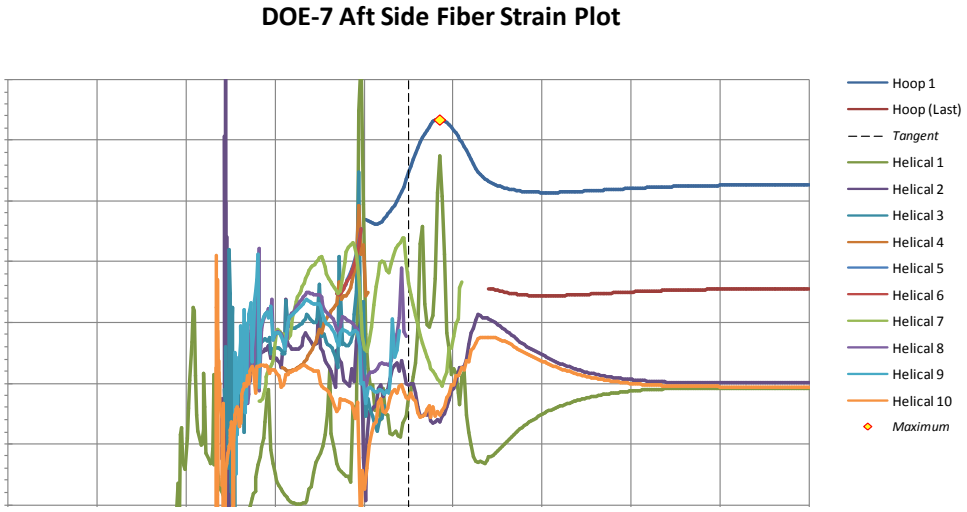

Figure 21. mWind fiber strain results of Vessel 7 aft end. The high peaks at approximately 9.5 inches are modeling anomaly due to material replacement.

The results of KWind and mWind versions of Vessel 7 design show that the vessel would have different burst modes. KWind predicts a cylinder failure, while mWind predicts an aft dome failure. The burst test conducted on Vessel 7 shows a mid cylinder burst and an aft dome burst at the tangent line. At the time of testing Vessel 7, it was thought the aft dome damage was caused by the mid cylinder burst. Figure 22 and Figure 23 show photos of the burst test on Vessel 7. These pictures revealed that the rupture could have occurred at both the mid cylinder section and at the tangent line of the aft dome, which is consistent with the results of both the KWind and mWind models. However, mWind predicts a worse failure mode of the two. For design purposes, it is preferred to use a tool that predicts the worst case.

Figure 22. Vessel7 after burst test

Figure 23. Vessel 7 aft dome after burst test

3.3.9 Vessel 13

Vessel 12 was the basis to start the design work on Vessel 13. The first step was to increase the first hoop layers to ensure the cylinder bridging was eliminated. Unfortunately, the increased number of hoop layers before a complete helical layer pushed extra bending into the dome near the tangent line. The layup for the end caps fabricated using AFP needed to have several more layers added to address the increased stresses. Vessel 7 used 10 layers for the end cap reinforcement, and Vessel 12 used 12 layers. Vessel 13 requires 19 layers in the forward end cap and 20 layers in the aft end cap. It is ideal to increase the number of end cap layers to maximize the benefits of AFP, eliminating the unnecessary fibers that would have been in place if those layers were filament wound.

Figure 24 and Figure 26 show the fiber strain results for Vessel 13 aft and forward ends respectively. Figure 25 and Figure 27 show hoop contour plots of the finite element model results for the aft and forward ends, respectively. The displacements of the model are magnified by 20 times to assess if any excessive bending exists in the dome.

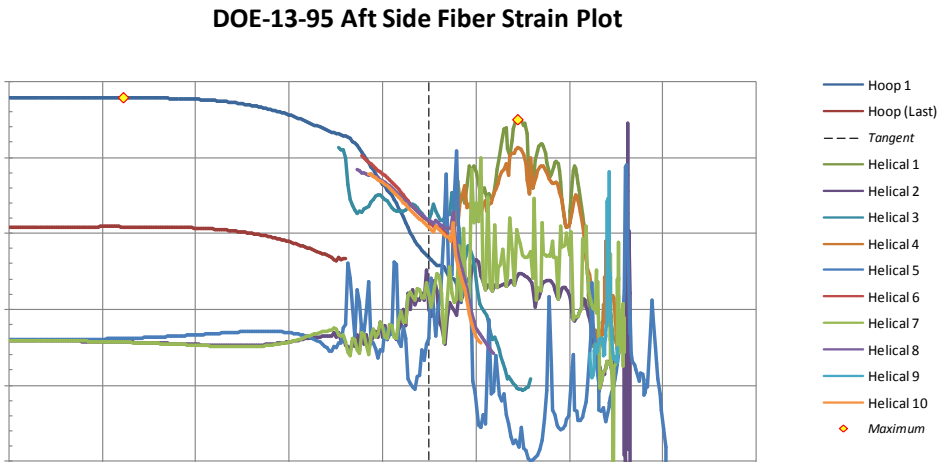

Figure 24. mWind fiber strain results of Vessel 13 aft end

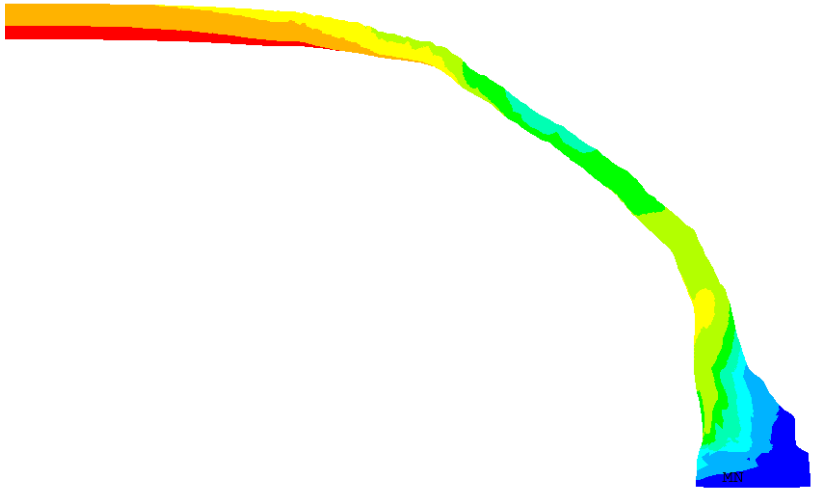

Figure 25. Hoop strain contour plot of Vessel 13 aft end

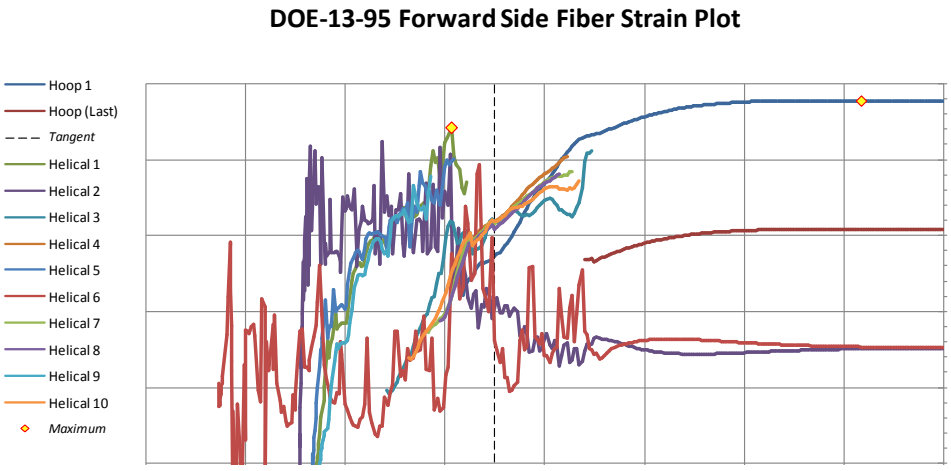

Figure 26. mWind fiber strain results of Vessel 13 forward end

Figure 27. Hoop strain contour plot of Vessel 13 forward end

Figure 28 reveals the composite build up near the tangent line from the model generated from mWind. This shows how extra hoops are used to fill the cylindrical section to the height of the AFP end cap material and should eliminate any bridging in the cylinder section.

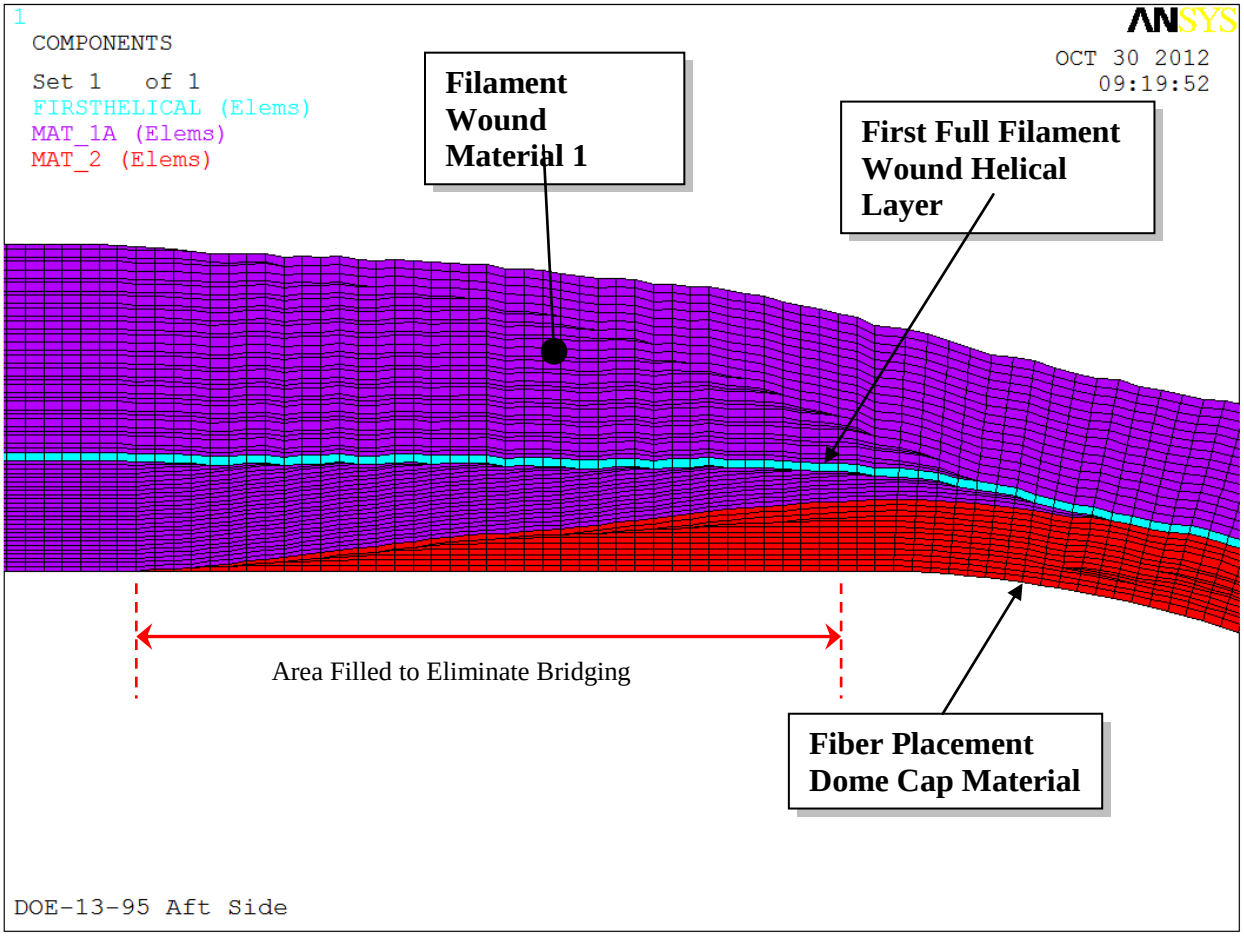

Figure 28. Vessel 13 composite layup near tangent line

The delivered AFP end caps were placed on the liner and setup for FW. At this point it was discovered that the length of the end caps on the cylinder section was incorrect and approximately one inch longer than the design value, which equals to two inches into the cylinder section.

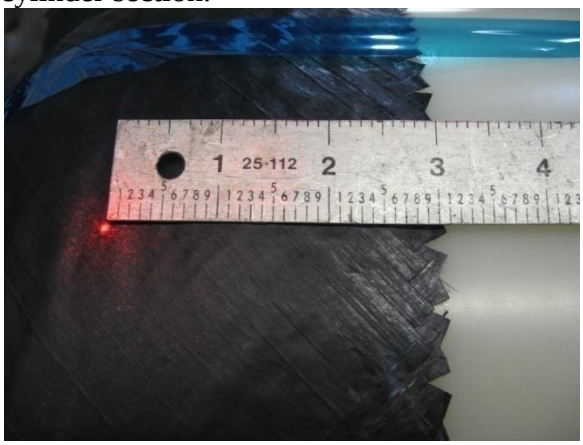

Figure 29 and Figure 30 show the forward and aft end caps on the liner installed on the winding machine, respectively. The laser point references the liner tangent point.

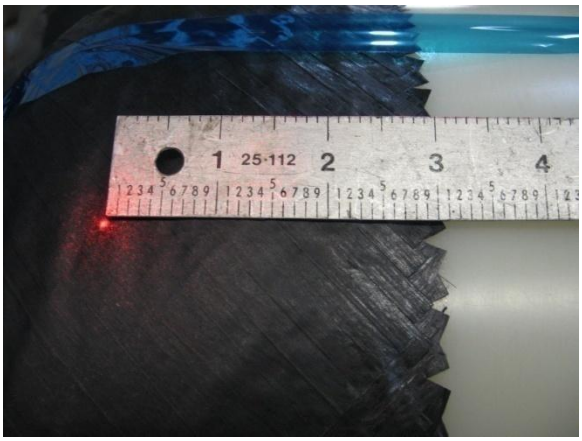

Figure 29. Forward end cap on liner

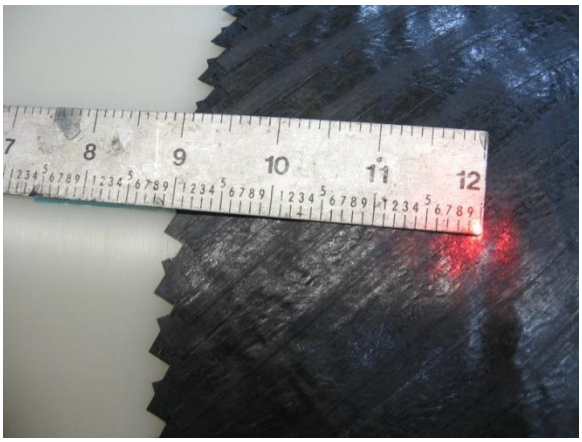

Figure 30. Aft end cap on liner

Discussions with Boeing revealed the tangent point defined by Boeing was 0.9" different from that of Quantum. Boeing defined the tangent point of each dome by measuring the liner with a CMM, while Quantum based the tangent point on geometry of the tooling used to make the liner. This places the tangent one inch outward from parting lines of the tooling. This "extended" configuration was analyzed on the aft end, and it showed the extra length on the dome cap would increase the fiber strains in the end caps by 90% at the termination of fiber on the cylinder side, which is shown in Figure 31.

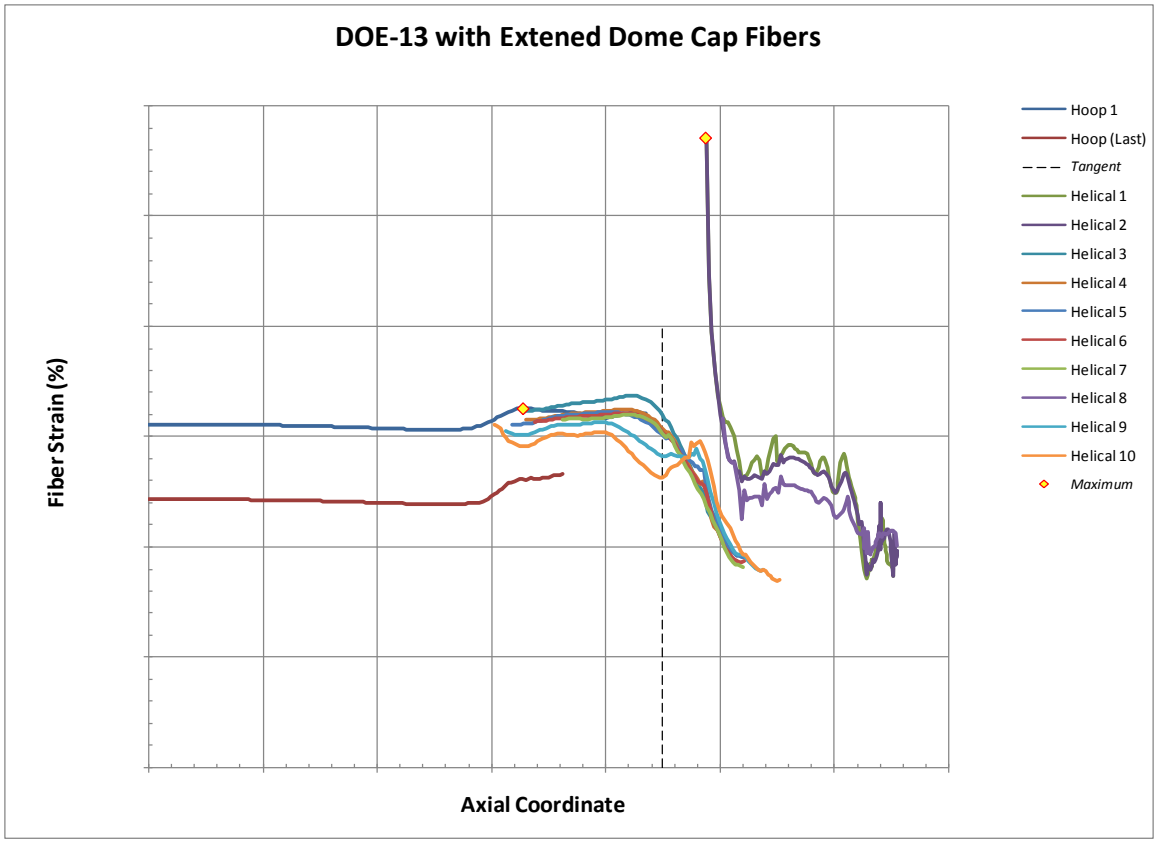

Figure 31. Vessel 13 aft end fiber strains with extended end cap

These results indicated that the end caps were unacceptable for the vessel design. Figure 32 shows the finite element model of Vessel 13 in the dome-cylinder transition area with the high fiber strains in the end cap material.

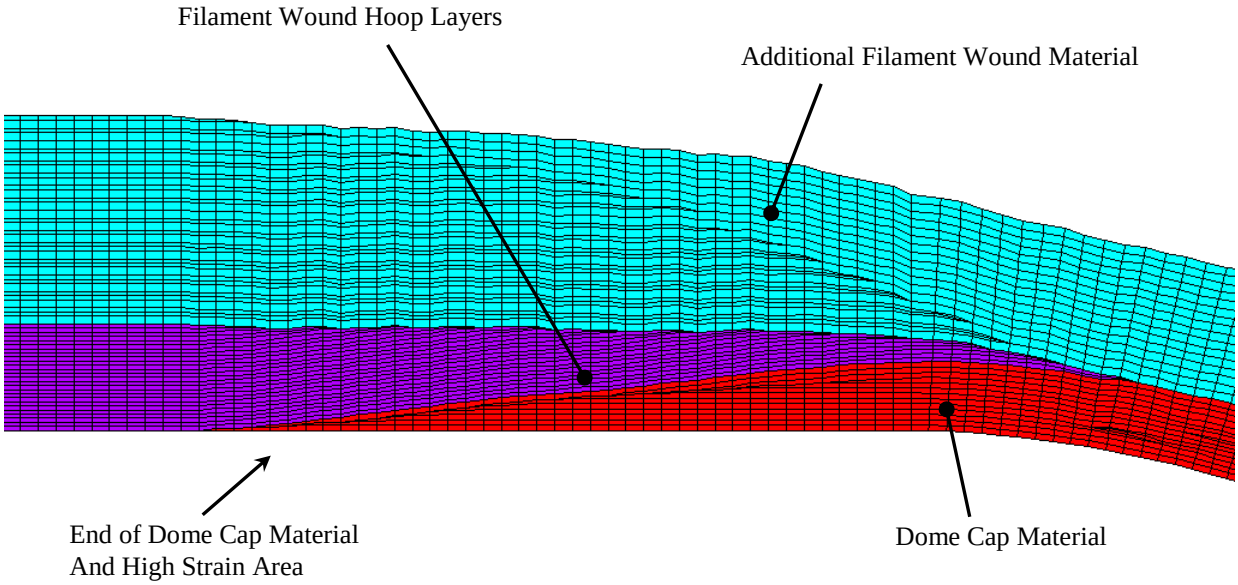

Figure 32. Finite element model of Vessel 13 aft end transition area

The end cap layers that terminate in the cylinder section are helical plies with a low wind angle between 10° and 20°. These end cap layers are overwrapped with filament wound hoop plies to build up the cylinder section to the maximum thickness of the end caps. The low angle end cap helical layers in the cylinder section are also tapper to reduce the thickness and better integrate the end cap material into the FW material.

The filament wound hoop layers have a low axial stiffness whereas the end cap helical layers have a high axial stiffness in the transition area. Since the filament wound hoop layers are much thicker than the end cap layers, and the axial stiffness of the hoop fibers dominates the overall stiffness of the composite in this area. The axial stiffness appears to be low which induces high axial strains which causes artificial high fiber strains in the end cap material. In the real world, micro cracks will probably be created at the interface between the end cap and filament wound materials. This will relieve the high fiber strains in the end cap material. The current finite element model does not account for micro cracking and the design is adequate for the required pressure loads.

When the cross-ply stresses and strains are high enough, micro-cracks are formed in the composite resin. Micro-cracks are often seen in the domes from the bending forces and higher cross-ply stresses. However, the finite element model does not take into account of micro-cracking in the resin because of the size of the micro-cracks are much smaller than the size of the individual elements.

Based on the above discussion, the high strains in the area where the end cap material ends is assumed to be a modeling artifact and not a real condition. It is assumed that micro-cracking will relieve the high axial strains and not transmit them to the fibers. Even though it was

assumed that the micro-cracking would relieve the high fiber strains in this area, the filament wound material layup was adjusted by adding additional localized reinforcement to help lower the axial strains.

The vessel winding layup was adjusted during fabrication to avoid fiber bridging in the dome-cylinder transition area seen on Vessel 12. The original number of hoop layers per design of Vessel 13 that was laid down between the end caps did not provide sufficient material to match the thickness of the end caps at the tangent points. **Figure 33** shows a photo of a straight edge and the gap that existed in the cylinder section of the vessel. The winding layup was adjusted to relocate some hoop layers from the outer layers to the inner layers. Figure 34 shows the layup with the relocated hoop layers needed to fill the gap.

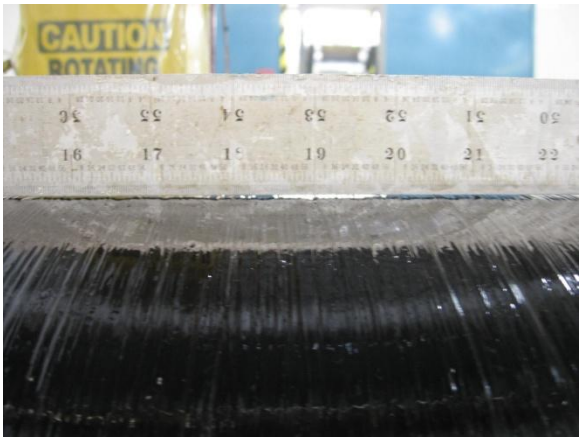

Figure 33. Initial hoop layers with gap

Figure 34. Hoop layers relocated to eliminate gap

The final helical and reduced hoops on the outer layers were adjusted to provide the most desirable predicted fiber strains for Vessel 13. Figure 35 shows the as-built aft end fiber strains of Vessel 13.

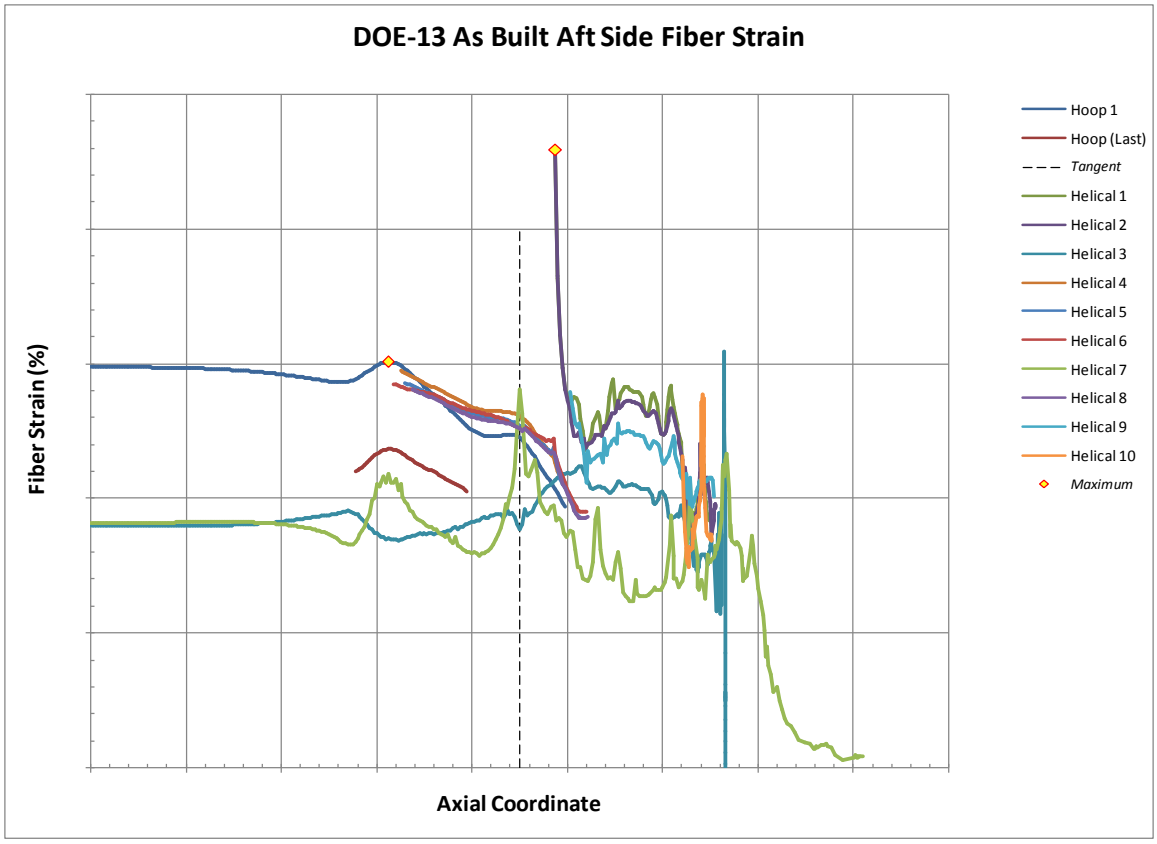

Figure 35. Final and as built fiber strains of Vessel 13 aft end

When Vessel 13 was completed with FW, the aft dome appeared to have a larger buildup at the aft polar boss than expected. Figure 36 shows two views of the composite buildup at the aft end. Bridging between layers was also observed in the aft end buildup during the winding operations. This type of buildup has been known to cause a reduction in burst strength in other vessels and was a concern for Vessel 13.

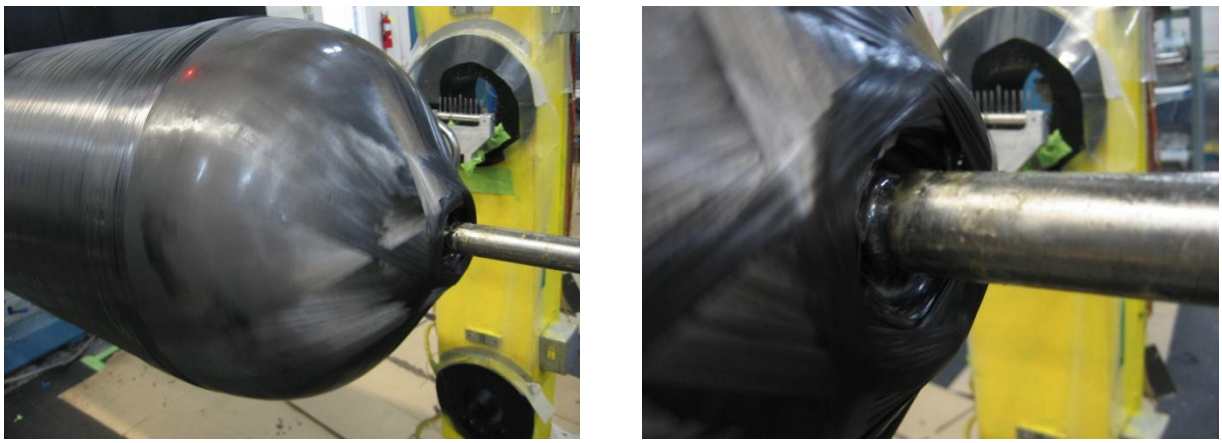

Figure 36. Vessel 13 aft end composite buildup

Before performing the burst test on Vessel 13, NDI in the form of CT scanning was done on the domes. The CT scan of the aft end dome shows bridging, which is illustrated in Figure 37.

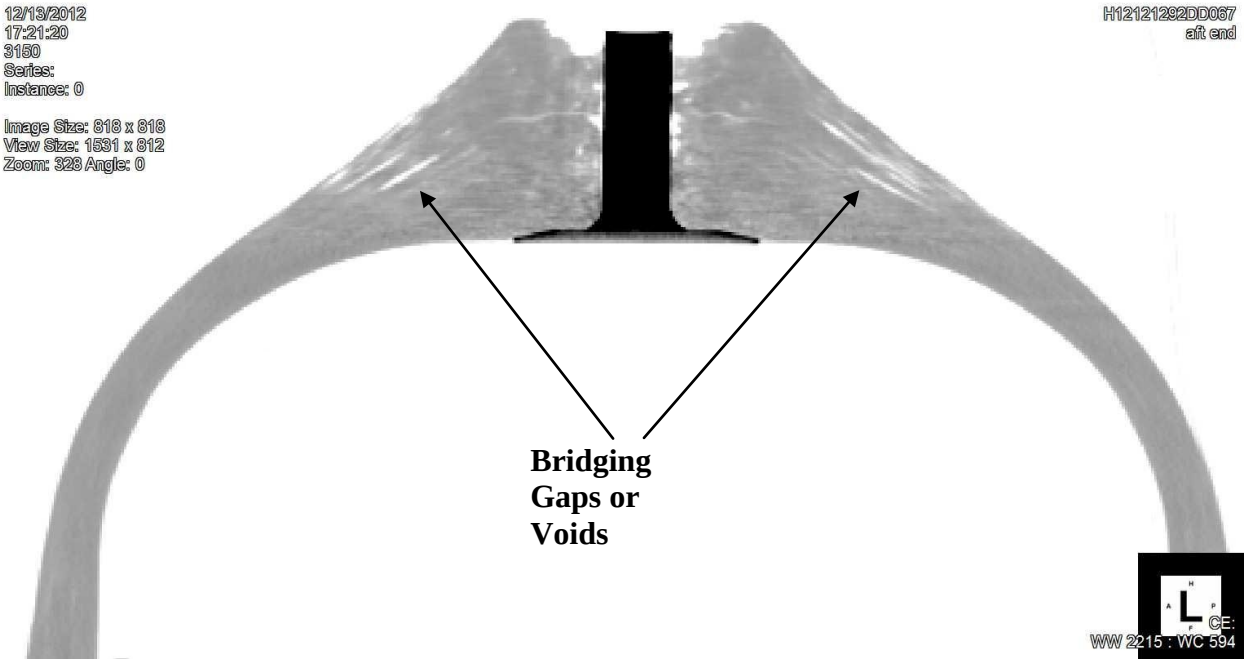

Figure 37. CT scan of the aft end dome

Figure 38 shows the final design layup for Vessel 13 in the same orientation as the CT scan image. The buildup near the aft polar boss is similar. Small adjustments to the buildup thickness will be made in mWind to better correlate the predicted and actual fiber buildup.

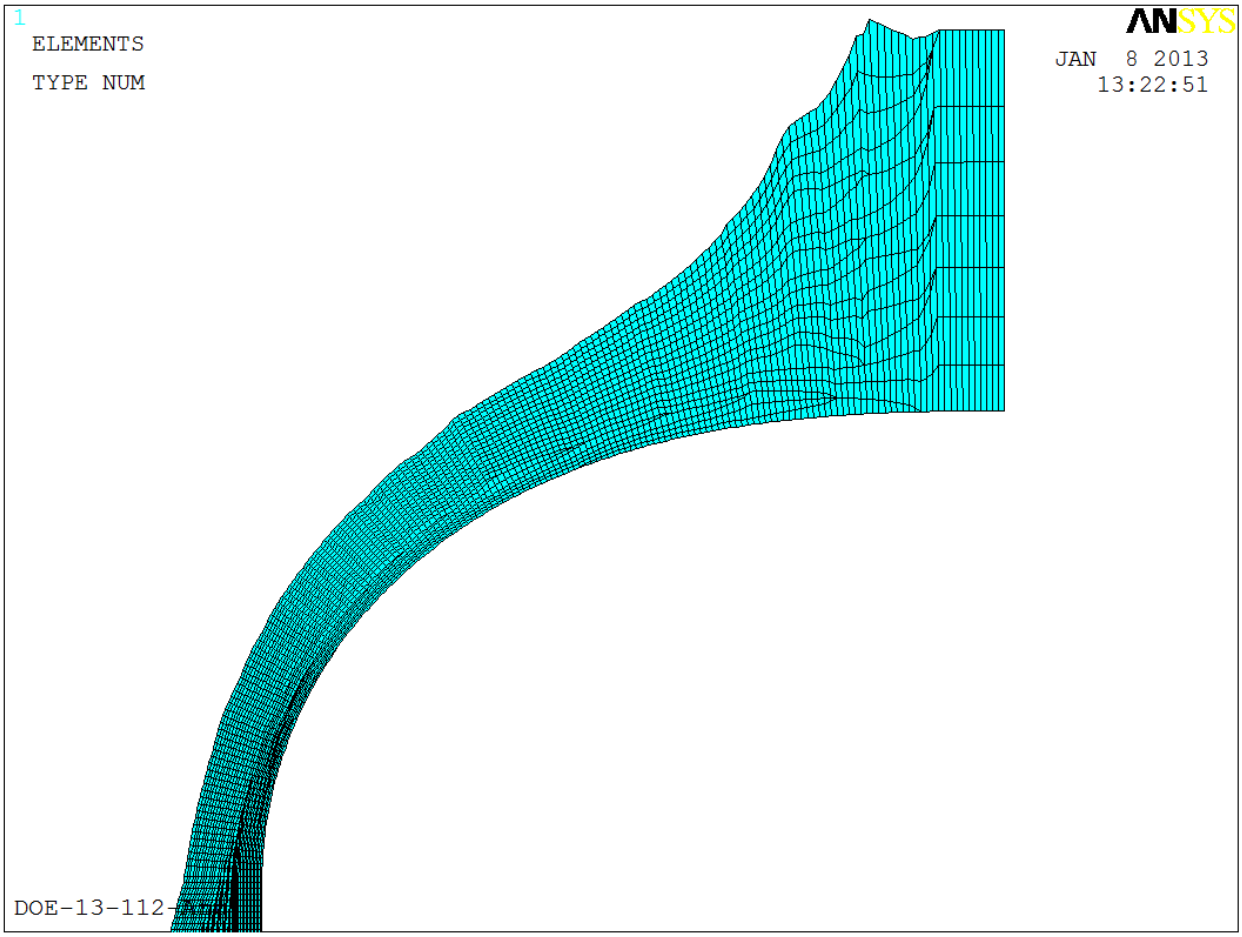

Figure 38. Aft dome finite element model buildup of Vessel 13

High speed camera was utilized to capture the burst location of Vessel 13. This valuable information would help design the subsequent vessel if necessary. The vessel ruptured with an internal pressure of 20,679 psi (142.57 MPa), achieving 91% of the burst requirement. Rupture occurred in the aft dome polar boss. Figure 39 shows three frames of the burst test high speed video.

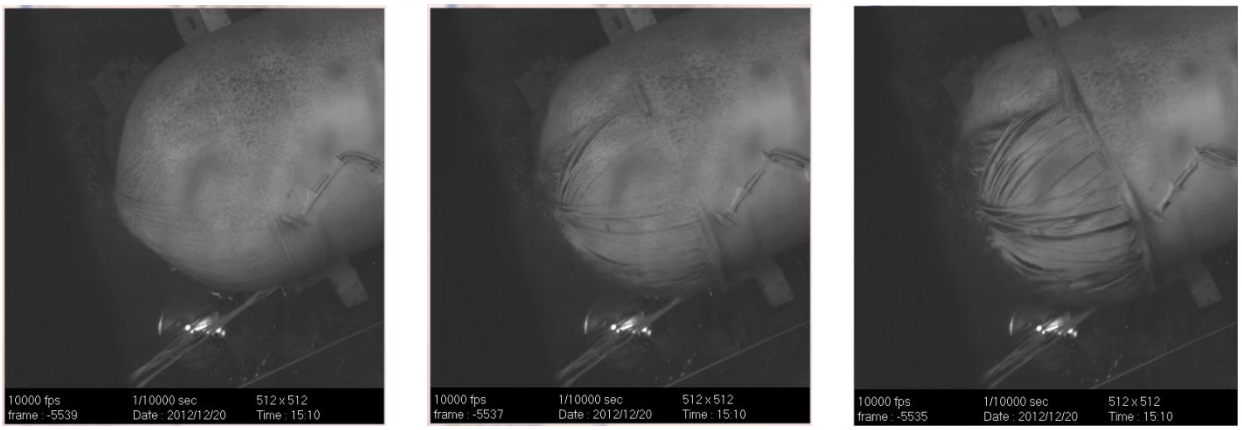

Figure 39. Vessel 13 burst test high speed video frames

The first frame is the vessel aft end right before rupture. The second frame shows the aft end just as failure starts to occur. The failure propagation is shown in the third frame. Each frame is 1/10,000 second.

The finite element generation software will be modified to more accurately model fiber buildup at the polar openings, which will result in a change to the composite layup for the filament winding of Vessel 14. The adjustments are necessary to reduce the voids in the aft end near the polar boss. The composite thickness measurements of the composite shell in the CT scans will be used to adjust the predicted thickness values of the mWind software.

3.3.9.1 Measurement Comparison between ARAMIS and Strain Gages

Strain measurements were performed on Vessel 13 prior to the burst test, both physically with strain gages and optically with ARAMIS, supported by Boeing. This was previously performed on Vessel 7.

Eight strain gages were attached on the vessel. At the transition area between the cylinder section and forward dome, as well as between the cylinder section and aft domes, strain gages were arranged to measure hoop strain, axial strain and strain at 45 degrees. On the cylinder section, strain gages were arranged to measure hoop and axial strains only. Figure 40 shows the locations of strain gages. This arrangement was chosen due to the limited number of channels on the data acquisition card.

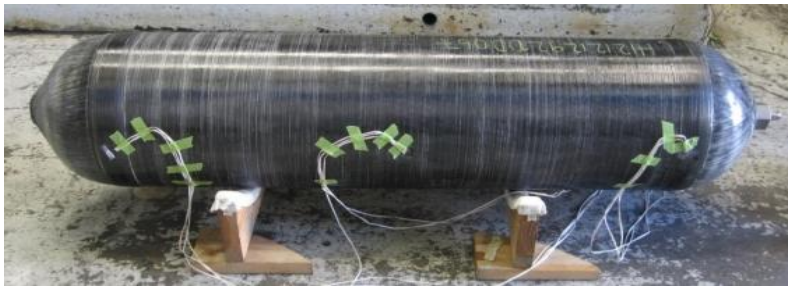

Figure 40. Vessel 13 with strain gages attached

To measure with ARAMIS, multiple pressurizations were performed on the vessel. A total of nine pressurizations were necessary because of measuring strains at different locations to cover the entire vessel – two times on the forward dome, five times on the aft dome and two times on the cylinder. The emphasis was on the aft dome because of previous experience with repeated burst at this location. Figure 41 illustrates the ARAMIS setup.

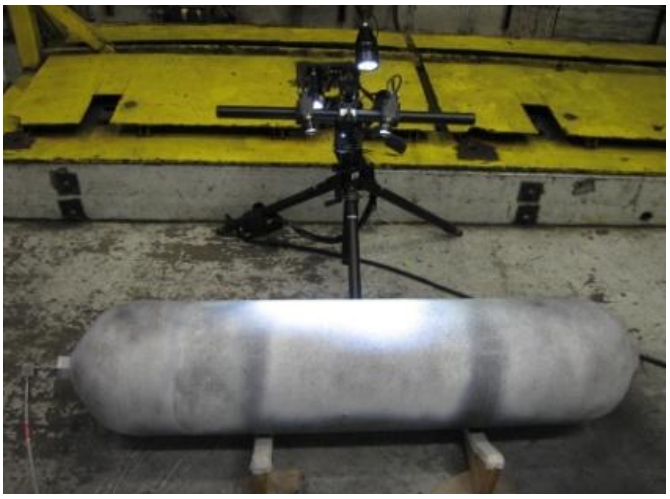

Figure 41. Vessel 13 measured with ARAMIS

After the first three pressurizations, five out of eight strain gages detached from the vessel. Fortunately the strain gage that was most interested – hoop strain at the transition between the cylinder section and aft dome – survived through all pressure cycles.

Strain gage measurements show the value is approximately 5,000 micro strain for hoop strain at the transition between the cylinder section and aft dome, while ARAMIS measures hoop strain of 4,000 – 5,000 micro strain at the same location (see Figure 42). This result shows that ARAMIS is sufficiently accurate that its measurements can be used to analyze the design and help verify the strain calculations from mWind.

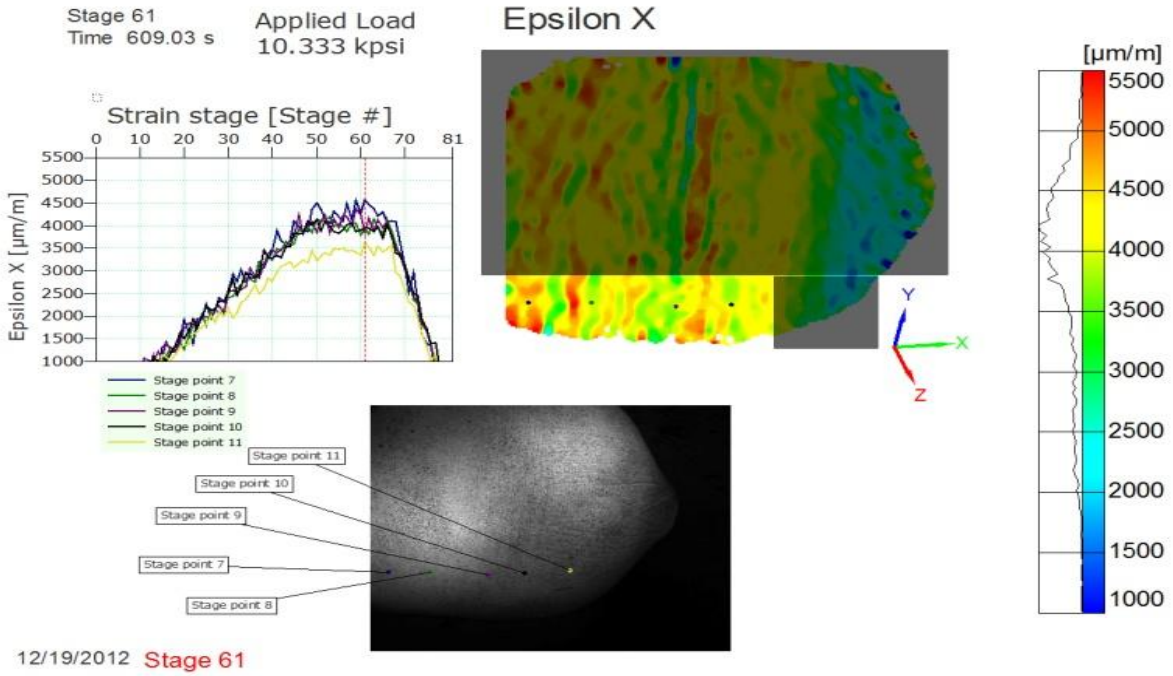

Figure 42. ARAMIS results of Vessel 13 by Boeing

3.3.9.2 Correlation between ARAMIS and mWind

The displacements of four points on the aft dome surface (Figure 43) were measured and compared to the results of the FEA results of Vessel 13 with the correct dome end buildup. Figure 44 shows a plot of the measured axial displacements at the four points and the predicted axial displacements. These results show a good correlation between the displacements except at the aft boss area. Two factors may affect the measurements at the aft boss: 1) The voids affected the stiffness of the material in this area and caused a larger discrepancy between the measured and predicted values and 2) the dome curvature affected the visual view of the optical measurement tool and obscured the measurement.

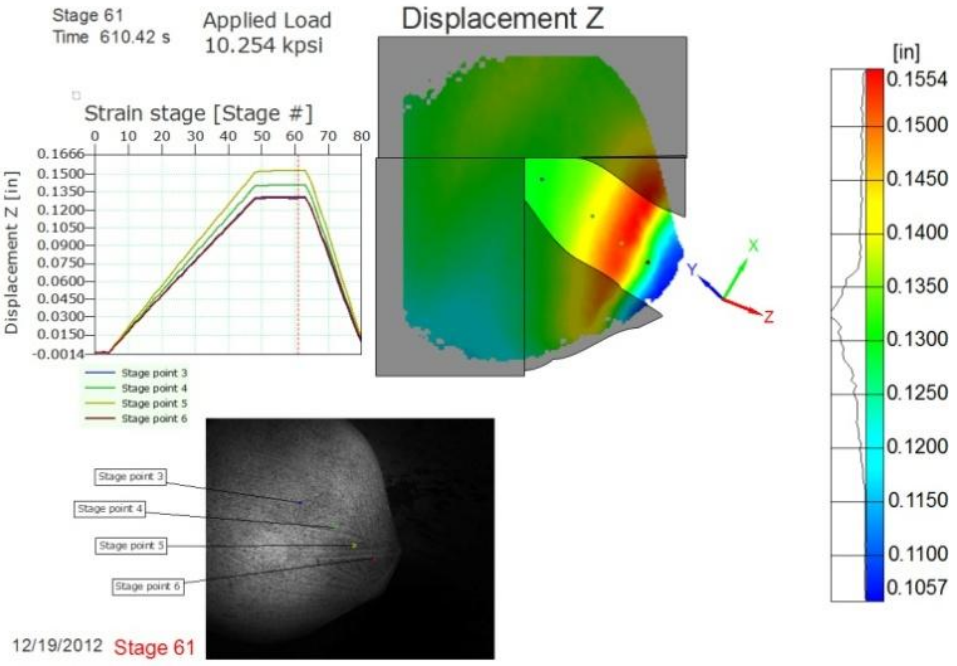

Figure 43. Optical displacement measurement with ARAMIS on Vessel 13 aft dome by Boeing

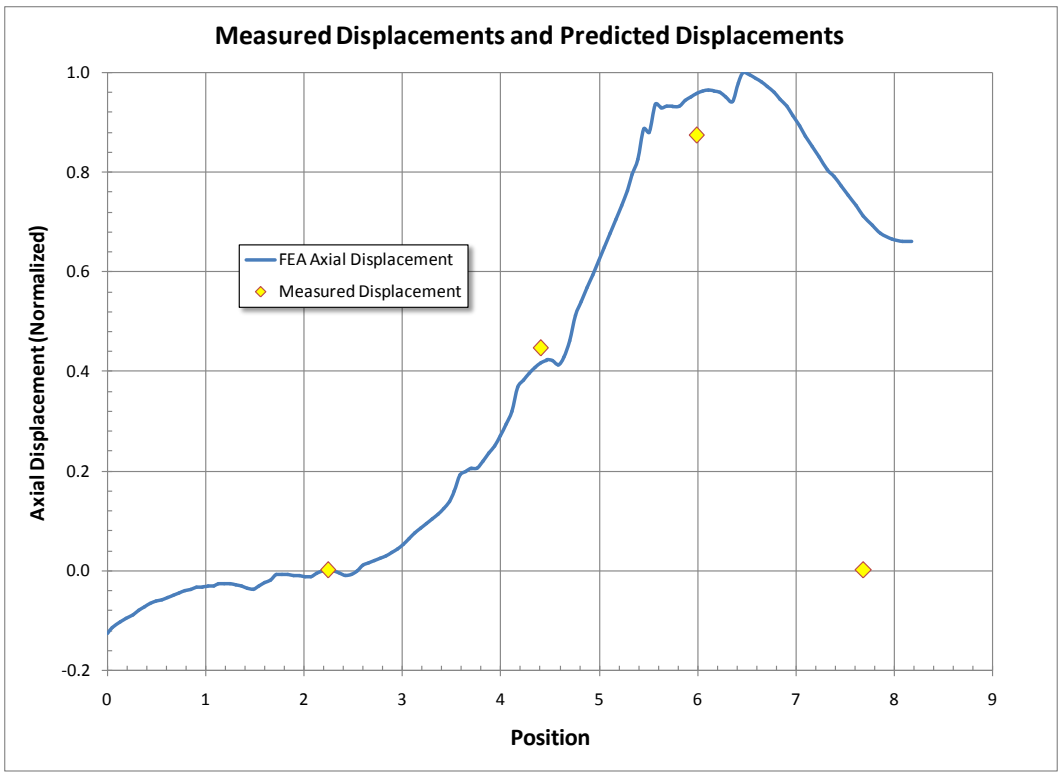

Figure 44. Vessel 13 aft dome measured and predicted displacements

Figure 45 shows the measured X or hoop strains obtained from the displacement measurements. Figure 46 shows the measured Y or axial strains. Figure 47 shows the hoop and axial strains predicted by the FEA model of Vessel 13. Again there is good correlation in the upper portion of the dome section. The predicted and measured strains tend to diverge near the polar opening part of the dome.

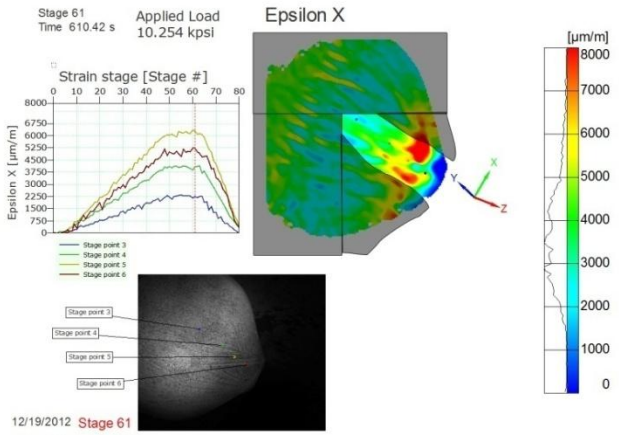

Figure 45. Measured X (hoop) strains

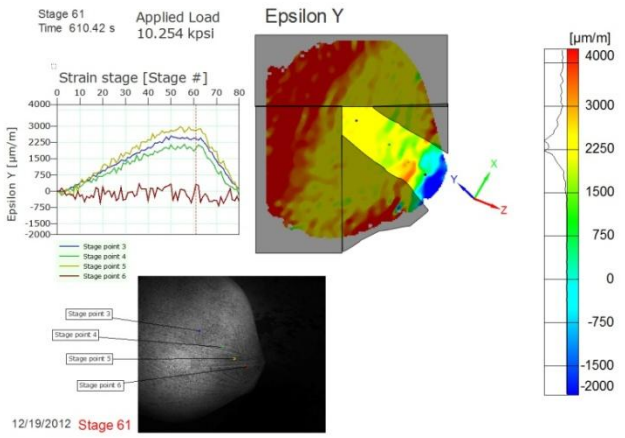

Figure 46. Measured Y (axial) strains

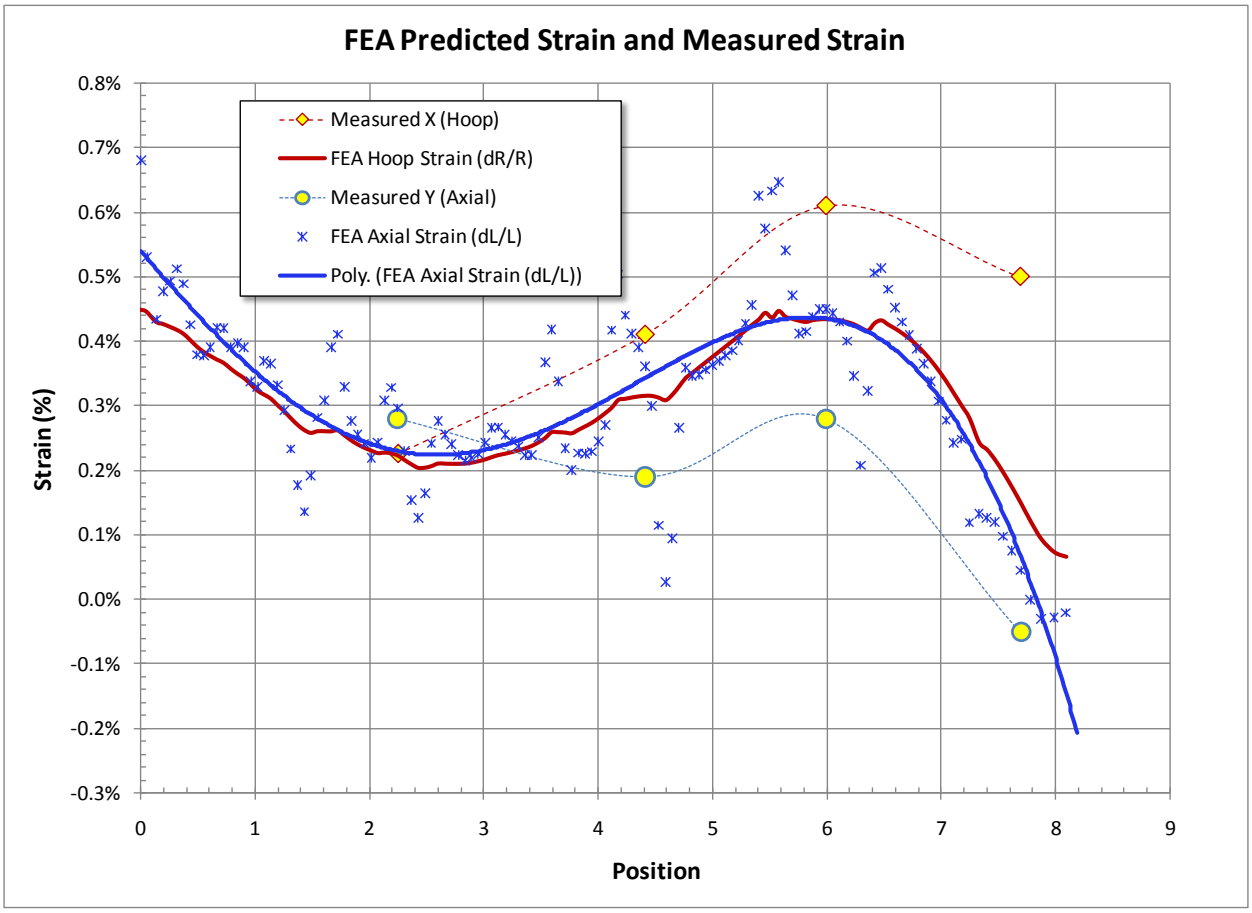

Figure 47. Predicted and measured X (hoop) and Y (axial) strains on Vessel 13

These results show that the FEA models provide a good prediction of the actual displacements and stress/strain conditions in a composite pressure vessel. Bridging and voids add uncertainties to the polar region of the composite dome and reduce the reliability of the model in these areas. Finer modeling details of the polar area will increase the predictability of composite material in these areas.

The end caps are generally farther away for the polar region and do not have the bridging and voids seen in this area. Thus, mWind and ANSYS are adequate to design the composite transition region where both FW and AFP layers exist.

3.3.10 Second mWind Software Update

The CT scan measurements on Vessel 13 were used to assess and adjust the predicted material buildup of mWind at the polar bosses. Figure 48 shows the CT scan of the forward dome with the measured and predicted profiles.

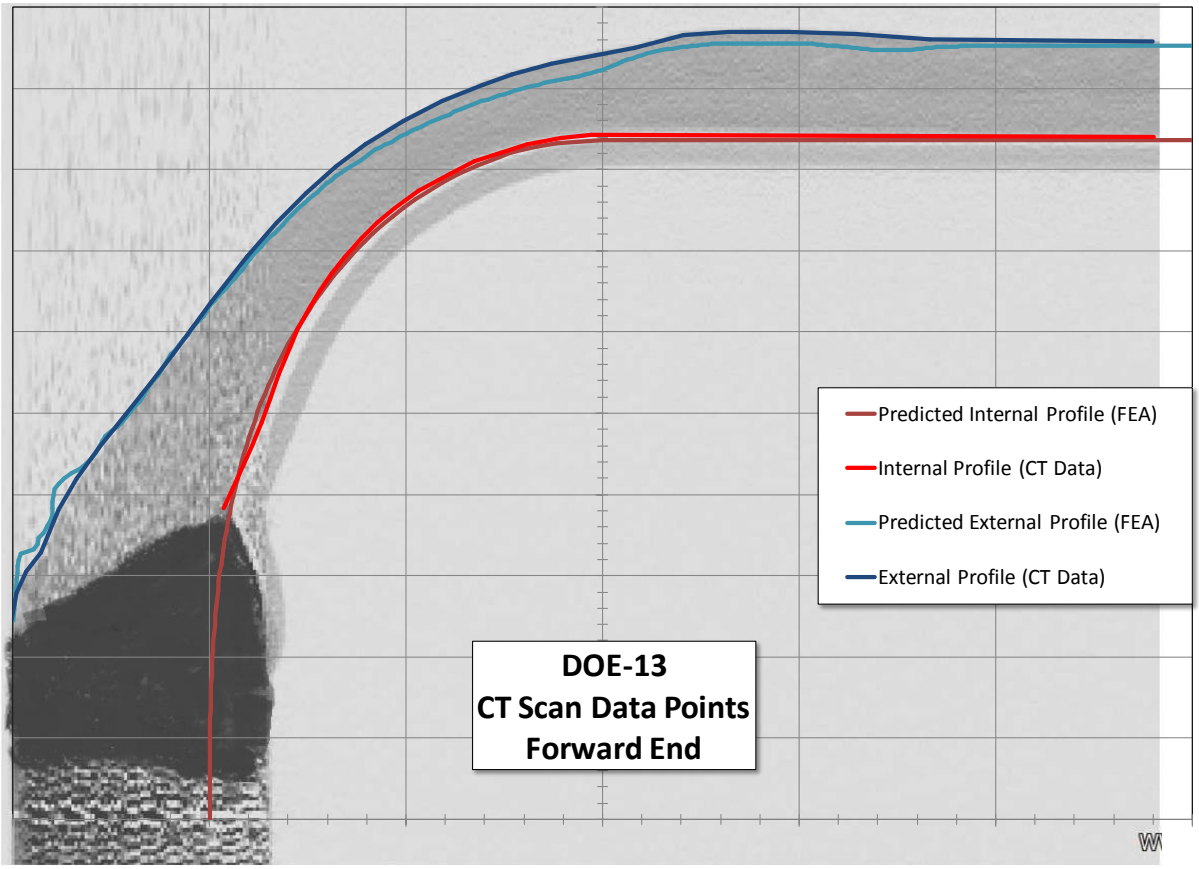

Figure 48. CT scan of Vessel 13 forward dome with predicted and measured profiles

The prediction of the material buildup in the forward dome is very close to the actual measured profile. Therefore, no modification to the buildup prediction was done to the forward dome. Figure 49 shows the aft dome buildup prediction and the actual measured profile obtained from the CT scans. This shows that the mWind prediction overestimates the actual thickness from filament winding. mWind has several variables to adjust the dome buildup, and these variables were adjusted to better fit the actual buildup.

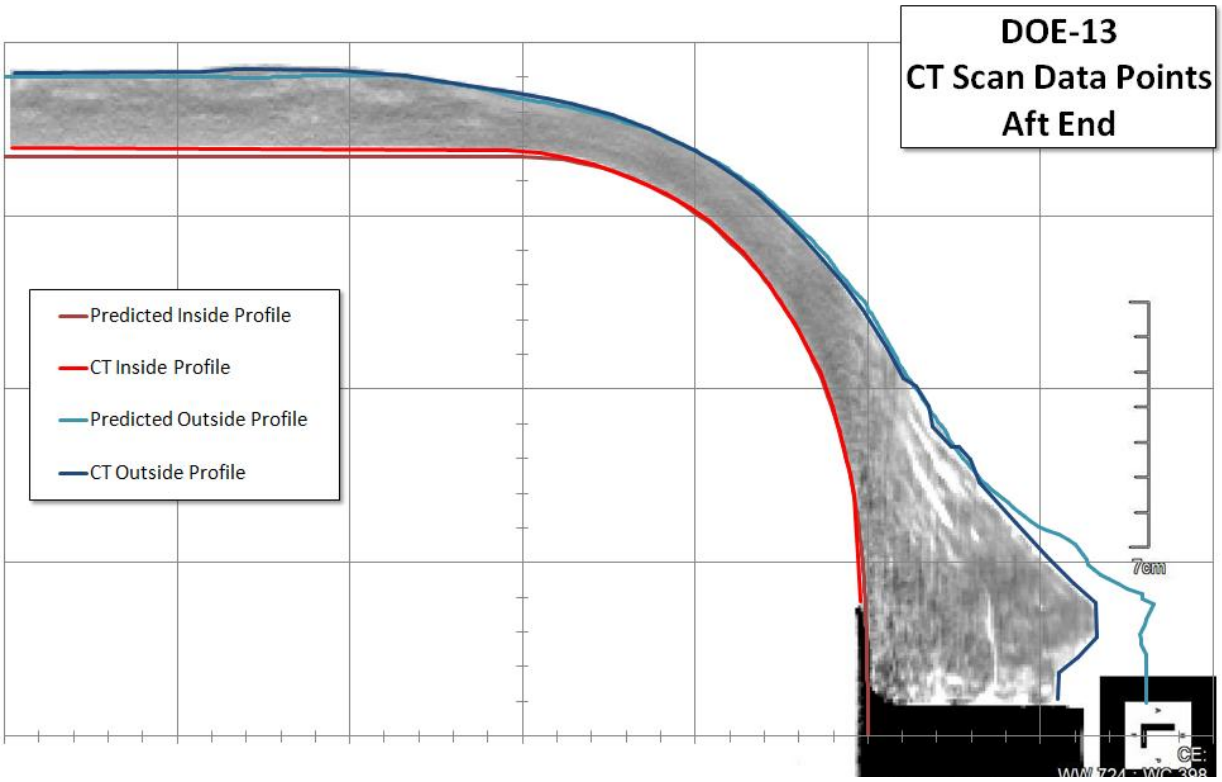

Figure 49. CT scan of Vessel 13 aft dome with predicted and measured profiles

The FEA model was re-run with the corrected buildup in the aft dome and compared to the design stresses without the corrected dome buildup. Figure 50 shows a plot of the aft dome fiber strains without the aft dome buildup correction factors, while Figure 51 shows the aft dome fiber strains with the corrected dome buildup factors. The fiber strains increase near the polar opening of the aft dome with the corrected buildup factors versus the model without the corrected buildup factors.

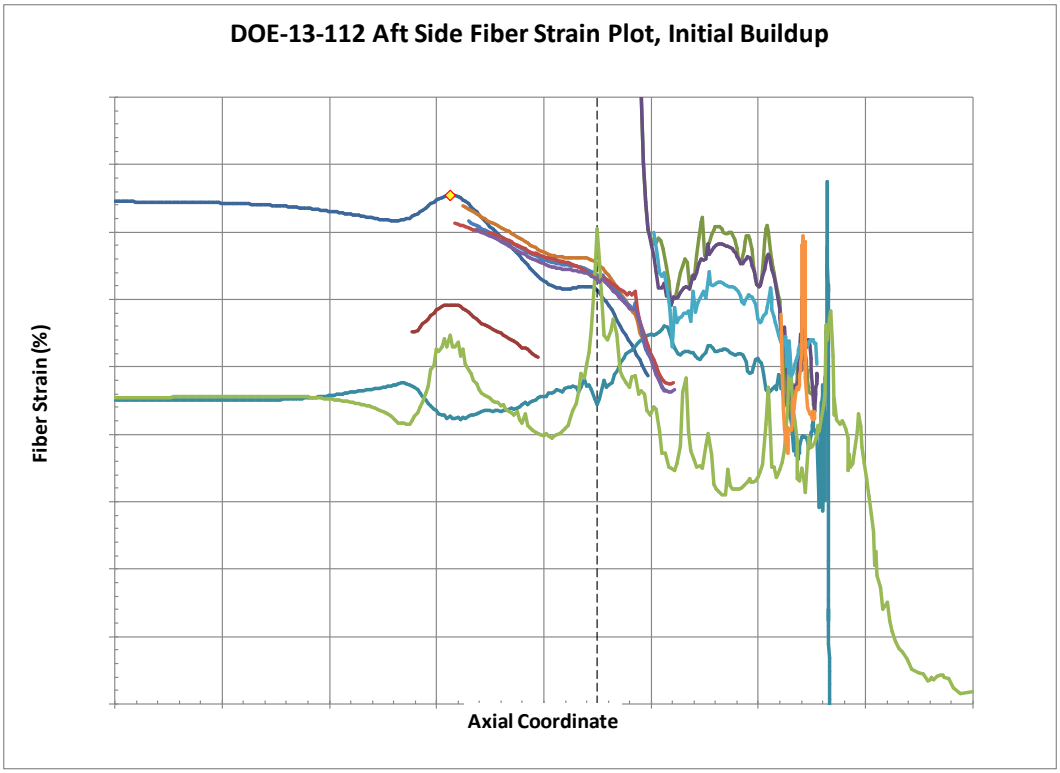

Figure 50. Aft dome fiber strain without corrected dome buildup

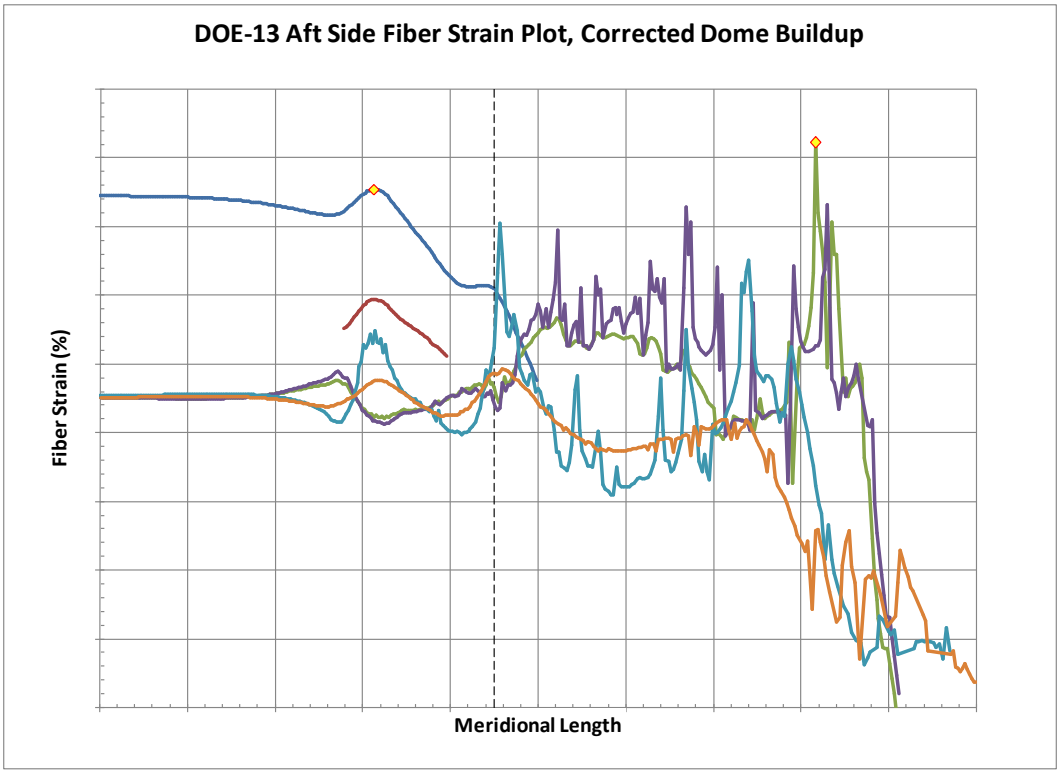

Figure 51. Aft dome fiber strain with corrected dome buildup

Figure 52 shows the hoop strain contour plot of the FEA model without the corrected buildup factors in the aft end. The displacements are magnified by 20 times to understand the areas of bending. Figure 53 shows the aft dome finite element model hoop strains with corrected dome buildup factor. Again the displacements have been magnified by 20 times.

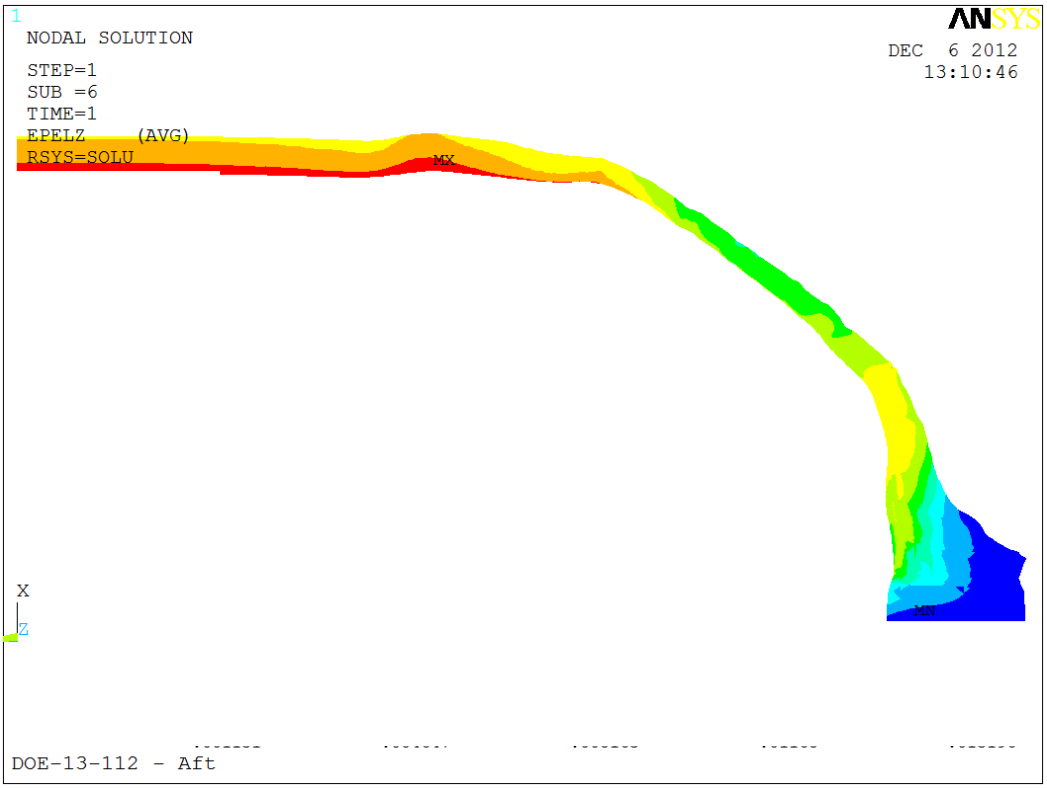

Figure 52. Aft end hoop strains on FEA without corrected dome buildup

Figure 53. Aft end hoop strain on FEA with corrected dome buildup

There is not a large difference between the two results. Both models do not account for the voids seen in the aft dome polar opening area. These voids greatly reduce the strength of the composite in this area.

3.3.11 Vessel 14

Many iterations of the composite layup design were completed for Vessel 14. The main focus during the design of Vessel 14 was to reduce the buildup in the aft dome to eliminate the voids and bridging issues seen on Vessel 13. The stresses and strains in other areas of the dome increased as layers were reduced in the polar opening. This caused Vessel 14 design to be significantly different than that of Vessel 13. A significant reduction of layers was accomplished with the latest design. Table 2. Design summary of Vessels 13 and 14 lists the design summary and differences between Vessels 13 and 14. The major difference is the calculated weight reduction of 5.6 kg (12.3 lbs).

Table 2. Design summary of Vessels 13 and 14

Vessel 13	Vessel 14

• 19 layers for end caps
• 42 filament wound layers
• 3 extra hoop layers at the transition
• Turnaround thickness:
  ○ Forward: 2.0” (50.8mm)
  ○ Aft: 2.25” (57.2mm)
• Weight: baseline
	• 14 layers for end caps
	• 38 filament wound layers
	• No extra layers in the transition
	• Turnaround thickness:
	  ○ Forward: 1.58” (40.1mm)
	  ○ Aft: 1.57” (39.9mm)
	• Weight: -12.3 lbs (5.6 kg)

Figure 54 and Figure 55 show the fiber strains in the forward and aft domes of Vessel 14, respectively. These plots show that the maximum fiber strain is in the hoop section without any spikes in the helical layers in the dome section.

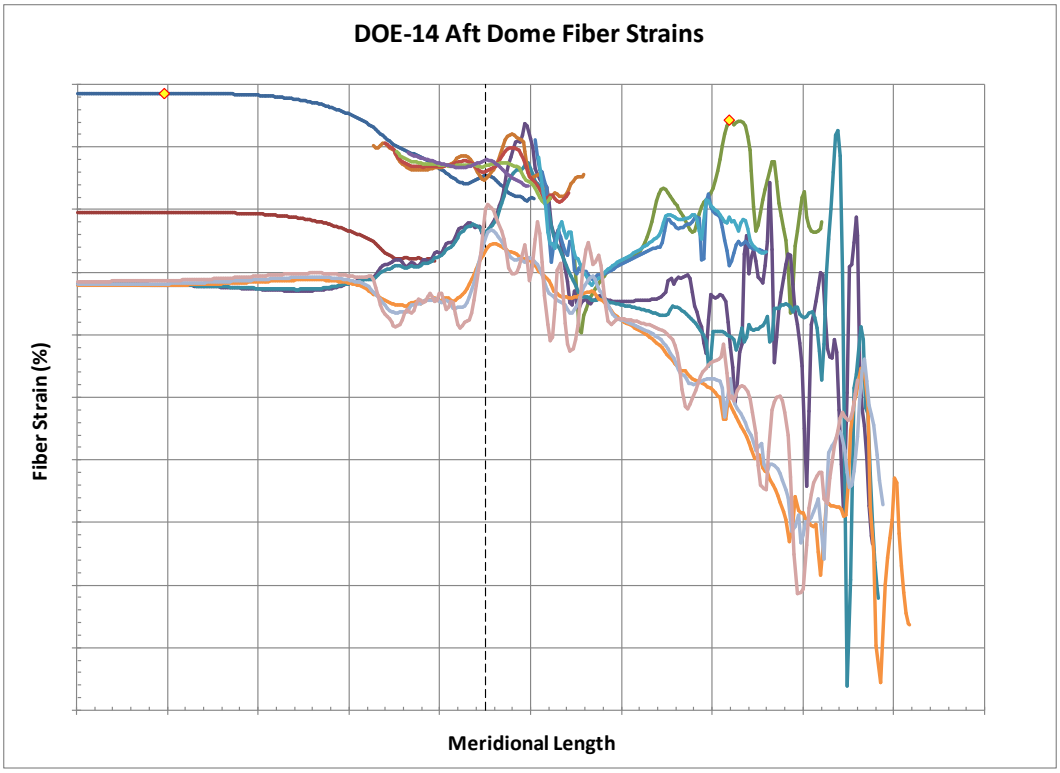

Figure 54. Vessel 14 aft dome fiber strains

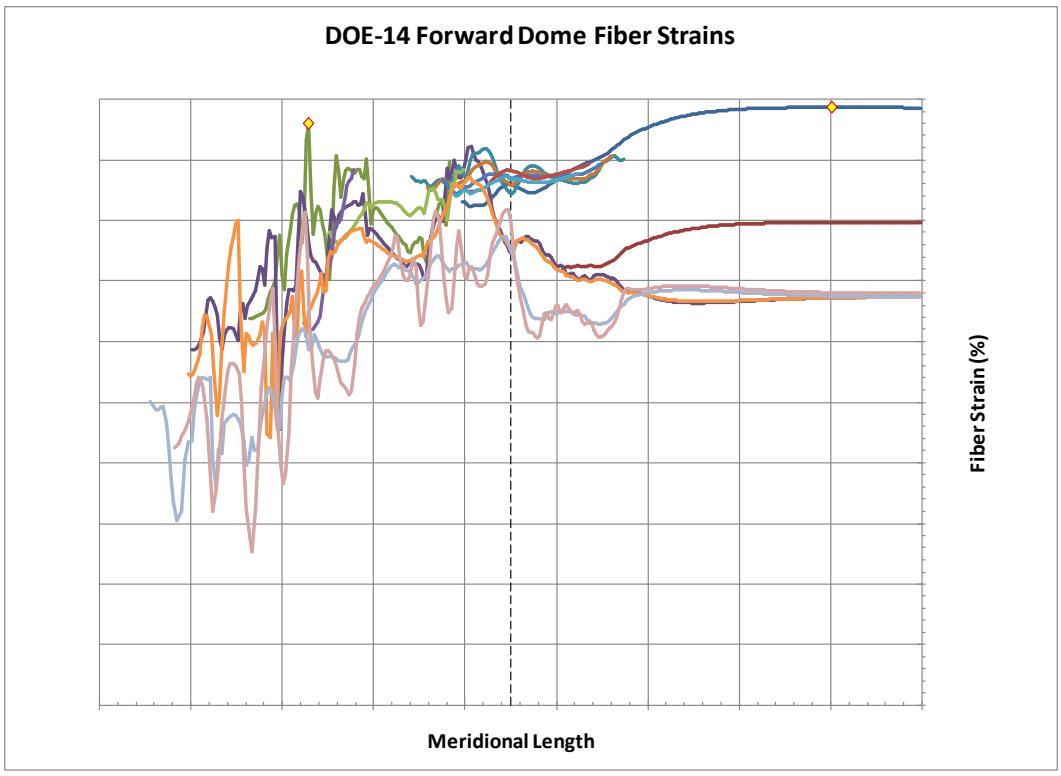

Figure 55. Vessel 14 forward dome fiber strains

During the build, when a partial helical layer was applied on the liner to pull the dome caps tight onto the liner ends, fiber bridging was observed across two different layers of the aft end cap as shown in Figure 56. Upon removing the partial helical, chopped fiber mixed with resin was used to fill the air gap as shown in Figure 57.

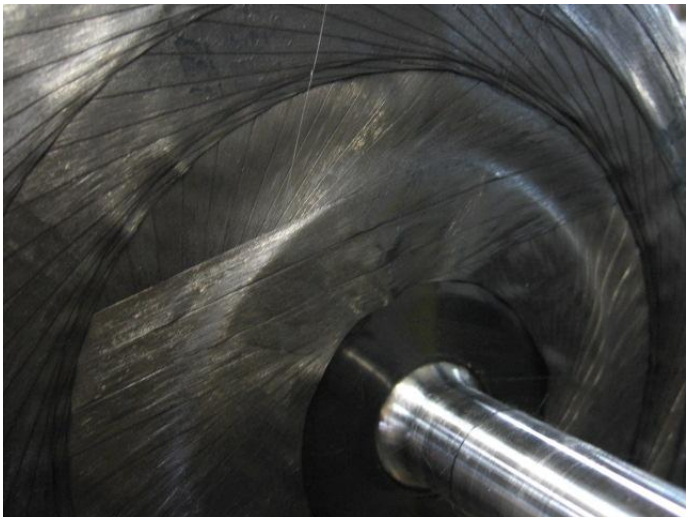

Figure 56. Bridging was observed after a partial helical layer was applied to pull the end caps tight onto the liner

Figure 57. Chopped fiber was used to fill the dip between two end cap layers

As the partial helical was re-applied onto the liner, slight amount of wrinkles was observed on the aft end cap. Instead of winding a partial helical, a complete helical layer was wound onto the vessel, with the expectation the helical pattern would be able to flatten out the slight wrinkles. At the same time, a heat gun was used to soften the end cap fiber to make it more pliable. However, the complete helical actually worsened the situation. The fiber tension eventually "collected" all the small wrinkles to form two larger wrinkles. This most likely was caused by a small difference in size of the fiber placement tooling and the liner geometry, thus resulting in a gap between the liner and the end cap. If the full helical was not wound at this time, these wrinkles would have formed on the vessel as the first helical layer is wound per design. Since this full helical was never in the design before the hoop layers were wound, it was removed before winding the vessel per design.

Day 1 of winding concluded with all the hoop layers applied to bring the cylinder section even with the end caps. In addition, the next helical layer was also applied. The composite was allowed to cure at room temperature overnight while rotating on the winding machine. The wrinkles on the aft dome were then sufficiently solid to allow smoothing of the high spots by filing. Figure 58 shows the result after filing down the raised spots. The size of wrinkle was kept to a minimal this way without affecting the next filament wound layers. The rest of the patterns were wound over the next two days.

Figure 58. Ridge formed on the filament winding layer was filed away to avoid bridging for subsequent fiber layers

Burst test was performed after the vessel was cured. It ruptured on the aft end at 20,499 psi (141.3 MPa), achieving 90% of the burst requirement. A high speed camera was again used to identify the burst location. The video showed the rupture initiated from the dome area, which led to believe the failure was caused by the dip between AFP layers on the aft end cap. Although chopped fiber was used as filler to avoid filament wound fiber from bridging across the high spots, the amount of voids in the filler could not be discounted.

3.3.12 Vessels 15 and 16 Build

Due to program timing, the project moved forward with the same end cap designs as Vessel 14. Instead of using chopped fiber as filler on the aft end caps, rings of various sizes were cut from carbon fiber woven fabric to fill the dip between the two AFP layers. Boeing delivered one of the aft end caps with fabric rings installed. The other had the rings separated per request, so that CMM measurements could be taken for the end cap profile to fine tune the fiber buildup calculations in the mWind software.

Upon installing the aft end cap and fabric rings on the liner, a very small dip still existed. However, only a small amount of chopped fiber was needed as filler, significantly reducing the amount of voids in the composite. From the CT scan results, no voids were observed at the locations where chopped fiber was used on both vessels. One of the scans is shown in Figure 59.

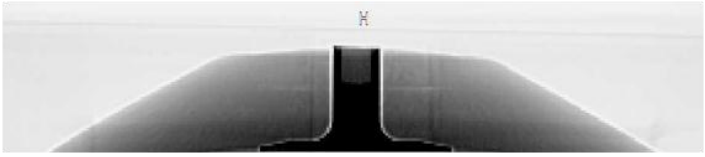

Figure 59 CT scan did not reveal any voids where chopped fiber was used

Since identical end cap designs to Vessel 14 were used, it was not necessary to develop winding patterns for these vessels. Further, to manufacture vessels at a faster pace for testing, two vessels

were built at the same time, utilizing two of the three spindles on the winding machine. One was designated for burst test, and one was planned for ambient cycle test.

On Vessel 8 that was built for cycle test in 2011, a release film was missed to be installed between the liner and composite to prevent mechanical bonding from happening due to the higher curing temperature of the Boeing resin system. That particular vessel did not pass the minimum cycle count of 15,000 due to excessive strain at the bonded location. For complete description of applying this release film on the vessels for the latest tests, please refer to the Boeing section 4.3.9 below under "Lessons Learned during Placement of Released Film on Liner".

As seen in Figure 60, the bottom vessel had the release film while the top vessel was a bare liner. With the convention to serialize vessels from the bottom up on the winding machine, Vessel 15 was sent to cycle test, and Vessel 16 was sent to burst test.

Figure 60. Released film installed for the bottom vessel planned for cycle test

3.3.12.1 Burst Test

A high speed camera was again utilized to capture the burst mode. Based on previous experience, the camera focused on the aft end in anticipation of a dome failure. The vessel achieved a burst pressure of 23,572 psi (162.5 MPa), exceeding the minimum burst requirement by more than 3%. The high speed video did not show the failure location on the aft end; the vessel simply traveled across the frame. Upon examining the vessel after burst test, it was determined that the burst location was mid cylinder, as shown in Figure 61. At the same time, the released film was discovered in the burst pit. The vessels had been serialized incorrectly and swapped as a result. The incorrectly serialized vessel weight was 62 kg, which translated to a 18.4% weight savings from the baseline vessel that weighted 76 kg. This vessel was 3.9 kg heavier than that of Vessel 7, which passed burst test previously. However, Vessel 7 only exceeded the minimum requirement by merely 0.4%. The vessel originally built for burst test was put in for the cycle test, hoping any bonding would not cause detrimental effects on the vessel during cycle testing.

Figure 61. Vessel 16 burst mode was mid cylinder per design

3.3.12.2 Ambient Cycle Test

The vessel originally built for burst test achieved 15,000 pressure cycles between 10% and 125% of service pressure without developing a leak or rupture. Although the vessel passed the cycle test, it is still recommended to apply the release film on vessels that will go through pressure cycle in the remaining tests.

3.3.13 Comparison of Actual End Caps to mWind Model Predictions

The geometry of end caps modeled by mWind was compared to measurements of actual end caps using a CMM. The comparison was done graphically using XY coordinate data from the CMM and the FEA model display plot. Figure 62 shows the forward end cap measurements vs. mWind FEA model, and Figure 63 shows the comparison on the aft end cap.

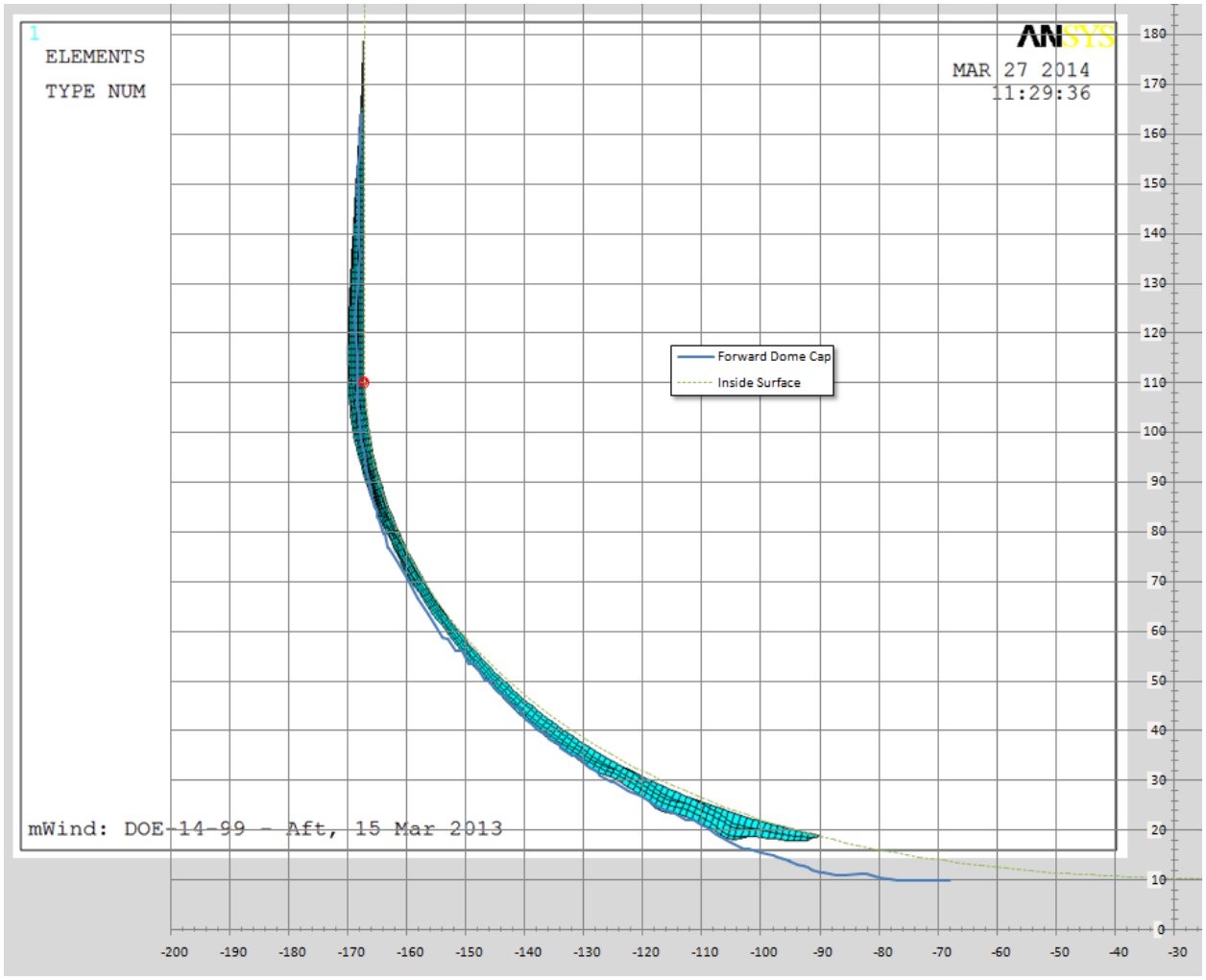

Figure 62. Forward end cap comparison between CMM and mWind model

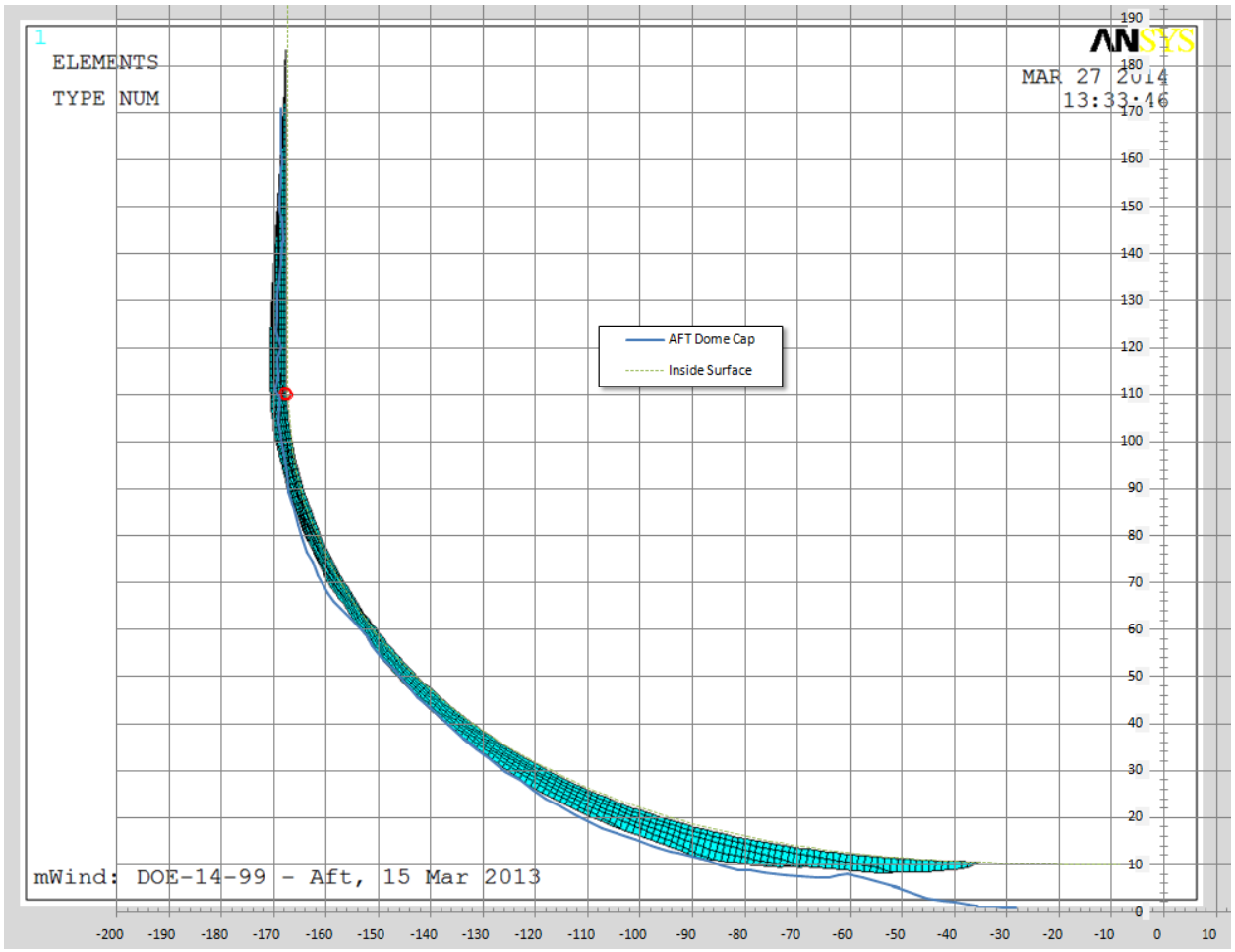

Figure 63. Aft end cap comparison between CMM and mWind model

These plots show good correlation between the actual measurements and mWind model predictions for most of the model. The mWind model does not match the actual buildup and shape at the polar boss openings. mWind uses a routine to smoothly taper the layer at the turn around points. The taper subroutine is not following the actual geometry and will be updated and modified to better model the actual geometry in the future.

One area where the model geometry at the end of a layer can be improved is detection of bridging and gaps. This would require a model assessment and subroutines after the model has been built to look for bridges and gaps and adjust the model in these locations.

mWind is predicting the composite layup throughout the majority of the model with sufficient accuracy to design a composite pressure vessel with intermittent or localized layers of material. The turnaround points near the polar bosses still needs some extra processing to detect and model bridging and gaps in the future.

3.3.14 Vessels 17 and 18 Build

Two additional sets of end caps, identical to the design of Vessel 15, were manufactured by Boeing for building Vessels 17 and 18. Both vessels were built at the same time on a winding machine. One was scheduled for impact damage test, and the other for accelerated stress rupture test.

3.3.14.1 Vessel 17 Accelerated Stress Rupture Test

The purpose of the accelerated stress rupture test was to evaluate the effectiveness of the resin systems to transfer load between AFP and FW layers and determine if there was a resin creep issue with discontinuous winding. The test was performed at 125% of service pressure (12,691 psi or 87.5 MPa) at 85°C (185°F) for 1,000 hours. 85°C is the upper design limit temperature. The vessel was kept inside an environmental chamber, which was then placed inside a pit to protect personnel from injuries in case of rupture during test. As part of the test, burst test was performed after the 1,000-hour hold to evaluate the vessel's residual strength. The minimum requirement is 85% of the nominal working pressure times the burst pressure ratio (85% x 70 MPa x 2.25), which is equivalent to 19,421 psi (133.9 MPa).

The vessel successfully passed the accelerated stress rupture test. The burst pressure was 22,191 psi (153.0 MPa), exceeding the minimum requirement by more than 14%. When compared with the virgin burst result (162.5 MPa or 23,572 psi) of Vessel 16, there was a 5.8% reduction in burst pressure.

The results showed the vessel design was capable of resisting creep degradation at the test conditions, even 1) two different resin systems (Boeing resin for AFP and Quantum resin for FW) were used on the hybrid design and 2) the AFP resin was cured at a lower temperature but longer duration due to liner processing temperature limitation.

3.3.14.2 Vessel 18 Foam Dome Installation

The foam domes and foam rings designed for the baseline (all FW) vessel were used on this particular vessel to prepare for the impact damage test. Since the hybrid design reduced the vessel diameter significantly, the foam domes had to be modified to fit onto the vessel. Foam dome material was removed to fit them over the smaller composite domes, as shown in Figure 64. In addition, the inside curvatures of the two halves had to be forced to conform to the composite dome profile. However, a perfect conformance was not possible due to the foam dome stiffness. Some air gaps were present as a result. In addition to the less-than-ideal foam domes, the composite domes were much thinner as a result of the hybrid design. This would further affect the outcome of the impact damage test.

Figure 64. The foam dome was cut to remove material to fit onto composite dome

3.3.14.3 Vessel 18 Impact Damage Test

The purpose of the impact damage test was to evaluate the vessel's resistance to impact damage even with an 18.7% weight reduction of composite. The vessel was tested in the following sequence:

1. Drop once from a horizontal position with the lowest position 1.83 m (72.0 in) above the ground.
2. Drop once on each end of the vessel from a vertical position with a potential energy of 488 J, but in no case shall the lowest end be more than 1.83 m above the ground. With this hybrid design, the drop height was 0.74 m (29.1 in).
3. Incline drop test with the valve end of the vessel positioned downward at a 45° angle with its center of gravity 1.83 m above the ground.

After the series of impacts, the vessel was then hydrostatically cycled between ≤ 2.0 MPa (290 psi) and ≥ 87.5 MPa (12,691 psi) for 15,000 times. Within the first 3,000 cycles, the vessel shall not rupture or leak. The vessel may leak thereafter during the remaining of pressure cycles.

Upon dropping the vessel, deformations and cracks were observed on the foam domes, as shown in Figure 65 and Figure 66. They were most likely caused by the air gap between foam domes and composite. This was inevitable when complete conformance was not achievable.

Figure 65. Foam dome deformation after impact

Figure 66. Foam dome cracked after impact

The vessel leaked after completing 11,658 pressure cycles, exceeding the requirement of 3,000 cycles. Upon cutting the forward composite dome section off the vessel, it was found that the liner exhibited fatigue cracks at the tip of the boss flange.

This observation revealed there was a mismatch of shape between the liner/boss and the AFP end cap resulting in a gap between the liner and composite. The vessel met the drop requirement, but there is additional work necessary in the future to improve fitment between the liner and AFP end caps.

3.3.15 Vessel 19

This final vessel was built for the extreme temperature pressure cycle test. The purpose of this test was to evaluate the compatibility of two resin systems to transfer load between AFP and FW layers effectively.

The test procedure involves pressure cycling the vessel hydrostatically between ≤ 2.0 MPa (290 psi) and ≥ 87.5 MPa (12,691 psi) for 7,500 times at both ≥ 85°C and ≤ -40°C. At 85°C the relative humidity is maintained at or above 95%. The vessel is conditioned for 48 hours before cycle test began. After completing the cycle test without evidence of composite degradation or tank leakage/rupture, a burst test is conducted to evaluate the vessel's residual strength. Minimum burst requirement is at least 85% of the nominal working pressure times the burst pressure ratio (85% x 70 MPa x 2.25), which is equivalent to 19,421 psi (133.9 MPa).

After conditioning the vessel for 48 hours at 85°C, the vessel completed 3,679 fill cycles before rupturing on the aft end.

The pre-mature rupture showed the load transfer mechanism could have been compromised with higher operating temperature and pressure cycling. With only a few inches of AFP and FW overlapping on both ends of the vessel for load transfer, this location could have been weaken under cycling. Due to the rupture, the test at -40°C was not able to be performed.

3.3.16 Vessel Weights with Latest Design

The latest vessels for technology demonstration were all based on Vessel 15 design. The average weights of forward and aft end caps are 0.82 kg (1.8 lb) and 1.04 kg (2.3 lb), respectively. The average FW composite weight is 49.5 kg (109.1 lb). Summary of each tank is shown in Table 3. PNNL revised the cost model with this latest composite usage information. The model details are shown under the PNNL reporting section.

Table 3. Tank results summary

Vessel #	Weight (kg)	Burst Pressure		Burst Location	Notes
		(psi)	(MPa)		
0	76	-	-	-	Baseline
Phase I					
1	64.9	23,771	164	Mid cylinder	Helical fiber rupture
2	Not Available	18,666	129	Aft	
Phase II					
3	67.1	21,658	149	Aft	
4	65.0	21,719	150	Aft	
5	54.4	20,500	141	Aft	
6	55.0	N/A	N/A	N/A	Same design as Vessel 5, Vessel cut for analysis
7	58.6	22,925	158	Mid cylinder and aft dome	Passed burst requirement
8	57.3	N/A	N/A	N/A	Cycle test, Cycled 13,500 times out of 15,000
Phase III					
9	59.6	22,083	152	Aft	With AF1, 2-day wind
10	59.4	22,388	154	Aft	Same design as Vessel 9, 1-day wind
11	59.6	20,026	138	Aft	Replaced some AF1 layers

					with baseline fiber
12	58.8	20,958	145	Aft	1st mWind design with AF1, fiber bridging observed
13	62.5	20,679	143	Aft	2nd mWind design without AF1, actual buildup different than model
14	59	20,499	141	Aft	3rd mWind design without AF1, bridging observed
15	62.0	N/A	N/A	N/A	Passed 15,000 cycles, same AFP caps as Vessel 14, fabric rings used
16	62.5	23,572	163	Mid	Built identically to Vessel 15, passed burst test
17	63	19,421	134	Aft	Built identically to Vessel 15, passed accelerated stress rupture test
18	59.5	N/A	N/A	N/A	Built identically to Vessel 15, passed drop test – leaked after 11,658 cycles
19	62.0	N/A	N/A	N/A	Built identically to Vessel 15, did not pass extreme temperature pressure cycle test – leaked after 3,679 cycles

4.0 Boeing Report

4.1 Phase I

The focus of Phase I was to develop a new tow head that works for the application of laying down fiber on pressure vessels. There were issues with the old design that made it unusable for this application.

4.1.1 AFP Machine Development – Six, Quarter-Inch-Tows Head

A new 6-tow head for quarter-inch tow (prepreg tape slit to a width of ¼-inch) was developed to achieve a tighter radius around both the forward and aft polar openings, as shown in Figure 67. This head (1) accurately tow-places with a minimal amount of tow wandering, (2) has individual cut/clamp/add mechanisms, and (3) makes the head more accessible for ease of maintenance. Issues with the old head design drove the upgrades and modifications to the new head development. These issues included downtime caused by frequent jamming and the time associated with clearing the jam, no individual cut mechanism for each tow, overall width of AFP head, and a need for better placement and guidance of each individual tow.

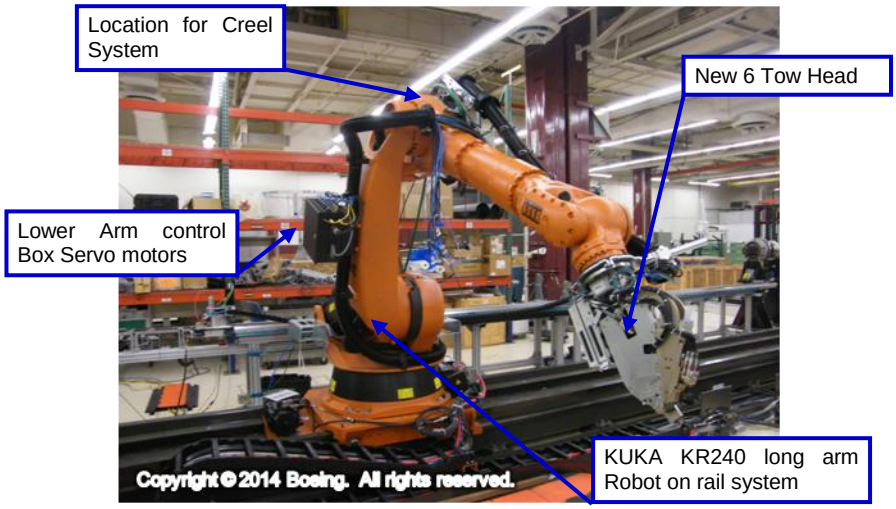

Figure 67. New 6-tow quarter-inch head design and features

The 6-tow quarter-inch head robotic cell can utilize a rail and a KUKA KR240 long arm system giving more control and flexibility during lay-up. The system is capable of adjusting its position up and down the rail to more easily lay-up on the pressure vessel tooling, as needed.

The new head design includes a reduction in total width by more than 0.5 inch, allowing for a minimum polar opening of less than 2.00 inches in diameter. The original head allowed for a minimum polar opening of 2.56 inches in diameter, giving an improvement of 0.56 inches. The head details are shown in Figure 68.

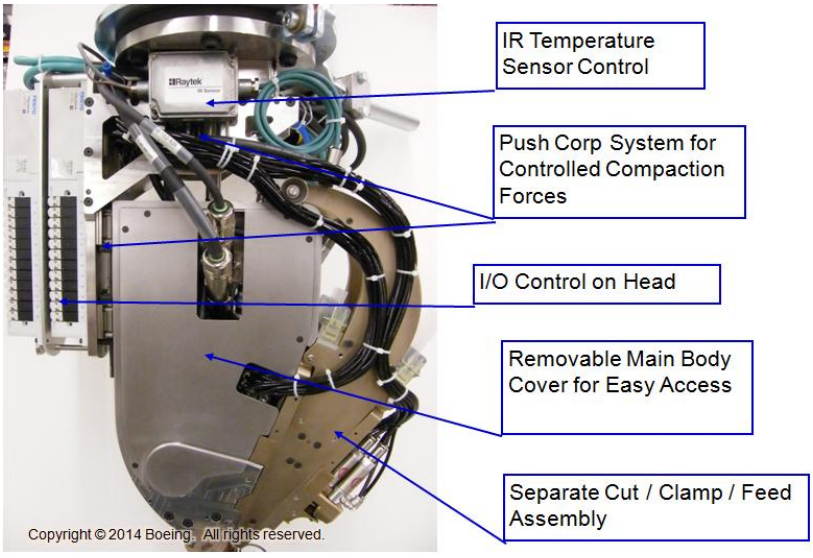

Figure 68. Details of AFP head design

Furthermore, the new head has incorporated individual cutters, reducing the crenulations or saw tooth from tow to tow. Reverse style cutters increase the cutter speed and add capability of allowing cutting on the fly. Cutters also have easy access to allow routine maintenance and cleaning to be performed with relative ease, requiring little downtime to complete.

A removable main body also allows ease of maintenance with better access to the guide plates and cut/clamp/feed mechanism for routine cleaning. Only two bolts are required to open both the upper and lower module for access to the tow. This feature allows for reduced downtime caused by material related issues that require opening the head to perform cleaning to clear the jam.

The new design incorporates a closed loop feedback system for the compaction system. This allows for a more consistent force to be applied when the head is in any orientation to the tool during lay-up.

A new infrared (IR) heater design, shown in Figure 69, was incorporated into the AFP head due to performance issues associated with the earlier hot-gas design. This solves these issues; (1) hot pockets around the compaction roller, (2) heated air in the cutter region causing the blade to buildup resin, (3) frequent cutter jams due to excessive heating in the cutter region unable to control heated area efficiently, (4) very noisy.

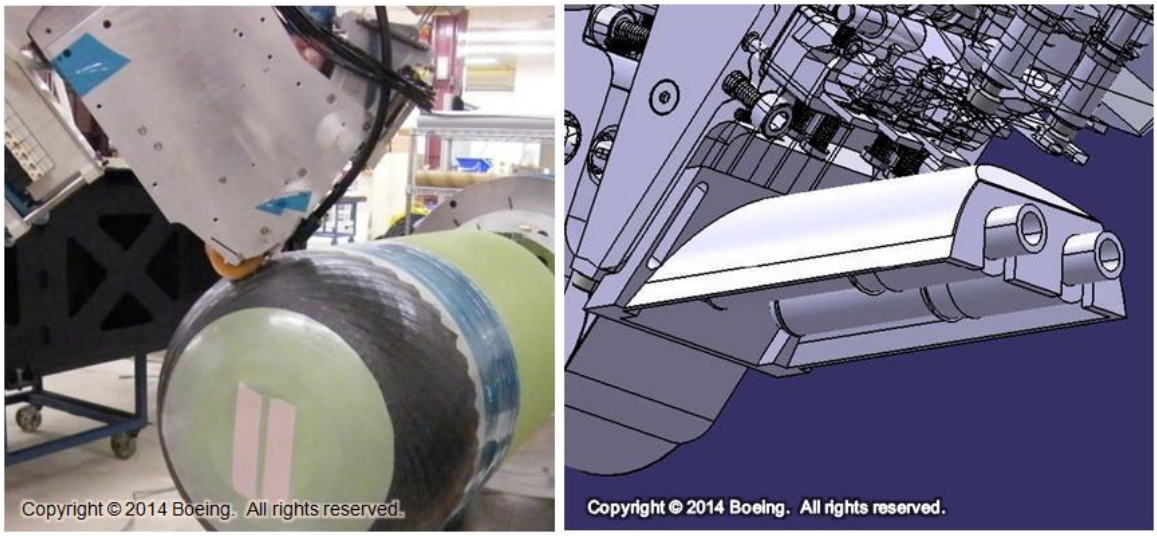

Figure 69. AFP operations (left) using new heater design (right)

The new IR heater system has increased the reliability and productivity of the system. The system has almost completely eliminated issues related to cutter jamming due to excessive heating of the cutter blade. The heated zone of the IR heater system is better controlled, allowing for a more efficient and effective system.

The AFP head robotic cell also incorporates a creel system with active tension control, shown in Figure 70. The active tension allows for a more controlled tow feeding system by (1) eliminating slack in the system, (2) having the ability to rewind excess tow during lay-up, (3) reducing the twists in tow caused by slack, (4) eliminating tow interference, and (5) producing better active control of tension. This system utilizes 6 individual servo motors attached to each spool chuck for active tension control. Each servo motor has a feedback loop that sends signals back for accurate count of tow velocity. A consistent drag is applied to each spool, and each spool is capable of rewinding excess tow during lay-up, eliminating slack related issues.

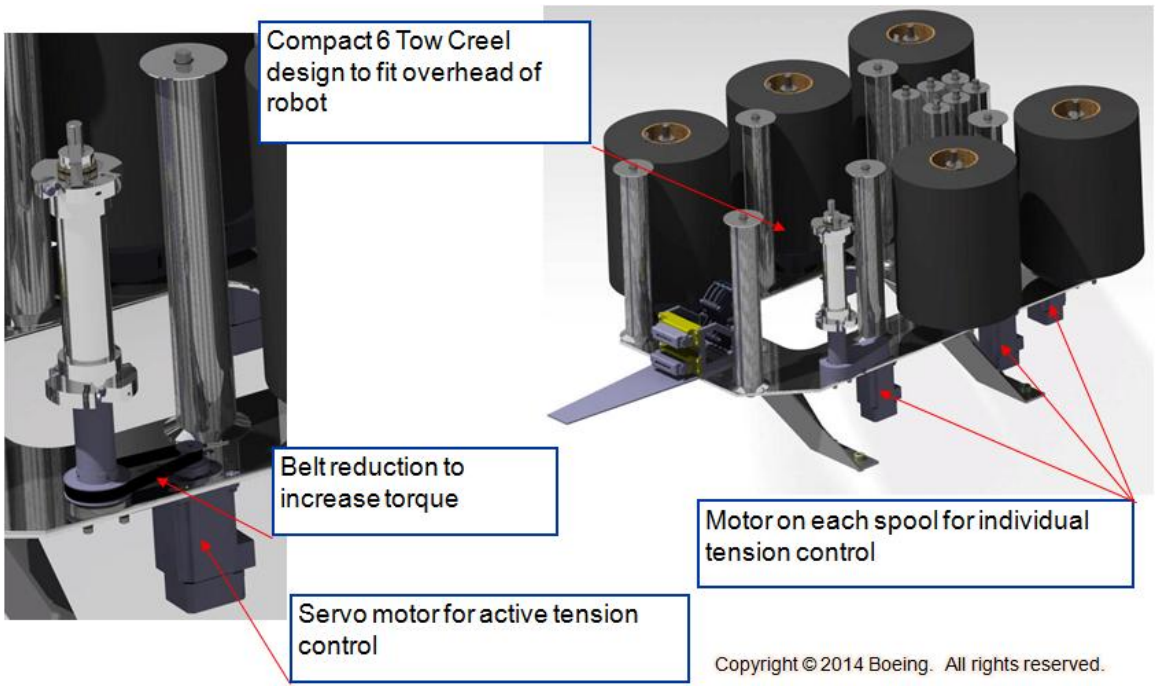

Figure 70. Creel system for AFP head

4.2 Phase II

Boeing integrated the new AFP head with the KUKA long arm robotic cell and performed calibration. In addition to laying down fiber using AFP on liner, tank or foam tool for building hybrid vessels, Boeing supported some of the post test composite analysis. The use of thermoformed shear protectors was also implemented to allow a better fit between the liner and AFP end caps.

4.2.1 Integration of the New 6-Tow, Quarter-Inch AFP Head

The new head was developed to meet the requirements of fiber placing material onto dome ends either as a separate layup on simplified tooling, on the vessel, or on the liner itself. The completed head was integrated into the AFP KUKA KR240 long arm robotic cell, whereby our first tests were conducted shortly after. Figure 71 illustrates the fully completed and integrated robotic cell. The integration included all instillation of components, plumbing, wiring of motors and heater system, and calibration of head unit.

Figure 71. New AFP cell fully integrated

The calibration test was conducted using a standard "T" test. The "T" test calibrated the cut and adds distances. It also dialed in the head alignment in order to have no overlaps or gaps and to assure that end-placement aligned with one another. Adding and cutting 6-inches of tow in one direction and then repeating this process in the opposite direction gives both the X and Y positions of the end-effector, as well as the cut and add placement for accurate alignment. This was then verified by crossing perpendicular to the original 6-inches of tow for accurate start and end placement. This was a critical step to determine actual robot end-effector positioning along with accurate tow placement during layup.

The integration also included kinematically linking between the robot and the head stock (rotation axis) that the foam tool was fixed to. This allows the translation and rotation between the motions of the robot and the foam tool to be linked to one another. Tests were conducted to make sure no slipping or misalignment was present in the layup that would be caused by the kinematics between the robot and the head stock.

4.2.2 Post-Test Analysis of Vessel 3

The forward end of Vessel 3 was received by Boeing in order to perform post test analysis. The primary objective was to use the vessel to determine how effective non-destructive techniques, such as ultrasound and CT scans, could be in evaluating the quality of future pressure vessels. Photomicrographs were prepared to further characterize the laminate.

Whereas the aft end of the vessel was where failure initiation occurred, the forward end also sustained considerable damage because of the vessel being propelled into the bunker wall. During the impact, the forward stainless steel boss was pushed into the vessel creating large-scale delamination and a broom-like effect (Figure 72). The analysis focused on both damaged and un-damage (not-shown) regions from the forward end of the vessel.

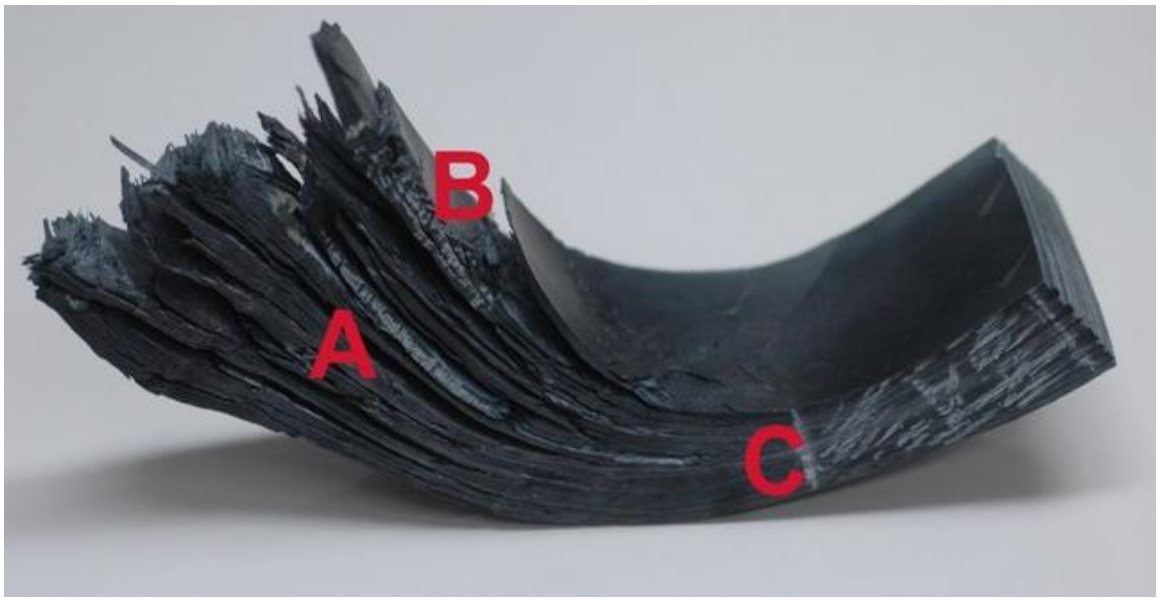

Figure 72. Section cut from the forward dome region of Vessel 3

Efforts to produce a meaningful ultrasonic scan of the undamaged areas were not successful. Methods of pulse-echo time of flight were used, since only one side of the structure would be available for inspection and due to the disbond between the liner and composite structure. The pressure vessel thickness, combined with the coarseness of the filament wound material attenuated (reduced) the sound to the point where a useful signal could not be obtained. Thus, it was concluded that ultrasonic methods are not effective in evaluating the quality of pressure vessels.

Efforts continued by exploring the use of a CT scan to evaluate quality. Key interest was in evaluating porosity and fiber waviness. Figure 73 reproduced one section from the CT scan results. Dark indications were probably porosity, as suggested by photomicrographs of adjacent regions, shown in Figure 74 and Figure 75. However, the dark indications could also be fiber rich areas or other anomalies. Further work was needed to determine which one was indeed the case. The scans were too coarse to determine the extent of any fiber waviness. Thus, the method provided useful information, but it was not effective in quantifying porosity or fiber waviness.

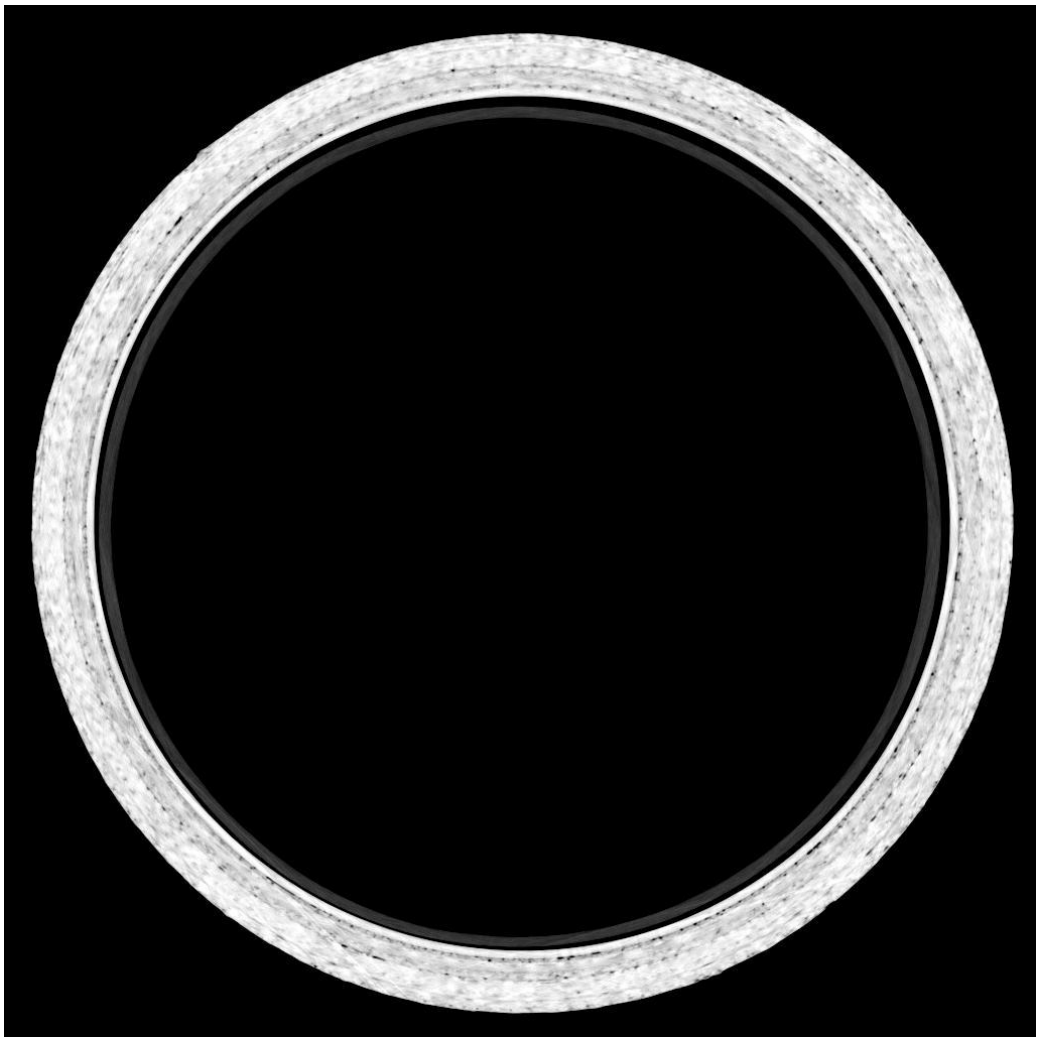

Figure 73. CT scan of Vessel 3 forward end

Figure 74. Polished cross-section photomicrograph showing tow-placed material in two regions near the top, and filament wound material elsewhere. The layup is in the proximity of region "C" in Figure 72 above.

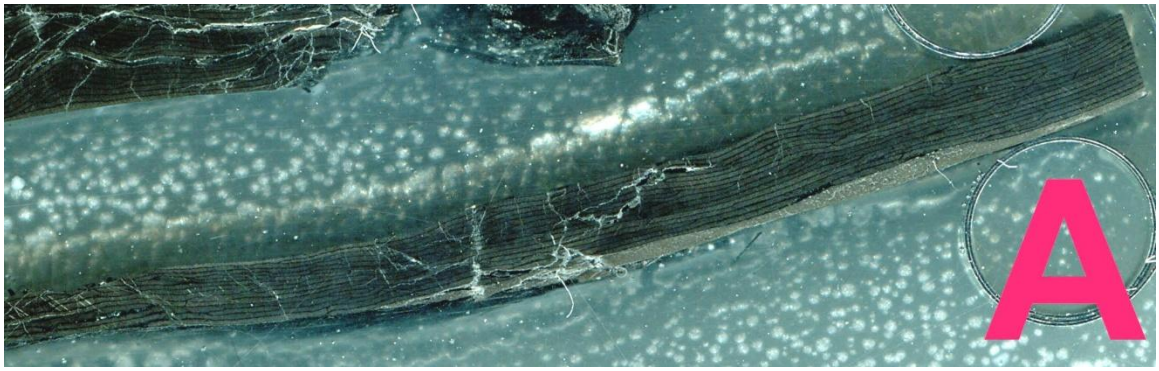

Figure 75. Photomicrograph of region "A" indicated in Figure 72. This particular region is from the second layer of tow-placed material extracted from the damaged area of the dome. Some fiber waviness is apparent.

The cross-section photomicrographs correspond to regions C and A (as indicated in Figure 72). In Figure 74, porosity was seen common to the filament wound regions, whereas the tow placed regions were mostly void free. The pressure generated from the FW was sufficient to completely compact and consolidate the tow placed material. Figure 75 shows a small amount of fiber waviness in the second layer of tow-placed material. Fiber-waviness can degrade the strength properties of the composite material.

4.2.3 Characterization of Wrinkling in the Tow Placed Layers

Lower burst values than designed observed in the recent vessels suggests that fiber wrinkling in the tow placed layer might be triggering the premature failure. The design of Vessel 1 used a single layer of AFP material on each of the dome ends. The more advanced designs of Vessels 2, 3 and 4 used two layers of AFP material, separated by discrete FW layers. The second layer of AFP material was applied against an irregular surface created by FW, and then was sandwiched by the outer heavier windings. It is believed the second AFP layer might become wrinkled due to the filament winding processes.

To show this is the case, cross sections of Vessels 1 and 4 were removed and evaluated for wrinkling. Figure 76 shows the blocks of materials removed from undamaged regions between the dome and cylinder section of the two vessels. These pieces were removed from the vessel post-failure, so cracking evident in the pictures may be due to the burst test. Two sides of each block were polished: one side was taken in the longitudinal direction of the tank, whereas the other was in the circumferential direction.

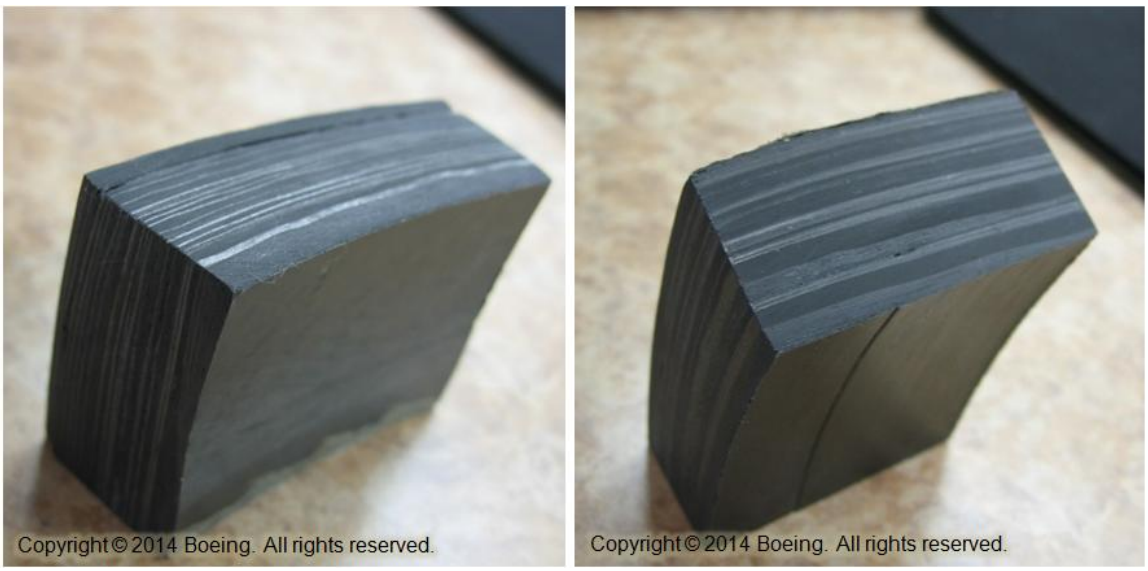

Figure 76. Sections removed from Vessel 1 (left) and Vessel 4 (right)

The AFP material was clearly identifiable in these cross-section photomicrographs in Figure 77 and Figure 78. The AFP material had near-zero porosity and little cracking. Significant cracking was clearly visible in Vessel 1 immediately above the AFP layer, creating a delamination. It could not be determined if this crack was due to the burst test or was pre-existing.

Fiber waviness was observed in AFP layers of both Vessels 1 and 4. Waviness was also observed in both the inner and middle layers. The differences in waviness between Vessel 1 and 4 may not be important, since it may be the middle layer that is sensitive to ply wrinkling. Furthermore since this was a cross section of only a small section of the vessel, it was difficult to generalize how prevalent or extreme the waviness was elsewhere, but it confirmed that waviness could be a cause of the low burst of the two-layer vessel design.

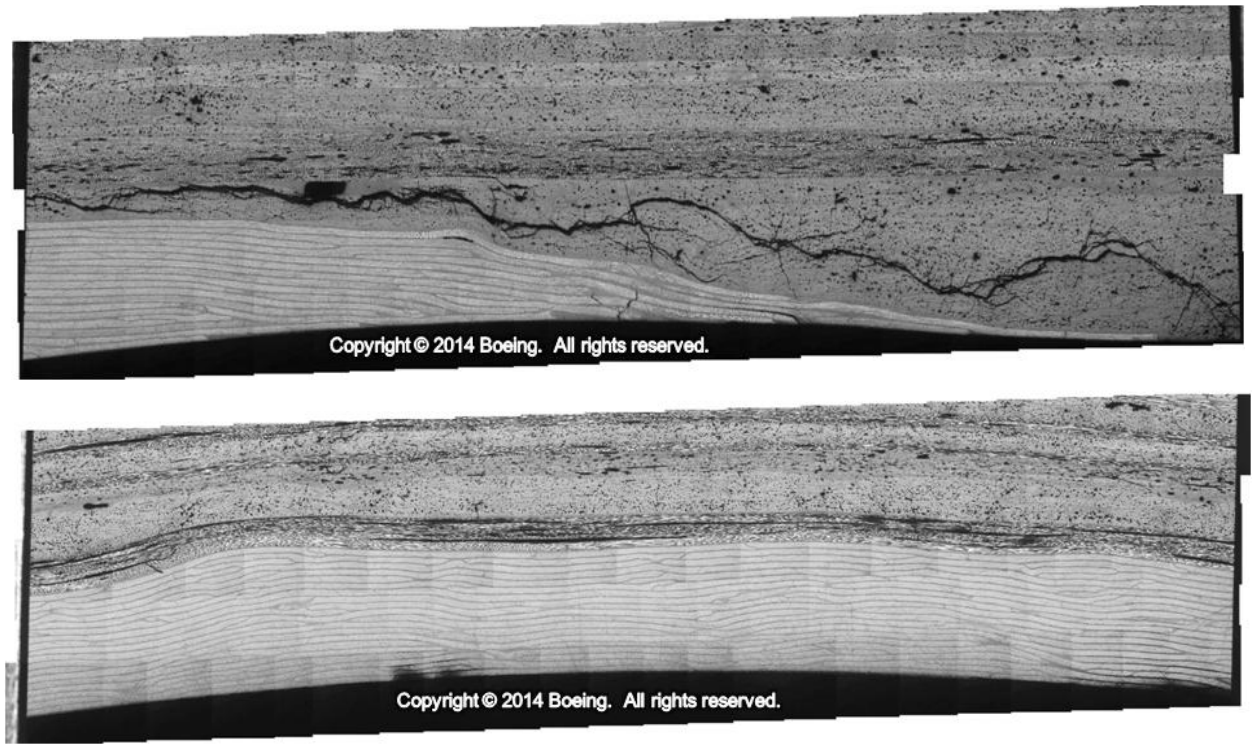

Figure 77. Cross sectional photomicrograph of Vessel 1. Top image was taken from the longitudinal direction. Bottom image was taken from the circumferential direction.

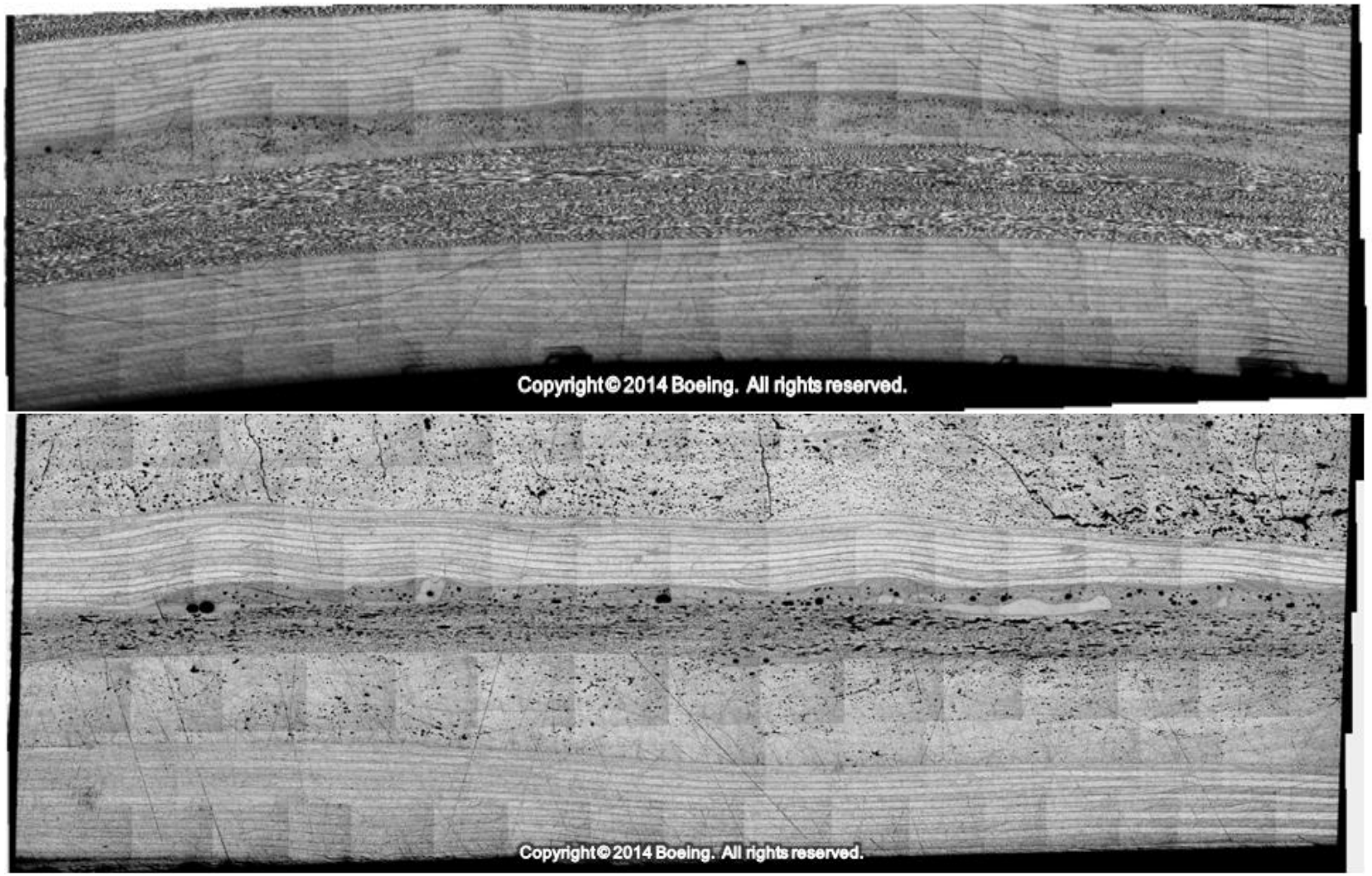

Figure 78. Cross sectional photomicrograph of Vessel 4. Left image was taken from the longitudinal direction. Right image was taken from the circumferential direction.

4.2.4 Reduction of Wrinkling Through Design Build Activities

The first attempts to build the AFP end caps resulted in wrinkling during FW. Figure 79 illustrates the type of wrinkling that occurred. The cause of this was traced to several factors, (1) the mismatch of the tool surface used to fabricate the end caps compared to the actual surface of the liner, upon which the end caps were placed, (2) the presence of stiff shear protectors that prevented the end caps from seating properly onto the liner prior to FW, and (3) inadequate modeling of the metal bosses at the forward and aft ends of the vessel.

Figure 79. Wrinkling due to poor fit of end cap to liner surface in earlier winding attempts

In order to eliminate all possible sources of ply wrinkles, the foam tool, which were used to wind the fiber placed end caps, were re-machined to a new, more accurate surface. Quantum shipped a new liner to Boeing. The contour of the liner was measured using a laser tracker system. The following figures show the measured deviation of the liner surface to the reference surface of Vessel 3. The liner cylinder area was found to be non circular as shown in Figure 80.

The forward end was found to be skewed in one direction relative to the foam profile used on Vessel 3 as shown in Figure 81. Near the polar opening it can be seen the contour appeared pushed in the +Z directions, whereas there appeared to be a more symmetric fit in the ±Y direction. This was more apparent in Figure 82, which collected data along intersecting planes that were oriented 90 degrees to each other rotated about the X axis.

To fit a new surface for the AFP end caps, it was determined to not compensate for the skew, but rather match the contour as best as possible based on data in the XY plane.

Similarly, data was collected from the aft end of the liner as shown in Figure 83 and Figure 84. Again the cylinder section was not round, but the errors on the dome section were more symmetric than the forward end, allowing a better fit of a new surface to the measured liner surface.

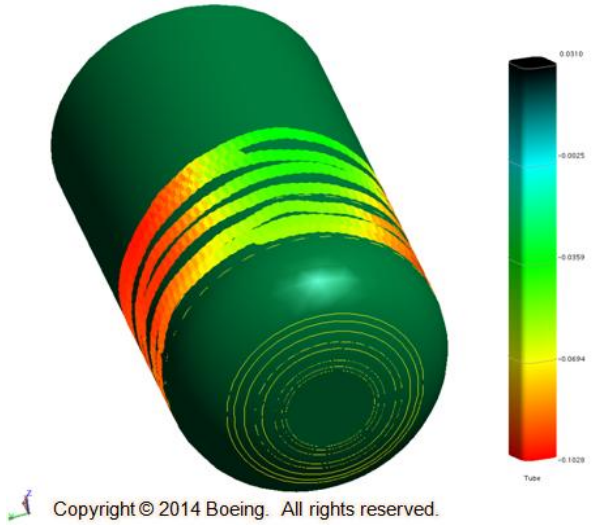

Figure 80. Liner cylinder section (toward forward) fit to Vessel 3 foam surface

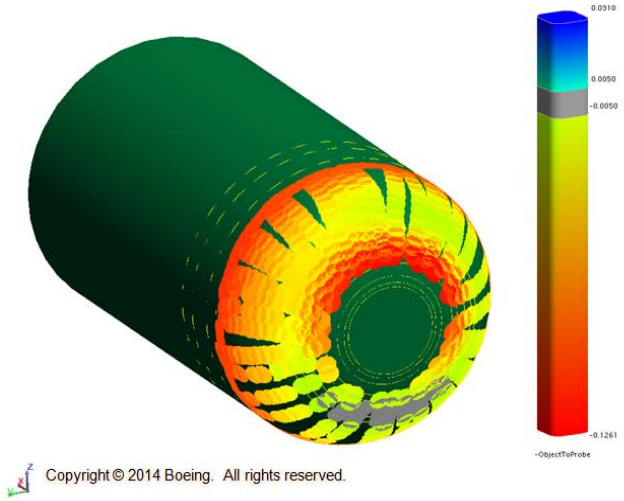

Figure 81. Liner forward section fit to the Vessel 3 foam surface

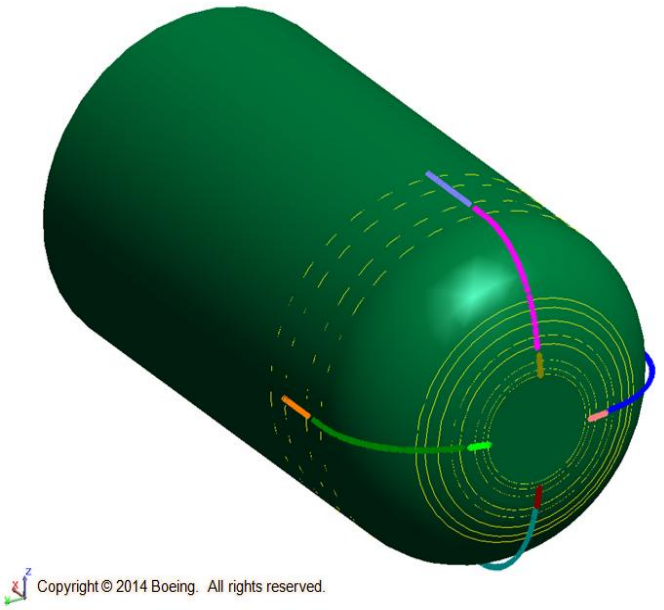

Figure 82. Planar section cuts used for defining profile for Vessel 3 foam surface

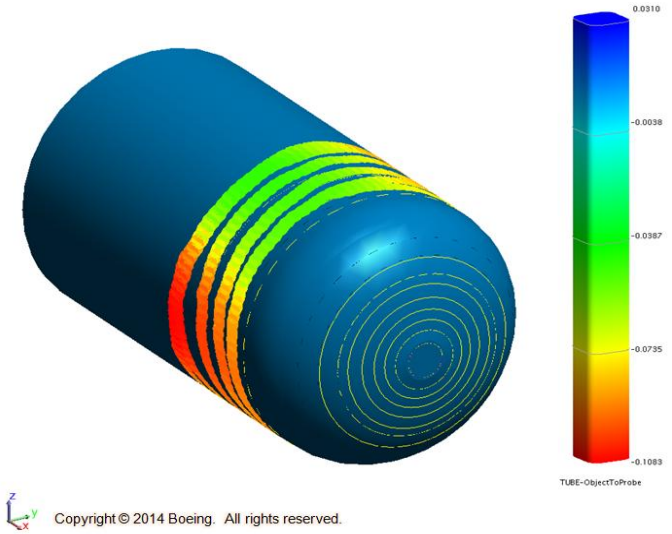

Figure 83. Liner cylinder section (toward aft) fit to Vessel 3 foam surface

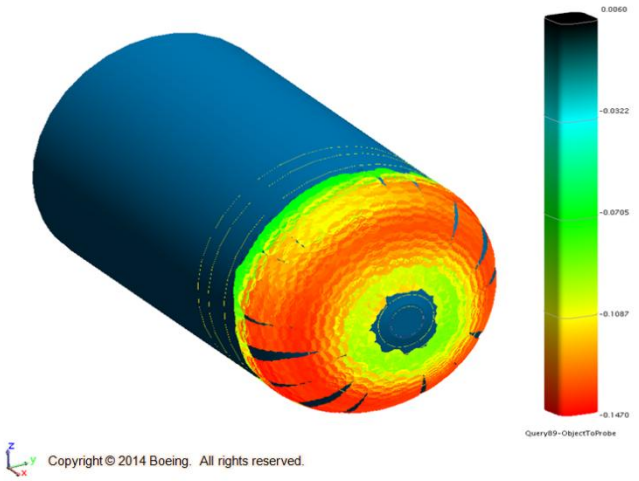

Figure 84. Liner aft section fit to the Vessel 3 foam surface

Surfaces were defined from the data generated off the liner. The existing foam tools were sent out for re-machining. The diameters of the new surfaces were smaller, so the entire foam tool was re-cut to the new surface. Even though the liner was measured as non-circular, the tools were machined with circular cross section. The foam surfaces also included higher fidelity of the boss features to minimize how much the bosses prevented the end caps from being held back from the liner. Tools were ordered also to thermoform the shear protectors, whose function was to cover the metallic bosses. The previous vessels used shear protectors cut from sheet stock, but their rigidity prevented the AFP end caps to fully seat onto the liner. With the formed shear protectors and the end caps that better match the boss features, the fit of the AFP end caps was improved.

These new AFP end caps were provided to Quantum for FW and structural testing. The fit of the AFP end caps with thermoformed shear protectors was superior to anything attained previously. No wrinkling was noticed during FW. Figure 85 to Figure 88 show additional pictures of the fit between liner and AFP end caps with the thermoformed shear protectors. With the new tooling and processes in place, end caps were shipped to Quantum to continue vessel fabrication and testing.

Figure 85. Forward end fit of AFP end cap on liner with thermoformed shear protector

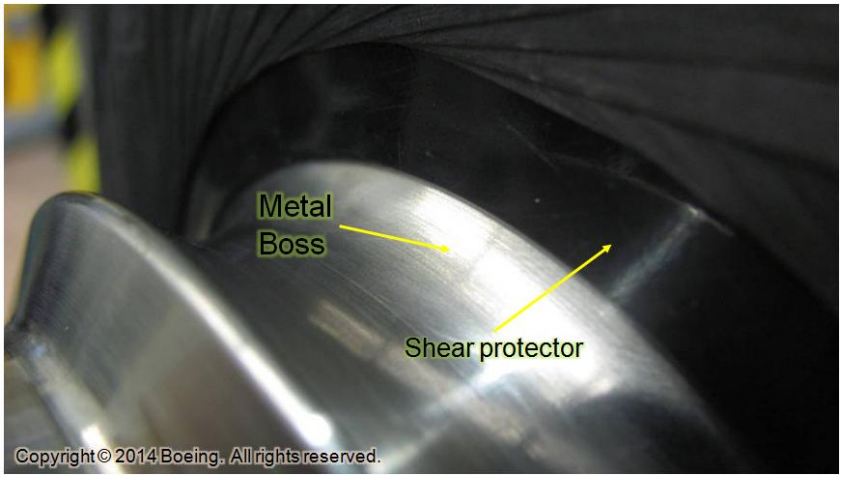

Figure 86.Close up of forward end cap fit to polar boss showing fit of shear protector and end cap

Figure 87. Aft end fit of AFP end cap on liner with thermoformed shear protector

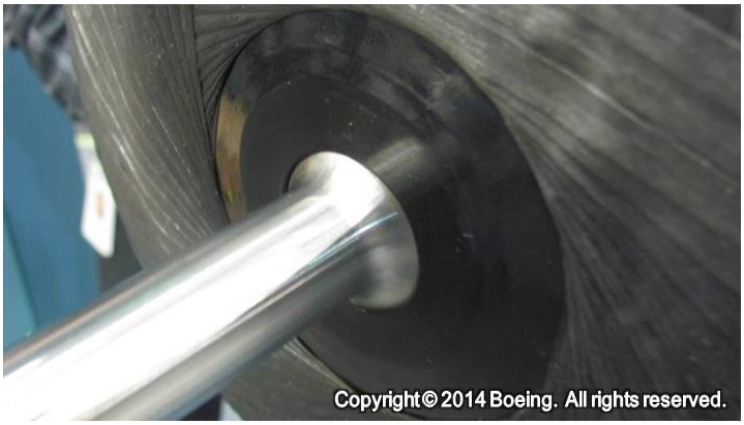

Figure 88. Close up of aft end cap fit to blind boss showing fit of shear protector and end cap

4.2.5 Process-Property Relationship for Tow Placement Candidates

The AFP material is Toray's 3900-2/T800H resin/matrix system. This material is used by Boeing for the fabrication of advanced composite aircraft structure. It is used for primary structure, and this is controlled and characterized very well. In particular, the standard aerospace cure cycle requires a 355°F cure for 2-hours under 90-psig pressure. For the hydrogen pressure vessels, the cure temperature is limited to 250°F due to the melting temperature of the liner.

The lower temperature, longer cure-time cycle will under-cure the 3900-2 resin system. The under-cure condition may contribute to lower strengths of resin-dominated properties. However, many epoxies can achieve significant strength and toughness at a lower degree of cure. Thus, additional testing was conducted to determine if the shear strength of the materials were being compromised due to the lower cure temperature.

In order to understand the consequences of the lower-temperature cure, the Mode II fracture toughness (shearing, Giic – see Figure 89) was measured for different materials, interfaces, and cure cycles. Three materials were screened in the study and were summarized in Table 4. Material "C" is Boeing's common 250°F cure material that achieves a high degree of cure after only 2 hours.

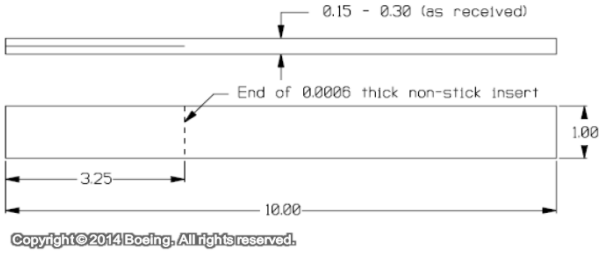

Figure 89. Giic, Edge Notch Flexure (ENF) type specimen used in the experiments. This measures shear type fracture toughness.

Table 4. Test matrix and results

Laminate	Cure Cycle	Interface Materials	Giic
A	**1**	**a/a**	21.4
B	**2**	**a/a**	12.7
C	**1**	**a/b**	8.9
D	**1**	**b/b**	8.1
E	**1**	**b/c**	9.4
F	**1**	**c/c**	8.8

Cure cycle is defined per Table 5 below.

Table 5. Test procedures

1. Base Line 250F/7-hr Cure Cycle	
1	Apply Full Vacuum
2	Apply 90 psig
3	Heat 3 F/min to 250 F
4	Hold for 7-hours based on part TC
5	Cool <5 F/min, Remove
2. Aerospace Standard 355/2-hr Cure	
1	Apply Full Vacuum
2	Apply 90 psig
3	Heat 3 F/min to 355 F based on part TC
4	Hold for 2-hours
5	Cool <5 F/min, Remove

Different interface configurations were created from combinations of the three different materials. These are given in Table 6, along with the results. The interfaces for these coupons were created from plies placed ±45 degrees to each other, in a cross-ply fashion. Thus, the crack propagated between orthogonal plies set at 45-degrees to the coupon direction. This configuration allowed the crack to jump from one interface to another, convoluting the results. Visual observation of the cracks confirmed that this was happening in most of the results.

Table 6. Three materials investigated in the study

Materials	
a	Toray 3900-2/T800H
b	Quantum T700 Wet Wind
c	Cytec 250 Cure Epoxy

Given the uncertainty in these results, looking at Table 4 Laminate "A", it is interesting to note that this under-cure case produced a significantly higher fracture toughness than the fully cured case (Laminate "B"). This particular set of coupons had uniform interfaces through the thickness, so crack jumping would not significantly affect the result. Furthermore, the value is also higher then Laminate "F", which is the standard 250°F cure material.

Overall, the shear strength of the interfaces are at acceptable levels, and no significant compromise is suggested by under-curing the 3900-2/T800H material system. Furthermore,

switching to a 250°F cure compatible material is not suggested since our current choice of materials, albeit under cured, are performing well.

4.2.6 Evaluation of Vessel 6

Vessel 6 was built specifically to be destructively-evaluated, using the current design and processes. Half-dome regions of the forward and aft ends of the vessel were sent to Boeing for detailed analysis. An X-ray of the forward dome is shown in Figure 90. The X-ray shows the internal structure, including the boss, liner, and composite shell, but does not show any high resolution details such as voids.

Figure 90. X-ray of the forward half-dome of Vessel 6

Higher detail of the composite was achieved by performing CT scan of the structure (Figure 91). The CT scan shows three-layer regions in the laminate, which are going from the inner radius to the outer radius: (1) fiber placed plies; (2) hoop filament wound layers, and (3) helically-wound layers. The CT scans were studied for regions suspected of having high porosity, cracking or delamination, or fiber wrinkling.

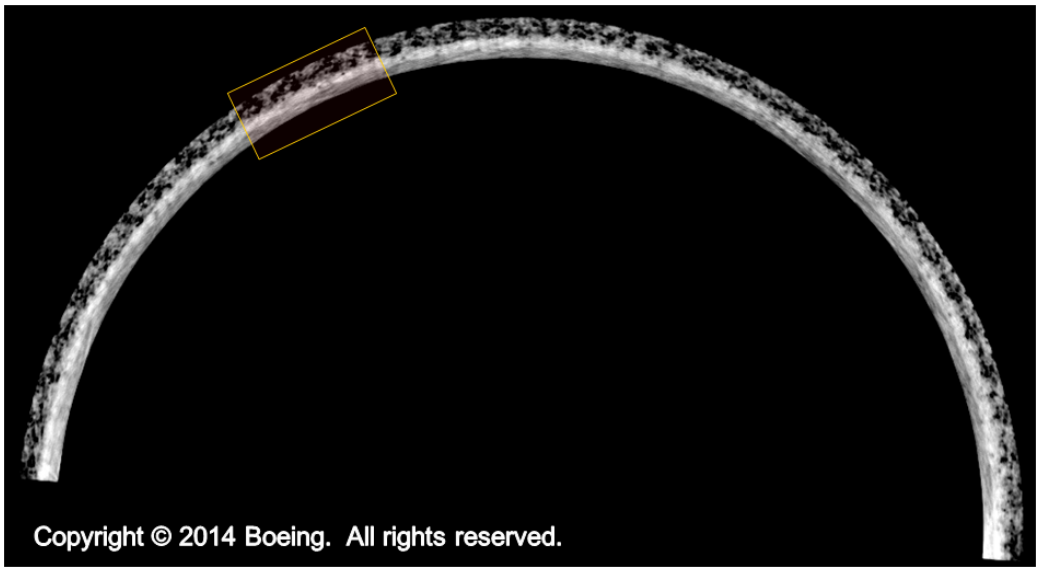

Figure 91. CT scan section taken from the forward dome region, showing suspected porosity in the helically wound material.

Several regions were sectioned for polished cross-section photomicroscopy at these suspected areas. One example is shown in Figure 92, again showing the three distinct regions identified in the CT scans. Porosity is observed in the outer, helically-would layers, although not to the extent suggested by the CT scans. In this region, resin-pooling or a less-uniform resin distribution may be contributing to the CT scan response. However, significant porosity was identified in the tip of dome regions; a problem which was later addressed in the fabrication of Vessel 7.

Figure 92. Cross section taken from region identified in Figure 91, showing the microstructure of the dome region.

One region suspected of having cracks, as identified by the CT scan, was later observed to be a resin-rich layer when observed through a microscope. Because the differences between resin and voids cannot be easily discriminated, the CT scan does not provide sufficient information to determine porosity or cracking directly.

4.2.7 Shipping of AFP End Caps

The first set of AFP end caps was built and shipped from Boeing to Quantum in June 2011. They were shipped supported by foam cutouts which were wrapped in FEP film and then placed in a disposable box with dry ice. Figure 93 illustrates the original packing method. This method caused the constant cylinder section of the end caps to stretch due to the diametric mismatch of the foam cutouts and the AFP end cap. This method also took excessive time to make the foam inserts for each set of end caps that were to be delivered to Quantum.

Figure 93. Forward end cap packaging (left), forward end cap fitted on liner (right).

When the package arrived at Quantum there was clear evidence that the end caps had indeed stretched around the constant cylinder section. Both the forward and aft end caps were fitted on liners at Boeing prior to shipping to Quantum, showing that the distortion was caused by shipping/packing issues.

A new method of shipment was developed to eliminate the damage. The method uses actual liner to support the forward and aft end caps. The caps are placed onto the reusable dome liners on top of FEP film. More FEP is placed over the composite end caps, and then a bag is placed over the entire layup to keep the dry ice from contacting the caps. This new method allows for a tight fit on the liners with no visible distortion created. Figure 94 shows the forward end cap placed on a reusable shipping liner and the reusable crate that both the forward and aft end caps are placed in for shipping back and forth between Boeing and Quantum. This method showed with no visible damage or distortion to the dome caps. There is a closer tolerance fit from the end caps to the liner, reducing any effects that would have been caused by the constant cylinder section mismatch.

Figure 94. Forward cap new packaging (left), new reusable shipping container (right).

4.3 Phase III

During Phase II of the program, many sets of dome caps were delivered to Quantum. Wrinkles were observed on the dome cap in the last few sets. One of Boeing's tasks during Phase III was to figure out the cause of wrinkles and how to eliminate them for subsequent deliveries.

4.3.1 AFP Layup Process Improvement

During the initial build and rebuild of Vessel 9 AFP end caps, it became evident that small amounts of wrinkling were being induced by the AFP process in the last several sets shipped to Quantum. This slight wrinkling or "marcelling" is a new phenomenon that was not previously observed, when end caps were fabricated on the original equipment. The wrinkling is limited to certain locations, which do not correspond to any failure locations during tank bursts. Nevertheless, the wrinkling is not acceptable for quality parts, and a significant amount of resources were tasked with resolving the causes for the formation of the wrinkling. An example of the visible marcelling can be seen in Figure 95 below. From the observation during layup, it is evident that the wrinkling is being induced on the first couple of plies of the lay-up on the inverted side of the polar opening. The wrinkles tend to be oriented around the polar opening of the first ply.

The approach to resolving the issues centered on tooling effects, fiber path generation effects and compaction effects.

Figure 95. Picture showing wrinkles in layup of Vessel 9

4.3.2 A Sealed Foam Tool for a Better Layup Surface

The process for all end caps fabricated previously was to stretch a 0.002-inch thick FEP film over the dome wrinkle free, secure it with tape, and layup onto the film. Once the dome was complete, it could be removed from the tool by cutting the FEP film and sliding it off. With the last re-machining of the foam tools to better match the liner contour, the foam was left unsealed which caused the foam to be more susceptible to damage during handling and layup of end caps. Previous end caps were built on sealed foam tools and did not show any signs of wrinkling. To be consistent and protect from wear and tear on the tools, both the forward and aft foam tools were sealed. Figure 96 shows the foam tool unsealed on the left and sealed on the right.

Figure 96. Picture showing unsealed and sealed foam tools

4.3.3 Wrinkling Caused by the FEP Film

Initial observations and speculation was that the thin layer of FEP was slipping against the foam tool and was the cause of wrinkles seen in the first couple of AFP plies. After observing multiple plies and layups, it was noticed that there was evidence of slipping between the FEP film that is stretched over the foam tool and the end cap itself. This problem became more

pronounced when the foam tools were sealed. The newly sealed surface made the interface between the tool and the stretched FEP slippery, aggravating the problem. The unsealed foam mandrel acted as a gripping surface holding the stretched FEP film in place. Figure 97 shows how the material slipped against the newly sealed foam tool and the resulting wrinkling.

Figure 97. Pictures showing wrinkles in layup after use of sealed foam tool and FEP film

After this initial effort, showing that the wrinkling induced during the layup had gotten worse, a second test was conducted without the use of the FEP film in order to determine if better results could be obtained using a more rigid surface. This process involved laying up fiber directly on the sealed foam tool.

4.3.3.1 Test 1: 3 Tows with Original Lay-up for Vessel 9 with no FEP

The first test conducted without the FEP stretched film kept all the parameters the same as they were for the build of Vessel 9. On the first ply there was steering with three tows causing some puckering of the tows. It was assumed that this also could be a cause of wrinkling seen in the first ply and would be reduced by having a stiffer surface since there was no FEP film. The wrinkles were still concentrated around the area close to the polar opening of the first few plies. Removal of the part was done by placing the entire foam tool in the freezer until both composite layup and foam tool were frozen. At this point the foam shrunk enough to allow the composite to release or "pop" off the foam tool with little work or stress to the composite layup.

After the layup was completed, wrinkling was still observed on both the outside and the inside surfaces of the end cap, concentrating around the area close to the polar opening of the first few plies. Removal of the part was done by placing the entire foam tool in the freezer until both composite layup and foam tool were frozen. At this point the foam shrunk enough to allow the composite to release or "pop" off the foam tool with little work or stress to the composite layup.

The wrinkling shown in Figure 98 was much less pronounced than what was displayed in Figure 97 from the first set of caps sent to Quantum. This demonstrated that the use of a more rigid surface could indeed help reduce the wrinkling effects that were noticed with earlier composite layups.

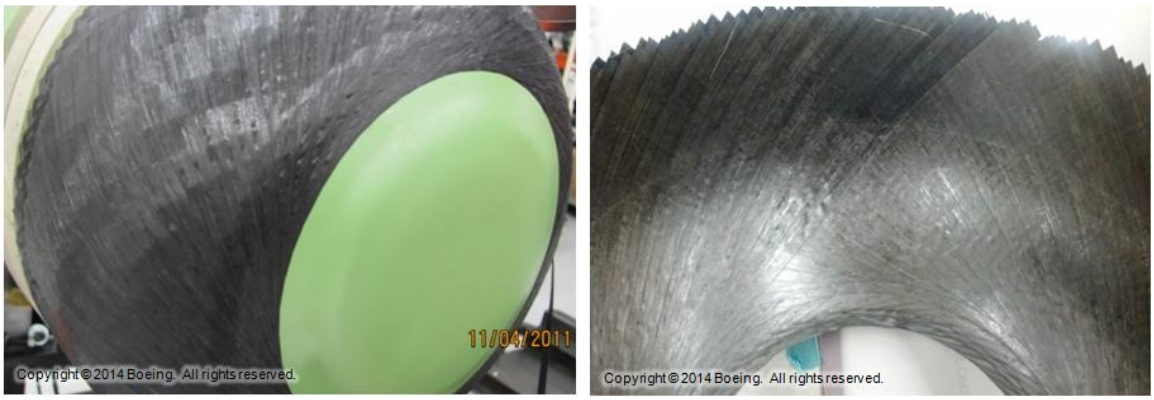

Figure 98. Picture showing wrinkles from first test with sealed foam tool and no FEP film

4.3.3.2 Test 2: Two Tows with Minimal Steering

The next test conducted was to repeat the first test, but to reduce the steering as much as possible. In CGtech software, two parameters control the steering, polar opening diameter and fiber angle. Under standard isotensoid designs, the vessel diameter and polar opening define the fiber angle that can be wound. With fiber placement, this is mimicked by defining the polar opening input, and the system calculates the resultant angle based. If any fiber angle other than the ideal isotensoid derived angle is entered into the programming system, the fiber path will be steered to fit both parameters. The greater the steering, the greater the chance for lateral slippage. The lateral steering and/or slippage can cause of the observed wrinkling. Almost all of the vessel designs rely on steering to meet polar opening and fiber angle definitions.

To study the effects of no steering, the polar opening was kept the same and the angle varied to the ideal isotensoid angle. The Vessel 9 design called for a 42-degree fiber angle and a 9.10 polar opening diameter. To eliminate steering, that angle was changed to 44-degrees with the same polar opening. Some wrinkling still occurred. Next, the programs were changed to only two tows, instead of three tows per course, in order to minimize the effects of parallel paths offset from the nominal path. The result of this trial was that the entire lay-up was virtually wrinkle free.

Figure 99 shows the first ply with the use of these parameters. Comparing this with those in Figure 98, it can be seen that there is no wrinkling around the polar opening. Extraction of the part from the tool without the parting FEP film, however complicates the process. The part and tool had to be cooled in the freezer long enough to eliminate the tack of the material and facilitate extraction. The part is then bagged and removed from the freezer in order to allow it to warm to ambient conditions, prior to removing it from the bag. A better means of removing the part from the tool is needed that does not unnecessarily encumber the production process.

Figure 99. Picture showing the layup with minimal steering and two tows

4.3.3.3 Observations

To completely eliminate the first ply wrinkling, the first two plies must use fiber angles that are close to the ideal isotensoid design, and only two tows per course can be used. Although this reduces productivity by 1/3 for these first two courses, it does eliminate the wrinkling. Additionally, a better means of extracting the part from the (FEP-less) tool is needed. One possible option is the use of a more rigid liner that can be attached to the tool for layup. The rigid liner will provide a solid base for layup, allow separation from the parent tool, and possibly aid in extraction from the tool without the need to freeze the material.

With the use of this new method the FEP film was eliminated from the process, but a new step was introduced. The removal of the layup from the foam tool needs to be conducted in a freezer to allow the separation of the two pieces.

4.3.4 Collapsible Tool Concept

In an effort to eliminate this difficult step of freezing the parts before extraction of end caps and make this process more production efficient, a three piece, collapsible tool concept was studied for incorporation into the production processes. This collapsible tool would allow for the removal of foam tool without the difficult freezing step. The concept uses three pieces as shown in Figure 100: the first piece is a wedge that slides out from the back of the tool. It will be bolted or pinned from the backside to secure it into position. After this wedge is removed the remaining two sections will hinge together and allow for the extraction of the composite end cap from the foam tool. By incorporating this collapsible tool into the robotic cell, the part can be removed with very little downtime, increasing the overall efficiency of the cell and process. This is conceptual only and many different collapsing processes/mechanisms can be utilized/designed to separate/remove the uncured composite part from the tool.

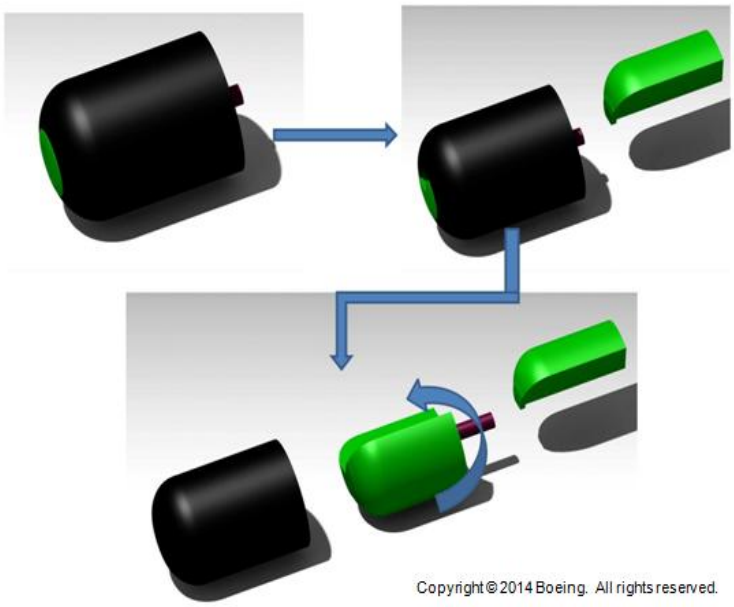

Figure 100. Collapsible tooling concepts

4.3.4.1 Scope

Design two multi-segmented collapsible room temperature tools for the fabrication of a thermoset composite pre-preg end caps. Two tools are required, one for the aft end dome and one for the forward end dome. Tools will mount in a 3-jaw chuck and will require a shaft and mechanical linkage for collapse/extend actuation.

4.3.4.2 Requirements

1. Minimum of three segmented collapsible tool but can be more if needed.
2. Initial separation of the tool from the composite should be initiated by a "peeling" action to facilitate part removal
3. Peel should be initiated in the thicker region of the layup minimizing distortion of the layup in the thinner regions. The thicker locations are on the dome at the polar opening of the layup
4. Surface material for the tool should be aluminum (vendor chooses grade)
5. Major mechanical linkages along with main shaft should be made of steel
6. Surface finish of tool should be Ra=16 or better
7. Provisions for a pneumatic vortex chiller to chill surface for each individual segment is required
8. Vortex chillers should be incorporated into tool, not having to remove during layup or during collapse/extend action
9. The outer tool surface should be capable of reaching less than 50°F
10. Tool needs to rotate and move freely during layup so a pneumatic slip ring is required
11. Slip ring passes pressurized air necessary to run chiller and pneumatic actuation for collapsing the tool (if pneumatic action is selected)
12. The tool will be exposed to room temperature only

13. No exposed lubricants allowed on any mechanical linkage or moving parts
14. Doesn't need to be vacuum tight, but seems need to be as tight as possible
15. Mechanical action
16. Needs to collapse inwards without distortion of uncured layup
17. Collapse action must only be sufficient to fully separate tool surface from the uncured composite end cap layup
18. Needs to collapse/extend while still in 3 jaw chuck
19. Need rapid collapse and rapid extent action (2 minute or less)
20. Needs to automatically re-index to original position after expansion
21. Tolerance and index to repeat profile tolerances (±0.020") after fully expanded to original layup state
22. Prefer pneumatic actuation for mechanical motion, but may accept other means for collapse or expansion of tool fixture
23. No servo, or electrically controlled mechanical motion
24. Consult with customer to determine best release coating for tool surface
25. Customer will supply surface definition along with surface tolerances, (surface tolerance of ±0.020")
26. Tool shall not deflect more than ±0.020" under a 100lb cantilever load given these conditions
27. Load normal to the axis of symmetry
28. Load applied at the farthest cylindrical portion of the tool from the mounting location
29. Deflection measured at the free end of the tool
30. Mount into three jaw chuck, vendor needs to supply tool fixture with a 3"(or appropriate) shaft and a grip length of no more than 8"
31. Provide a hinged/latched storage crate for both forward and aft dome caps capable of housing fixtures while not in use.

4.3.4.3 Ply Layup Definition

Forward End Cap

Layup is approximately 1/4" thick at polar opening and tappers down to approx. 2 plies (0.015in thick). Constant cylinder section is approximately 13inches in diameter and layup height is approximately 12-14inches.

Aft End Cap

Layup is approximately 3/8" thick at polar opening and tappers down to approx. 2 plies (0.015in thick). Constant cylinder section is approximately 13inches in diameter and layup height is approximately 12-14inches.

4.3.4.4 Supplemental Information

Figure 101 demonstrates the current process for laying up uncured pre-preg composite material onto a foam tool. The tool is cantilevered on one end in a 3-jaw chuck with the load being applied to the far extremity of the foam tool.

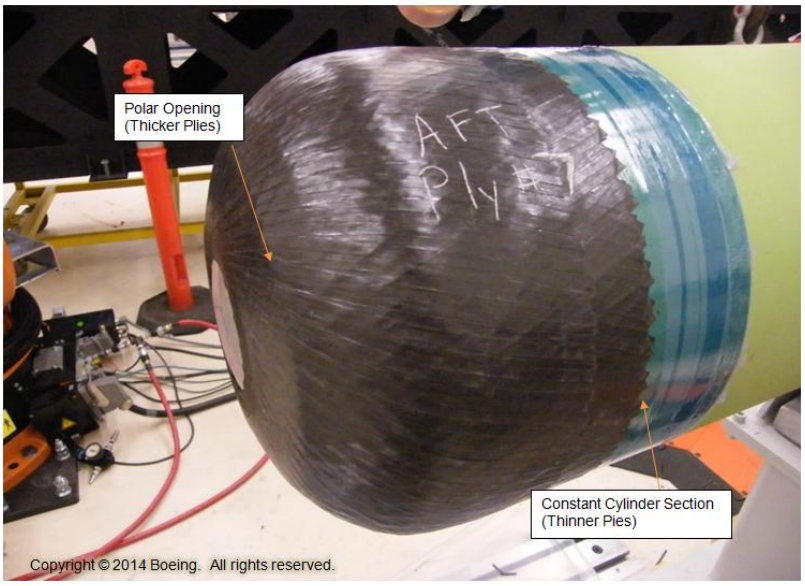

Figure 101. Current foam tool used to layup composite end cap

Figure 102 shows the dimensions and surface finish of the collapsible tool. As shown the actual tool surface shouldn't be more than 16 inches in length with an approximate diameter of 13 inches (the surface model will provide the actual data needed for diameter as well as dome radii). The shaft will need to be 8 inches in length with a diameter of 3inches (or appropriate length).

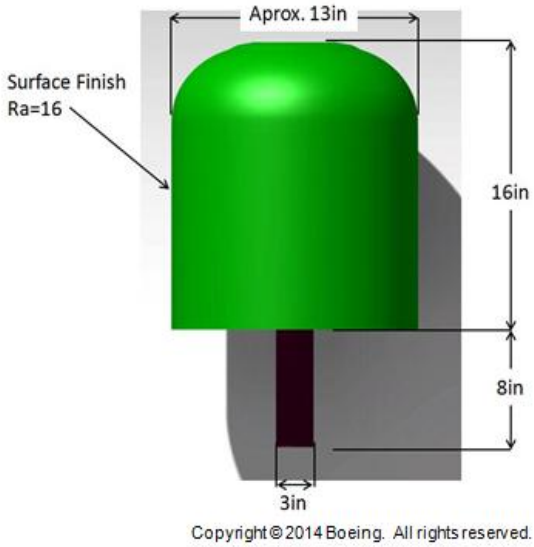

Figure 102. Dimensions of collapsible tool

4.3.5 Refinement of the Fiber Tensioning System

A new design on the dynamic tensioner system (shown in Figure 103) was designed and built due to the response rate of first generation tensioner system. The first generation system relied on programs within the motor to control various tension conditions based on direction and rate of movement of prepreg tow. This system created undesired levels of tension during directional

change of tow and during the feed portion of each course. This undesired level of tension can cause loss of placement accuracy as well as induce unwanted wrinkling, caused by the high tension. This later system did however reduce slack in the system during articulation of the robotic arm and created a more consistent level of tension throughout the duration of each course path on each ply.

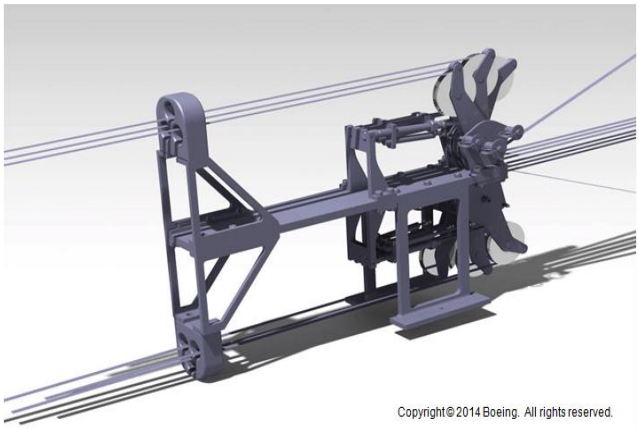

Figure 103. 3D model of new tension control system

Boeing installed a new smart-motor control system from *Animatics* onto their existing creel system, along with a newly designed dancer system. The *Animatics* motors allow for better control and higher torque output as compared to previous motor control systems. This system also allows for a dynamically-control, closed-loop-active tow tensioning, allowing for consistent tension on each tow regardless of tow direction or speed. This will greatly reduce spikes in system tension caused by the articulation of the robot's arm movement while building AFP end caps.

Figure 104 shows the creel system with the installed smart motors and integrated dancer mechanism. The dancer system has linear actuators that are used to control tension. Linear potentiometers are installed to send feedback information to the smart motors for closed-loop control of tension. This allows the tension to be consistent regardless of spool diameter, speed, and direction of fiber movement.

Figure 104. Upgraded closed loop tension control

The final control logic was integrated into the upgraded creel system. This controller allows the linear potentiometers that are associated with each individual dancer arm to send information back to the motor that it is affixed to, creating a more-refined tension control system. Each motor controls an individual tow; thus, each of the six tows is controlled independently of each other. Each motor will output the correct torque for its particular lane so that tension across all six tows is consistent, regardless of differences in drag from lane to lane.

The motors also allow for the material to be wound back up or re-spooled when the head articulates in a manner which creates slack. Having this function keeps the material from coming into contact with any unwanted or foreign materials, while keeping consistent tension on the tows at all times.

4.3.6 Processing of End Caps for Vessel 13

Vessel 13 end caps were built using the new process utilizing the sealed foam tools and method for extracting the dome caps from the foam tool. The new dome caps differed from previous caps in that the transition point where the dome caps merge with the FW process was extended an extra 2 inches. The end caps were also thicker by doubling the plies from 10 to approximately 20 for both the forward and aft. The layup process was successfully completed with no visible wrinkles or defects.

Figure 105 shows the in-process layup of the aft dome cap on the sealed foam tool. This layup shows a ply placement that will be AFP'd over in a few later plies.

Figure 105. Layup of aft dome cap

Figure 106 and Figure 107 show the pictures of the exterior and internal surfaces of both forward and aft AFP end caps after they were vacuum bagged, respectively. The end caps were vacuum bagged to the foam tool to de-bulk the composite and allow for a more accurate CMM

comparison to the software prediction by Quantum. CMM data was also taken from both forward and aft end caps for validation from Quantum's software to the actual.

Figure 106. Pictures of forward and aft end caps external surfaces (after vacuum bagged)

Figure 107. Pictures of forward and aft end cap internal surfaces (after vacuum bagged)

No visible wrinkles in the dome region of the forward and aft end caps were seen. Slight wrinkling around the most extreme polar opening was seen. This was primarily caused by steering violations exceeding the ¼-in tow's capabilities.

Boeing AFP end caps met the requirements within 2° of the angles provided and less than 0.05-inches in polar openings for both the forward and aft end caps.

4.3.7 Processing of End Caps for Vessel 14

Boeing built the next set of end caps for Vessel 14 using the newest design configuration provided by Quantum. Boeing utilized the sealed-foam layup tool (described earlier) to form the end caps during AFP. The caps were extracted from the tool after AFP. The new end caps differed from the earlier versions by the number of plies, which were reduced from 20 to 14. The layup sequence, ply angles and polar openings also differed. A correction in the tangent point definition – where the dome region meets the constant cylinder section definition was used. This resolves an earlier issue associated with differing definitions between FW and AFP.

Quantum's layup parameters were fiber placed by Boeing to within 2° of the angle specified, and the polar openings to within 0.05-inches for both the forward and aft domes. Furthermore, little to no wrinkles were seen on either of the end caps. These end cap designs were utilized on all the vessels subjected to testing per EC79.

4.3.8 Lessons Learned during Placement of End Caps onto Liner

Boeing participated at Quantum in the filament winding of Vessel 14. The earlier process for installing the AFP end caps onto the liner was to press them into place. This method tended to cause the end caps to deform due to handling. Since the liner's outside surface and the dome cap's inside surface are net to one another, the fit is difficult. For this reason it was decided to freeze the liner, allowing it to shrink enough, so that the end caps would slip onto the liner. This allowed for easier and more accurate placement (locating), making the dome caps and the liner concentric to one another. After this step, the assembly was sat out at room temperature, allowing the liner to lock onto the end cap. This step was repeated for the other end. Once fully assembled, the liner and end caps were mounted onto the filament winding machine.

Figure 108 shows the tight fit between AFP end cap and the liner using the above described method. It also shows that no distortion to the end caps was induced during the handling and processing of these steps. Note, if the liner is allowed to cool too much, condensation can occur once removed from the freezer. To minimize this, the liner is only placed in the freezer for 1-2 minutes, just enough to shrink the liner and allow for accurate placement of the end caps.

Figure 108. Placement of dome cap on liner

4.3.9 Lessons Learned during Placement of Release Film onto Liner

Quantum has conducted pressure cycle tests that require the vessel to be pressurized and depressurized numerous times. Since the cure process takes the liner up to the softening temperature, allowing it to co-mingle with both the AFP and FW materials, a mechanical bond is created between the liner and composite. A high temperature release film was stretched over the liner to prevent the composite material from mechanically bonding to the liner during cure. This bond can cause a premature failure due to high stress concentrations where the two materials are

bonded. This release film has ability to withstand the temperatures and to stretch over the complex geometry, along with it being a Boeing-approved contact material for composites.

Figure 109 shows the process for stretching the release film onto the dome ends. First double back tape is placed all the way around the constant cylinder section, approximately 18" from the end of the dome. The film is slowly worked around the dome region, being stretched as it's worked. This process takes a bit of work to finesse the film and stretch it around the dome without tearing it. Once stretched, the excess is cut off, and the liner with the stretched FEP film is placed into the freezer for a couple of minutes to shrink the liner for installation of end cap.

Figure 109. Process for stretching release film onto liner

Once the end caps are placed over the stretched film, more work is needed to wrap the film over the constant cylinder section. This is done by first cutting away the excess stretched film and then removing the double back tape. New film is then place over the constant cylinder section and taped to the stretched film with blue Mylar tape. This process is difficult and time consuming, and it still creates wrinkles in the film.

Since the film is stretched over the dome region, stresses are introduced into the film. Once the film is cut away from the double back tape, it pulls away relaxing these stresses, moving the end cap and causing a separation (gap) between the liner and the cap. Figure 110 shows this separation. This was fixed by reworking each end through the freezer process in order to re-seat the caps back to their proper locations. This added an extra step in the process of placing the film and then locating the end caps.

Figure 110. Picture of gap caused by cutting stretched film

A new method for placing the film onto the liner was developed to eliminate the extra steps and the problems associated with the composite cap separating from the dome region on the liner. This method starts by placing the film on the constant cylinder section first, followed by taping one end with Mylar tape, so that the film won't move when stretched over the opposite dome region. On the end that the film is stretched over first, double back tape is placed on top of the film, so that the tape doesn't come in direct contact with the liner. The film is next stretched over the dome region as before, but this time there is no need to cut the film and retrieve the double back tape since it is not touching the liner directly. After the excess film is removed from the stretching process a strip of blue Mylar tape is used to secure the stretched film in place. This is repeated for the other side leaving a nicely stretched taught film over the liner. Figure 111 shows both ends of the liner with stretch film. Figure 112 below shows the completed process with stretched film onto the liner.

Figure 111. Picture of domes with stretch film by new method

Figure 112. Completed process for stretching film onto liner

5.0 PNNL Report

5.1 Testing of Polymer Vessel Liner Material in Hydrogen

In the course of this project, PNNL has completed extensive hydrogen compatibility studies of polymeric liner materials in order to determine hydrogen degradation effects and changes in materials properties as a function of high pressure hydrogen exposure. While the detrimental effects of hydrogen are well known for metals and even some ceramics, the body of knowledge on the effects for polymers is relatively scarce. This knowledge gap was addressed by providing results on hydrogen blistering and both ex-situ and in-situ tensile testing of structural polymers in high-pressure hydrogen. The results, given in detail below show that polymers, like metals, degrade in hydrogen. This exposure can result in blistering, void formation, and a reduction in tensile strength. While some of these results, like the voids and blisters, are permanent, some of the reductions in strength are transient, and the polymer recovers after the high-pressure hydrogen is removed. This is by no means an exhaustive study, and more work is needed in this area to fully understand the effect of high-pressure hydrogen on polymer materials critical to the hydrogen economy.

5.1.1 Blistering

PNNL investigated the effects of high-pressure hydrogen as a function of temperature and crystallinity on the surface damage of polymer films with the goal of developing a model to understand hydrogen degradation of the polymer liner in high-pressure composite vessels. Most polymer liner candidates are semicrystalline material like high-density polyethylene (HDPE), consisting of amorphous and crystalline regions. In order to separate the effects of hydrogen in the two different regions, PNNL investigated amorphous and crystalline materials separately to better develop a model for degradation, with the finding that damage occurs in amorphous polymers and not in perfectly crystalline polymers under identical conditions. As well, the damage is strongly a function of temperature with more blistering occurring as the temperature increases and the viscosity decreases.

To investigate this effect, polymer films with ultra-low roughness surfaces were exposed to high-pressure hydrogen while mounted on a thermal gradient stage developed at PNNL for this project. The thermal gradient stage is a unique experimental capability that allows *in-situ*

combinatorial studies of hydrogen degradation over a large temperature range (see Figure 113 a & b). Samples were exposed to high-pressure hydrogen for one day and underwent controlled decompression under the elevated temperature gradient. Samples were then evaluated with optical microscopy for possible surface degradation. The smooth surface condition greatly aids in observing any potential damage.

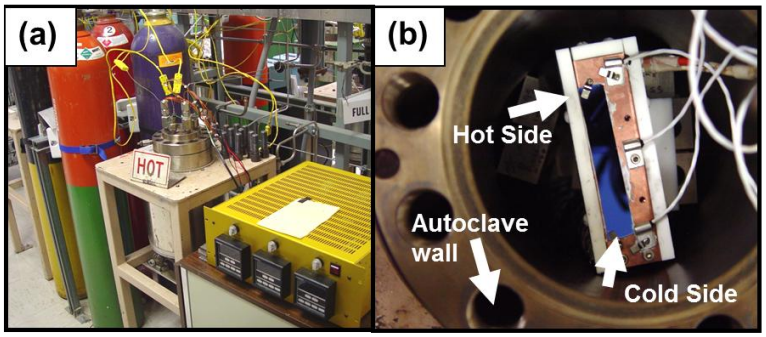

Figure 113. (a) High-pressure hydrogen autoclave setup. Two autoclaves are capable of charging samples at 100% H_2 or D_2 atmospheres at up to 6,000 psi and 300°C. (b) Additionally an in-situ thermal gradient stage for combinatorial thermal testing in the hydrogen environment was developed.

PNNL observed extensive surface blistering in the amorphous polymer materials. Blistering occurs when the polymer absorbs a significant amount of hydrogen and the external pressure is released. The hydrogen can collect around a defect and the depressurization leads to unmatched forces resulting in the formation of a void or blister (see Figure 114a). The observed blisters in the polymer were on the order of 10-50 microns (see Figure 114b) in amorphous (polystyrene) where blister size and density varied strongly with temperature. For the amorphous samples, blistering only occurred at temperatures above the glass transition temperature (transition from glassy solid to viscoelastic liquid). Note that most semi-crystalline polymer liner candidates have glass transition temperatures below room temperature, which allows them to have superior mechanical properties, including ductility.

This temperature dependence is likely due to two main effects. The first effect is that of hydrogen solubility. Hydrogen solubility in polymers is thought to be strongly a function of free volume which increases as the polymer is heated. Thus, the solubility should increase with increasing temperature. The second effect is that of viscosity. The polymer viscosity changes over many orders of magnitude with heating past the glass transition as the polymer goes from a glassy solid to a viscoelastic liquid. Thus, mass flow is markedly enhanced at temperatures above the glass transition and more damage is expected to occur.

Preliminary tests of crystalline films with a nearly identical polymer (isotactic vs atactic polystyrene of identical molecular weight) over the same temperature range shows no observable blistering (Figure 114c). This is thought to be due to the comparatively decreased free volume of the crystalline polymer as compared with the amorphous case. The hydrogen solubility should be lower and the material stiffer and more resistant to damage from hydrogen.

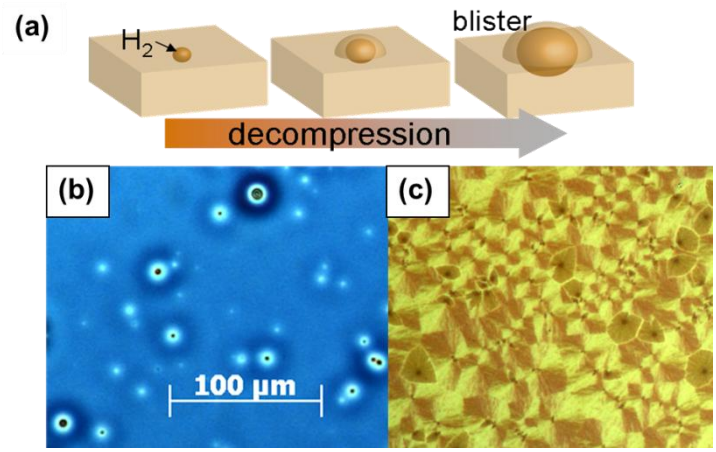

Figure 114. (a) Blistering occurring in a purely amorphous polymer after 2,000 psi hydrogen for 24hrs above the glass transition of the polymer and rapid 5 minute decompression. (b) 100% crystalline polymer of the same molecular weight shows no blistering after identical treatment. The texturing on the crystalline sample are the different crystalline regions (spherulites) that appear under polarized light. As semicrystalline materials (e.g. HDPE) are comprised of both amorphous and crystallite regions, it is expected for the material to exhibit some combination of the above effects.

5.1.2 Ex-Situ Mechanical Properties after Hydrogen Exposure on HDPE

Ex-situ modulus testing was also carried out after exposure to high-pressure hydrogen. Standard high density poly-ethylene (HDPE) sheet stock along with material from Quantum was measured ex-situ to investigate the effects of hydrogen on the mechanical properties, including peak load and tensile modulus. The change in mechanical properties is important to understanding the vessel life-cycle and durability. From initial testing, a 10 to 20% decrease in HDPE modulus was observed immediately after 7 day exposure to 3,000 psi hydrogen. Surprisingly this marked decrease in modulus recovered after a period of 1-2 hours. Additional HDPE materials were then tested at three different pressures (3,600 psi, 4,000 psi, and 4,400 psi) and different dwell times in hydrogen. The modulus decrease and recovery were measured as a function of time to compare these with the average concentration of hydrogen in the material.

For these tests, ASTM D638 type III standard tensile samples were machined from ½" thick standard HDPE sheet stock from McMaster-Carr. This is roughly twice the nominal thickness of the usual vessel liner. The rationale behind the thicker test material is that the hydrogen desorption time is thickness dependent and thus thicker materials yield a longer recovery time. This is especially important since only pressures up to ~4,500 psi can be reached and not the 10,000 psi that a working vessel would experience. Tensile coupons were rough cut using a band saw and were routed to exact dimensions with a tensile cut guide. Once the samples were machined, 7 of the ½" thick samples were tested to determine the statistical variation of the modulus in the material. The remaining samples were loaded into a high pressure hydrogen autoclave in batches of 18. The autoclave was charged with 4,000 psi (high purity) hydrogen and held for varying times between 7 and 21 days at 30°C. Long dwell times are required to achieve hydrogen saturation in these thick samples. For the ½" thick samples we would expect

about 98% saturation at 10 days and 99.95% after 21 days based on our absorption calculations with literature values for H_2 diffusion in HDPE. Only a slight variation was observed between the 11-day and the 21-day run indicating that the shorter dwell time is likely sufficient for subsequent measurements. After venting the hydrogen atmosphere from the autoclave, the samples were pulled as a function of time after exposure (recovery time) with a 20 kpsi Instron load frame.

The standard control set of ½" McMaster HDPE tensile samples showed an average modulus of 0.8 GPa with a standard deviation of 30 MPa based on a secant modulus analysis starting at zero load and ending at 3.4% strain. These starting and end values were chosen to allow easy comparison with the accepted literature values of 0.8GPa for HDPE. It should be noted however, that the stress/strain curve is not linear even for low strain and the modulus values are highly dependent on these endpoint choices. Please see Figure 115 for a comparison of stress/strain curves at different recovery times after annealing. A plot of the modulus as a function of recovery time is shown in Figure 116. The hydrogen effect is still observed regardless of the choice of the secant endpoints.

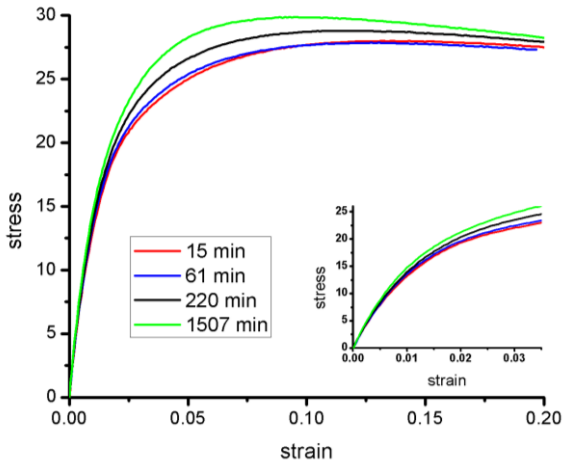

Figure 115. Comparison plot of the stress/strain curves at different times after high-pressure hydrogen exposure for HDPE. The inset shows the same data sets for low strains.

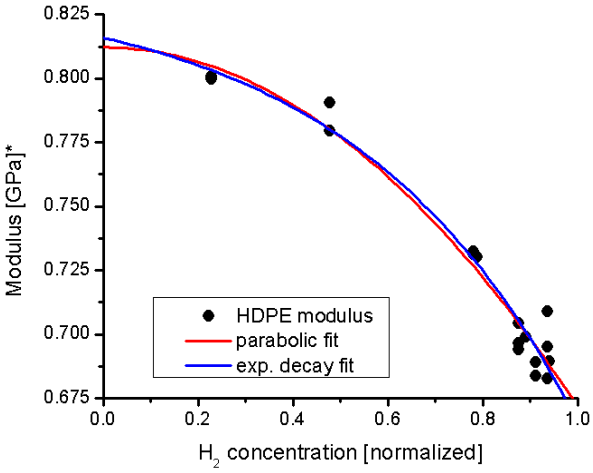

Figure 116. Plot of the HDPE modulus as a function of calculated H_2 concentration after removal from the autoclave. *Note that the modulus is calculated as described in the text.

The samples that were exposed to hydrogen for either 10 or 21 days showed an approximately 14% decrease in modulus (calculated as discussed above) that appeared to recover within a period of 1 to 2 hours. This is in good qualitative agreement with our earlier measurements at 3,000 psi hydrogen loading.

5.1.3 In-Situ Experiments

As discussed above, it was discovered that the drop in material properties was time dependent and was influenced by hydrogen desorption from the polymer. This effect made it difficult to ascertain the full effect of the high-pressure hydrogen as the hydrogen fully desorbed over the course of 1 hour and it took 15 minutes to fully vent the system, pull samples out, and initiate testing. The limitations of the ex-situ testing suggested the need for an in-situ hydrogen tensile sample test rig, as shown in Figure 117. A solenoid based pull system was decided upon due to swelling issues associated with the Nd based magnets in a more classical motor driven system. The first incarnation of this test rig also showed a drop in the UTS of the polymer material, but a comparative analysis was not possible due to lack of a feedback loop to control the strain rate.

Figure 117. Photograph of the in-situ tensile test rig showing the various components: (1) load cell, (2) grips, (3) LVDT, (4) solenoid, and (5) frame.

After realizing the limitations of the initial in-situ rig, the rig was redesigned to have a feedback from the LVDT into the solenoid voltage to give constant, programmable strain rate. The initial frame was also replaced with a stiffer, tubular frame to reduce flexing and unwanted compliance during testing noticed in the initial setup. Finally, everything was reduced to a single program computer control to improve reproducibility over the manual switching and separate LVDT and load cell controls of the initial system.

After completion of the build and debugging, the in-situ frame was tested in air many times and the stress/strain curves were cross-correlated with identical samples and strain rates in a standard tensile test frame equipped with a strain gauge. This allowed us to obtain the "effective" gauge length of the polymer samples. Samples used were miniature tensile "dog-bone" geometry from ASTM standards with the tabs reduced for the miniature grips. A procedure for reproducibly mounting the samples and setting the solenoid initial displacement was developed during this air testing to ensure high reproducibility. Even so, some tests showed either minor, or major jumps in the stress/strain curves at low strain within the elastic limit that are likely caused by sticking somewhere in the system and indicate some minor design modifications are needed. Due to funding limitations, we instead tested a larger number of samples and disregarded tests where there was a major jump in the stress/strain curve that indicated sticking. After analysis, minor inflections in the stress strain curve in the elastic limit were considered acceptable for analysis of the UTS degradation in high-pressure hydrogen.

Testing was carried out in a high-pressure hydrogen autoclave at pressures of 4,000 psi, 4500 psi, and 5,000 psi. This represents the upper safe working limit of the autoclave. Multiple tests were carried out at each pressure. Tests exhibiting no inflections (signs of mechanical sticking) in the stress/strain curve are shown in Figure 118. From simple examination of these curves, it appears that changes in the modulus are minimal, but there is a clear decrease in the UTS with increasing hydrogen pressure.

Figure 119 shows the data around the UTS demonstrating a clear decrease in the UTS of up to nearly 10% for tests performed at 5,000 psi hydrogen compared to those in air. This marked decrease is similar to what was seen in ex-situ measurements previously by PNNL. Again, these data are only those with no inflections in the elastic region. Figure 120 shows the average UTS as a function of hydrogen pressure and in-air data. There appears to be a potentially non-linear behavior to the data with the UTS decreasing more after 4,500 psi, but that cannot be confirmed without further testing at higher pressures not attainable with the current autoclave system.

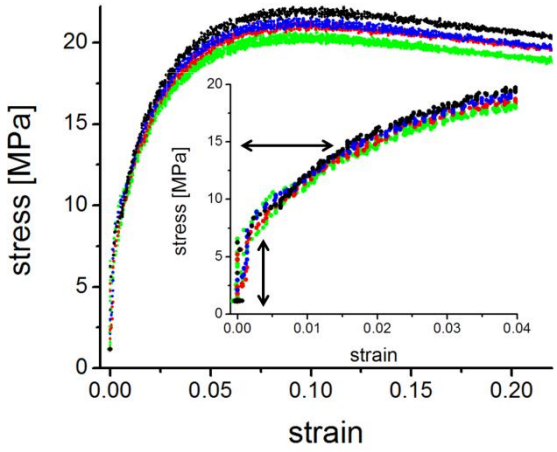

Figure 118. Stress-strain plot of the HDPE under in-situ high-pressure hydrogen at various pressures: black (in-air), blue (4,000 psi), red (4,500 psi), and green (5,000 psi).

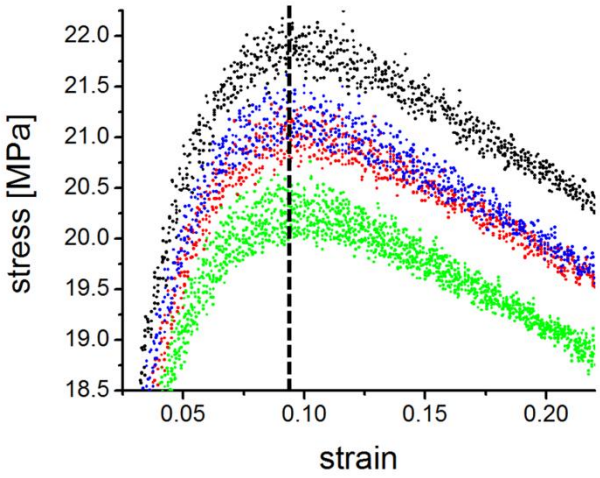

Figure 119. Zoom in on the stress-strain plot peak in the data indicating the UTS of the polymer at the different pressures: black (in-air), blue (4,000 psi), red (4,500 psi), and green (5,000 psi).

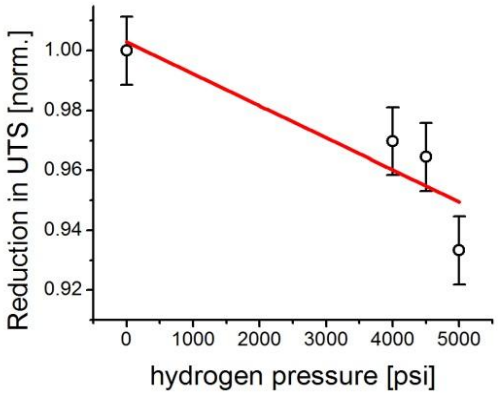

Figure 120. Plot of the reduction in UTS as a function of the in-situ pressure of hydrogen. Data is scaled to the in-air data.

5.2 Vessel Manufacturing Cost Analysis

A manufacturing cost analysis was performed to estimate the reduction in vessel cost that is achievable with advanced hybrid composites compared to filament winding alone. Quantum and Boeing specified the manufacturing equipment and obtained the equipment cost estimates for the FW and AFP composite layup methods. The hybrid composite designs developed for the prototype vessels (manufactured by Quantum and Boeing) provided the FW and AFP masses to estimate the cost and processing times for each process. Costs associated with composite curing, inspection, and testing were considered separately from the composite layup costs. The cost model includes materials, labor, overheads, manufacturing equipment and factory space costs, plus the balance of system costs. The equipment cost and required factory space were estimated for the FW and AFP tank layup. The number of manufacturing cells was estimated for production of 500,000 units per year. Table 7 summarizes the information and assumptions used in the cost analysis of the FW and AFP layup equipment and factory space.

Table 7. Cost modeling information for filament winding and advanced fiber placement processes

Item	Value
Filament Winder (3 axis)	Equip. Cost: $349,600 Factor Space: 436 ft^2 Layup Speed: 13.2 kg/hr (per axis)
Advance Fiber Placement Robot plus Tape Layup End-Effector	Equip. Cost: $184,040 Factor Space: 203 ft^2 Layup Speed: 0.9 kg/hr
Production Rate	500,000 tanks / year
High Volume Material Costs: High Strength Carbon Fiber Epoxy Resin	 $28.6/kg ($13/lb) $8.25/kg ($3.75/lb)
Factory Construction Cost	$80/$ft^2$
Equipment Fixed Charge Rate Economic Life = 20 years Depreciable Life = 10 years Rate of Return = 10% Federal + State Income Tax = 38.9%	14.14%
Factory Fixed Charge Rate Economic Life = 30 years Depreciable Life = 20 years Rate of Return = 10% Federal + State Income Tax = 38.9%	14.42%

Quantum's 129-liter, Type IV, FW vessel was the baseline for weight and cost comparisons. This vessel size can store 5 kg of usable hydrogen at room temperature and 700 bar. Two bounding scenarios were evaluated for integrating the FW and AFP layup processes. The first scenario considered fully integrated processing where thin layers of FW and AFP composite could be alternated in the domed ends to optimize the composite layup without concern for machine efficiency. This serial process results in inefficient machine usage because the FW (13.2 kg/hr) must wait for the slower AFP process (0.9 kg/hr). The second scenario considered parallel manufacturing of the FW and AFP layers with 100% machine usage. In this case the AFP reinforcing layers would be manufactured off-line and inserted on the tank domes at discrete times during the layup.

5.2.1 Cost Evaluation of Hybrid Composite Vessels Tested during the Project

During project year FY2011, Vessel 1 produced by Quantum and Boeing exceeded the required burst pressure and saved 11.1kg of the 76 kg baseline mass (a 14.6% savings). The hybrid design removed 12.6 kg of parasitic FW composite in the vessel cylinder section and replaced it with 1.5 kg of AFP composite reinforcing the domed ends at the optimum ply angles. Table 8 summarizes the cost analysis of Vessel 1. The baseline cost of the Type IV FW vessel was estimated to be $25.34/kWh, which is similar to the estimated cost of $23/kWh reported by Lasher [8]. Note that DOE has since provided updated vessel cost estimates that will be

compared against later in this report. The composite cost (FW + AFP = $2,172 to $2604) is 84% to 90% of the total vessel materials cost. Manufacturing equipment and factory costs are small in each case ($36 to $66/vessel), suggesting that efficient machine usage is a secondary consideration behind optimizing the composite layup for reduced composite mass. The hybrid process with reduced composite mass improves the specific energy (increased from 1.5 to 1.67 kWh/kg) and the cost efficiency (reduced from $25.34 to $23.40/kWh).

Table 8. Comparison of the baseline FW Type IV vessel with hybrid manufacturing of Vessel 1

		Type IV Tank	Hybrid FW + AFP Reinforced	
Summary Table		**Baseline 129L**	**Fully Integrated**	**Separate**
		Filament Wound	**FW and AFP**	**FW and AFP**
Composite Mass, kg	**FW**	76	63.4	63.4
	AFP		1.5	1.5
Total Composite Mass, kg		76	64.9	64.9
Composite Mass Savings		0%	15%	15%
Composite	**FW**	13.2	13.2	13.2
Placement Speed, kg/hr	**AFP**		0.9	0.9
Composite	**FW**	5.8	4.8	4.8
Placement Time, hr/tank	**AFP**		2.5	1.7
Total Place Time, hr/tank		5.8	7.3	4.8
# Manuf. Cells for 500K/yr	**FW**	191	242	159
	AFP		484	165
Tank Costs				
FW Composite		$2,604	$2,172	$2,172
AFP Composite			$103	$103
End Boss		$250	$250	$250
Manufacturing Equipment		$36	$66	$41
Factory Space		$7	$10	$7
Total Tank Cost		$2,897	$2,601	$2,573
% Tank Cost Savings		0%	10%	11%
DOE Measures				
Specific Energy, kWh/kg [1]		1.50	1.67	1.67
Cost Efficiency, $/kWh [2]		$25.34	$23.56	$23.40
[1] 5 kg H2 * 33.31 kWh/kgH2 / (Tank+OtherComponents+H2 mass, kg) OtherCompMass=30kg				
[2] (Tank+OtherComponents $$) / (5 kg H2 * 33.31 kWh/kgH2)				

During project year FY2012, Vessel 7 successfully exceeded the 22,850 psi burst pressure with a lower composite mass of 56.2 kg. Both Vessels 1 and 7 were produced with single layers of AFP composite in the dome sections. Vessel 1 applied the composite tape directly to the HDPE liner ends, requiring sequential manufacturing of the AFP and FW steps. However, Vessel 7 formed the AFP dome reinforcements on a mandrel in a parallel manufacturing line, and then transferring them to the vessel liner for direct over-wrapping with filament wound composite. Exceeding the required burst pressure with Vessel 7 showed that the dome reinforcement can be successfully made in a parallel manufacturing line, allowing optimized machine usage.

Table 9 estimates that parallel AFP and FW processing lines can reduce the vessel manufacturing time from 8.2 hours to 4.3 hours. This reduces the required number of FW cells by 48% and the number of AFP cells by 52% (for 500,000 units per year), which is a $27 per tank savings in manufacturing cost.

Table 9. Comparison of the baseline FW Type IV tank with hybrid manufacturing of Vessel 7

		Type IV Tank	Hybrid FW + AFP Reinforced	
Summary Table		**Baseline 129L**	**Fully Integrated**	**Separate**
		Filament Wound	**FW and AFP**	**FW and AFP**
Composite Mass, kg	**FW**	76	56.2	56.2
	AFP		2.4	2.4
Total Composite Mass, kg		76	58.6	58.6
Composite Mass Savings		0%	23%	23%
Composite	**FW**	13.2	13.2	13.2
Placement Speed, kg/hr	**AFP**		0.9	0.9
Composite	**FW**	5.8	4.3	4.3
Placement Time, hr/tank	**AFP**		4.0	2.6
Total Place Time, hr/tank		5.8	8.2	4.3
# Manuf. Cells for 500K/yr	**FW**	191	273	142
	AFP		546	264
Tank Costs				
FW Composite		$2,604	$1,926	$1,926
AFP Composite			$164	$164
End Boss		$250	$250	$250
Manufacturing Equipment		$36	$72	$45
Factory Space		$7	$11	$8
Total Tank Cost		$2,897	$2,424	$2,393
% Tank Cost Savings		0%	16%	17%
DOE Measures				
Specific Energy, kWh/kg [1]		1.50	1.78	1.78
Cost Efficiency, $/kWh [2]		$25.34	$22.50	$22.31
[1] 5 kg H2 * 33.31 kWh/kgH2 / (Tank+OtherComponents+H2 mass, kg) OtherCompMass=30kg				
[2] (Tank+OtherComponents $$) / (5 kg H2 * 33.31 kWh/kgH2)				

Further optimization of the vessel composite layups in FY2013 produced Vessel 15 with an even lower mass that also exceeded the required burst pressure. Table 10 compares the mass and cost savings of the successful vessel designs 1, 7, and 15. The hybrid composite manufacturing costs assume the AFP dome reinforcements are produced off-line with no reduction in machine utilization. Table 10 shows that Vessel 15 reduced the total composite mass by 32% and the estimated cost by 27%.

Table 10. Mass and cost comparison of Vessel designs 1, 7, and 15 that exceeded the 22,850 psi burst pressure

Summary Table		Baseline 129L	Filament Wound + Advanced Fiber Placement		
		Filament Wound	Tank 1 Layup	Tank 7 Layup	Tank 15 Layup
Composite Mass, kg	FW	76	63.4	56.2	49.6
	AFP		1.5	2.4	1.9
Total Composite Mass, kg		76	64.9	58.6	51.5
Composite Mass Savings		0%	15%	23%	**32%**
Composite	FW	13.2	13.2	13.2	13.2
Placement Speed, kg/hr	AFP		0.9	0.9	0.9
Composite	FW	5.75	4.80	4.25	3.75
Placement Time, hr/tank	AFP		1.65	2.64	2.05
Total Place Time, hr/tank		5.75	4.80	4.25	3.75
# Manuf. Cells for 500K/yr	FW	191	159	142	125
	AFP		165	264	205
Tank Costs					
FW Composite		$2,604	$2,172	$1,926	$1,699
AFP Composite			$103	$164	$128
End Boss		$250	$250	$250	$250
Manuf. Equipment		$36	$41	$45	$40
Factory Space		$7	$7	$8	$7
Total Tank Cost		$2,897	$2,573	$2,393	$2,124
%Tank Cost Savings		0%	11%	17%	**27%**
DOE Measures					
Specific Energy, kWh/kg [1]		1.50	1.67	1.78	1.93
Cost Efficiency, $/kWh [2]		$25.34	$23.40	$22.31	$20.70
[1] 5 kg H2 * 33.31 kWh/kgH2 / (Tank+OtherComponents+H2 mass, kg) OtherCompMass=30kg					
[2] (Tank+OtherComponents $$) / (5 kg H2 * 33.31 kWh/kgH2)					

5.2.2 Comparison with the DOE Updated Cost Standard

In FY2012-2013 DOE funded Strategic Analysis (SA) to perform an updated manufacturing cost analysis to serve as a standard of comparison for the other DOE hydrogen vessel development programs [9]. SA's vessel cost model is based on vessel masses from a finite element analysis of a 147.3 L, type IV, carbon fiber composite vessel capable of holding 5.6kg of usable H_2 at room temperature and 700 bar pressure. This modeling work done by Ahluwalia et al. [10] at Argonne National Laboratory (ANL) estimated composite tank masses for a progressive series of filament wound design optimizations: 107.4 kg with no doilies and 90° hoop angle; 102 kg with no doilies and varying hoop angle; 92.6 kg with integrated end caps by resin transfer molding (RTM); and 91 kg with doilies and varying hoop angle. The term "doilies" refers to angled local dome reinforcement layers similar to the AFP end caps manufactured in our project. The composite mass of 91 kg for the most optimized design was chosen as the standard for the 147.3 L, type IV, 700 bar composite tank. SA's cost estimate for this design resulted in the component costs listed in Table 11.

Table 11. Estimated component costs for the 147.3L, 700 bar vessel modeled in the SA cost analysis

Item	Estimated Cost per Tank
Tank Composite: 91 kg, Carbon Fiber $28.6/kg, Epoxy Resin $8.25/kg	$2146 (includes processing)
End Boss	$14
Polymer Liner	$23
Balance of Plant	$940
Assembly	$14
Total Tank System Cost	$3134

The costs estimated by SA in Table 11 are quite different from Quantum's cost data used in the analyses of Table 8 and

Table 9. The prototype vessels developed and tested in this project are also a smaller 129L size compared to the 147.3L tanks modeled in the SA and ANL analyses. Therefore, the average FW composite cost ($2146 / 91kg = $23.58) and the component costs in Table 11 were used to recalculate the cost efficiencies for direct comparison with SA's updated vessel cost standard of $16.8/kWh. The AFP composite (using automated tape layup) was estimated to be twice the FW cost per kg, as was estimated in the initial cost analysis of Table 8 and

Table 9. Table 12 presents the revised cost estimates for the 129L vessels manufactured in this project. The baseline 76 kg FW tank has an estimated cost of $16.7/kWh, and the hybrid composite vessels have lower costs down to $13.5/kWh for Vessel 15 with 32% composite mass savings. Based on the composite design of the 129L FW vessel, Quantum estimated that a similar 147.3L tank would have a mass of approximately 87 kg. This is significantly lower than the 102 kg estimated by ANL for a similar FW vessel layup. However to be consistent with the SA results, Table 13 scaled the vessel mass and cost savings to the 91 kg, 147.3 L vessel size. Similar to Table 12, the FW vessel has an estimated cost of $16.8/kWh, and the hybrid composite vessels have lower costs down to $13.4/kWh for Vessel 15 with 32% composite savings.

Table 12. The 129L vessel costs recalculated to be consistent with the DOE 2013 vessel standard

Summary Table		Baseline 129L	129L Filament Wound + Advanced Fiber Placement		
		Filament Wound	Tank 1 Layup	Tank 7 Layup	Tank 15 Layup
Composite Mass, kg	FW	76	63.4	56.2	49.6
	AFP		1.5	2.4	1.9
Total Composite Mass, kg		76	64.9	58.6	51.5
Composite Mass Savings		0%	15%	23%	**32%**
Composite	FW	13.2	13.2	13.2	13.2
Placement Speed, kg/hr	AFP		0.9	0.9	0.9
Composite	FW	5.8	4.8	4.3	3.8
Placement Time, hr/tank	AFP		1.7	2.6	2.1
Total Place Time, hr/tank		5.8	4.8	4.3	3.8
# Manuf. Cells for 500K/yr	FW	191	159	142	125
	AFP		165	264	205
Tank Costs (Consistent with the DOE 2013, 700 bar, 147.3L storage system cost analysis)					
FW Composite		$1,792	$1,495	$1,326	$1,169
AFP Composite			$71	$113	$88
End Boss		$14	$14	$14	$14
Liner		$23	$23	$23	$23
Balance of Plant		$940	$940	$940	$940
Assembly		$12	$12	$12	$12
Total Tank System Cost		$2,781	$2,554	$2,428	$2,246
%Tank Cost Savings		0%	8%	13%	**19%**
DOE Measures					
Specific Energy, kWh/kg [1]		1.5	1.7	1.8	**1.9**
Cost Efficiency, $/kWh [2]		$16.7	$15.3	$14.6	**$13.5**
[1] 5 kg H2 * 33.31 kWh/kgH2 / (Tank+BOP+H2 mass, kg) BOP=30kg					
[2] (Tank+BOP $$) / (5 kg H2 * 33.31 kWh/kgH2)					

Table 13. The equivalent 147.3L vessel costs recalculated to be consistent with the DOE 2013 vessel standard

Summary Table		DOE 2013, 147.3L	147.3L Filament Wound + Advanced Fiber Placement		
		Filament Wound	Tank 1 Layup	Tank 7 Layup	Tank 15 Layup
Composite Mass, kg	FW	91	75.9	67.3	59.4
	AFP		1.8	2.9	2.2
Total Composite Mass, kg		91	77.7	70.2	61.6
Composite Mass Savings		0%	15%	23%	**32%**
Composite	FW	13.2	13.2	13.2	13.2
Placement Speed, kg/hr	AFP		0.9	0.9	0.9
Composite	FW	6.9	5.7	5.1	4.5
Placement Time, hr/tank	AFP		2.0	3.2	2.5
Total Place Time, hr/tank		6.9	7.7	8.3	6.9
# Manuf. Cells for 500K/yr	FW	229	191	170	150
	AFP		197	316	245
Tank Costs (Consistent with the DOE 2013, 700 bar, 147.3L storage system cost analysis)					
FW Composite		$2,146	$1,790	$1,588	$1,400
AFP Composite			$85	$136	$105
End Boss		$14	$14	$14	$14
Liner		$23	$23	$23	$23
Balance of Plant		$940	$940	$940	$940
Assembly		$12	$12	$12	$12
Total Tank System Cost		$3,134	$2,863	$2,712	$2,494
%Tank Cost Savings		0%	9%	13%	**20%**
DOE Measures					
Specific Energy, kWh/kg [1]		1.5	1.6	1.8	**1.9**
Cost Efficiency, $/kWh [2]		$16.8	$15.3	$14.5	**$13.4**
[1] 5.6 kg H2 * 33.31 kWh/kgH2 / (Tank+BOP+5.8kg H2 mass, kg) BOP=30kg					
[2] (Tank+BOP $$) / (5.6 kg H2 * 33.31 kWh/kgH2)					

6.0 LLNL Report [Phase I]

The Potential of Dry Winding for Rapid, Inexpensive Manufacture of Composite Overwrapped Pressure Vessels

Andrew Weisberg, Salvador M. Aceves

6.1 Introduction

As a universal transportation fuel that can be generated from water and any energy source, hydrogen (H_2) is a leading candidate to supplant petroleum with the potential to ultimately eliminate petroleum dependence, associated air pollutants and greenhouse gases [11]. The predominant technical barrier limiting widespread use of hydrogen automobiles is storing enough hydrogen fuel onboard to achieve sufficient (500+ kilometers) driving range in a compact, lightweight, rapidly refuelable, and cost-effective system [12].

Whether at ambient [13] or at cryogenic temperature [14-15], compressed hydrogen storage in composite overwrapped pressure vessels (COPVs) is necessary for long-range automotive hydrogen propulsion. However, COPVs are expensive and their production processes may be challenged to ramp up fast enough for a large-scale transition to hydrogen-fueled transportation. COPV's rely on filament winding to obtain the full strength of the fiber. Filament winding is a slow, sequential process. New processes that can reduce composite manufacturing cost without compromising strength may have broad applicability for reducing costs of COPVs.

In collaboration with industrial partners Quantum and Boeing [16], we have researched methodologies that may contribute to addressing the remaining composite pressure vessel cost efficiency hurdles to enable a rapid transition to hydrogen-fueled automobiles. We propose a manufacturing process that may offer manufacturing speed and cost advantages independent of the choice of fiber material.

6.2 Approach

In an effort to reduce COPV manufacture cost and time vs. today's wet winding process, we consider the potential for increasing winding speed. Fast winding has the potential to reduce cost by increasing fiber throughput through expensive vessel manufacturing and curing machines. An important question therefore surfaces: what prevents the proven wet winding composite fabrication processes from being sped up? Production capital and labor cost components are both inversely proportional to the duration that the part being built spends on a particular piece of equipment. The process that puts all of the costly structure mass into a pressure vessel has intrinsic physical speed limitations.

If one tried to speed up wet winding, process consistency would fall apart. Density variations, fiber not following straight paths, long bubbles between plies, perhaps a large variety of fluidics with insufficient equilibration time would arise with a few-fold speed increase. Substantial (e.g. order of magnitude) speedup in wet winding processes is therefore unlikely.

The proposed "Dry Tape" process pays attention to viscous flow and diffusion. It aims at an order of magnitude or more improvement in winding speed – the key rate-limiting manufacturing step. The process is likely to achieve these aims because the viscous flow equations are subsets of the convection-diffusion equations, and diffusion times vary inversely as length squared. The target is achieving bond formation on sub-millisecond timescales.

The proposed dry winding approach may allow considerable cost savings through centralized tape manufacture and fast winding with no need for oven curing. The technique can be easily scaled up to satisfy the growing demand for inexpensive pressure vessels. The first step in the dry winding approach consists of making fiber tape at a central facility. Fiber is wetted with polyester resin and then squeezed into rollers, maximizing the ratio of fiber to resin. The tape is rigid and is therefore sliced into narrow (~1 cm) strips, enabling it to curve around end dome contours without crumpling. The sliced dry tape is then rolled into reels and transported to the vessel winding facility in a refrigerated container. At the vessel production site, the tape is wound at very high speed (200 m/s vs. 20 m/s for today's wet winding processes).

In the future, we envision the use of this procedure for making vessels in a very short time (~10 minutes vs. 3 hours for wet fiber winding) without the need for oven curing. The proposed two-vendor sequence would be a series processes very similar to electronics manufacturing. The technique can be easily scaled up to satisfy the growing demand for inexpensive pressure vessels.

The proposed vessel winding process has potential for reduced cost vs. today's wet wound vessels due to a synergistic combination of advantages:

- Fast winding reduces capital cost of winding machine (per kilogram of composite) and labor cost of the machine operator.
- Inter-tape bonding is performed at ambient temperature. No oven curing is necessary.
- High volume production is possible with a single winding machine instead of multiple winding machines and ovens requiring multiple operators.
- High ratio of fiber to resin reduces the cost of resin. It also reduces the wall thickness for any necessary strength, increasing the packaging efficiency of the vessel and reducing weight.
- Tape manufacture in large scale in a central facility minimizes tape handling and distribution costs.

Figure 121 illustrates where the proposed approach lies within all available composite manufacturing process choices, with dry winding tape technology on its rightmost edge. Other efficient approaches to vessel manufacture (wet wound, fiber placement) are being researched by team members Quantum and Boeing as a part of this project. Alternatives at the left of the figure lead to undesirable characteristics due to sacrifice of maximum tensile strength and/or imprecise net shapes.

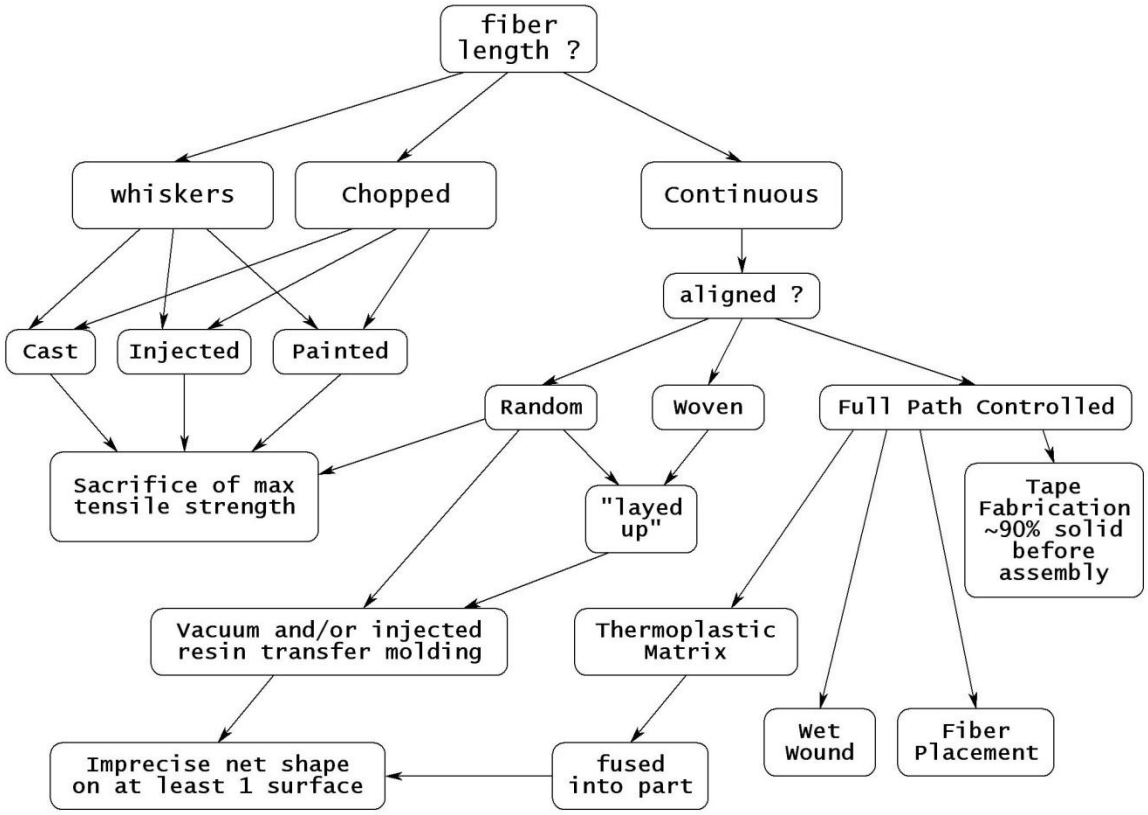

Figure 121. Bubble diagram dissects the various options for manufacturing composite vessels, starting from choices of the geometry of the individual composite fibers. Two undesirable characteristics of the final composite part are shown at the left of this diagram. The team of pressure vessel innovation partners (Quantum Technologies and Boeing) seeks to combine characteristics of wet winding and fiber placement, both of which avoid the undesirable consequences. LLNL's proposed tape technology, also on the right of this diagram, avoids the negative consequences and combines features of two proven processes being improved by team members.

6.3 Results

The proposed approach combines many of the features of proven high-strength processes, except that it seeks to perform them at high speed to drastically reduce manufacturing cost. Other features and drawbacks of the tape process could affect materials costs and vessel performance, but the effects are likely to be slight and positive. Until the reality of significant manufacturing cost improvements is proven, the investigation of vessel performance effects and potential restrictions on fiber choices would be inconsequential. Therefore we estimated how much the proposed process might save in manufacturing (capital and labor) cost. Figure 122 and Figure 123 break that cost down in a fundamental way, first into what the process equipment adds to manufacturing cost as a function of how much material goes through a costly piece of production equipment how fast (the 'throughput'), and then how much 'throughput' that equipment can achieve when laying down a tape of a particular cross section at a particular speed. Attempts are

made in these figures to roughly characterize our process with the conventional competing process – wet winding.

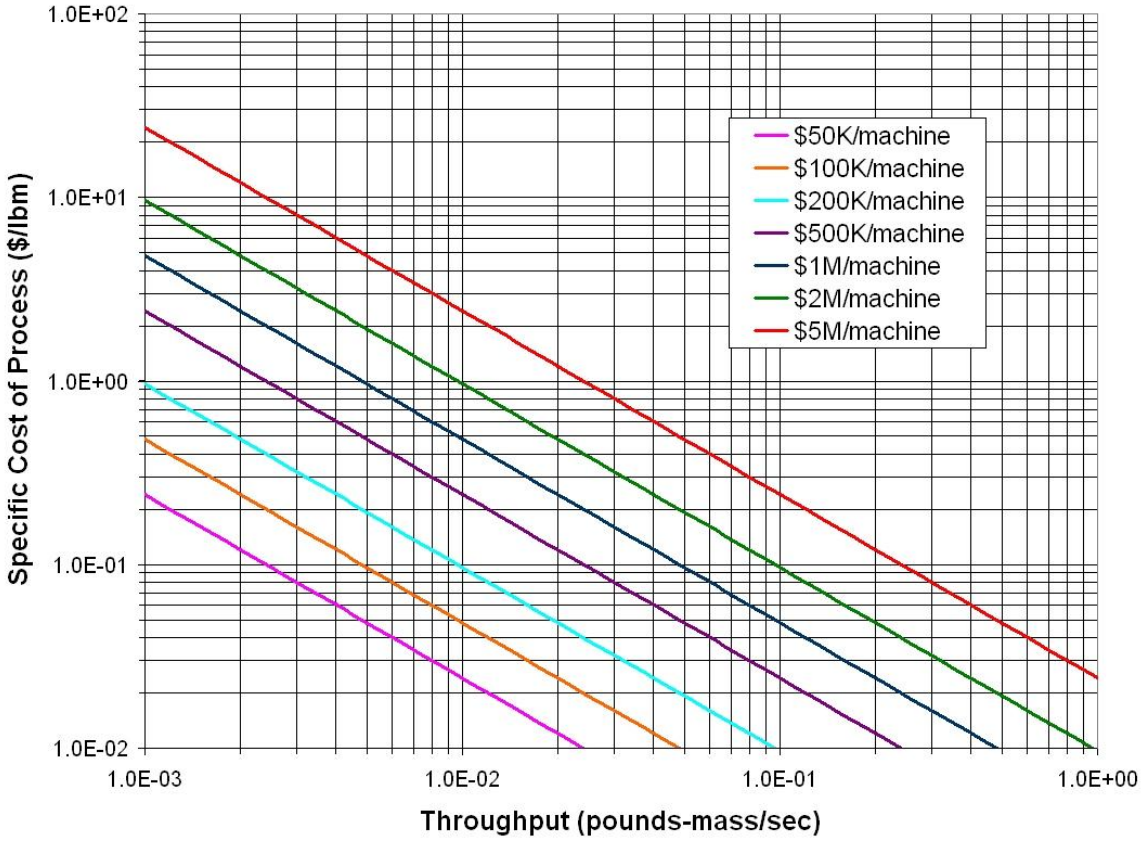

Figure 122. Cost to perform a composite manufacturing process versus the composite material processing rate ('throughput' in units of mass-per-unit-time), at various levels of production capital cost (presuming a 3 year return on investment). This graph applies to all composite manufacturing processes, with conventional wet winding processes occurring in roughly the middle of its left hand edge. The proposed dry tape process projects operation in the middle of the bottom edge of this graph.

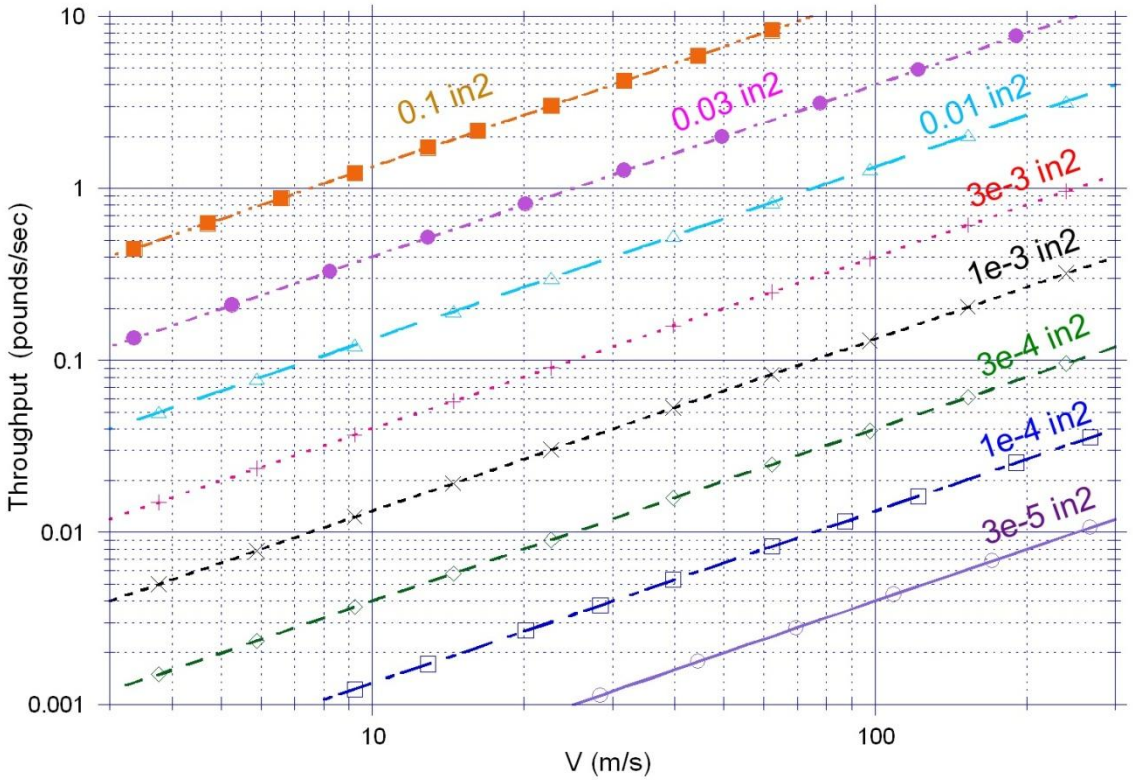

Figure 123. Tape material processing rate ('throughput' in units of mass-per-unit-time) as a function of tape velocity, at various levels of tape cross sectional area. This graph applies to all continuous filament fiber production processes, and current wet winding processes occupy the lower left corner. We project dry tape process operation in the upper right corner of this range.

Although many fiber and matrix material choices should be compatible with LLNL's tape innovation, very few provide the confidence to quickly perform our proof of concept experiments. In particular, the repeatability of (rapidly testable) bonding is at risk from airborne contamination and perhaps from humidity. Low material sensitivity to environmental conditions is therefore important. Clean facilities are available to meet these challenges, and plans to procure tape and (slightly hazardous) bonding materials are compatible with standard laboratories' safety and environmental regulations.

6.4 Proposed Proof of Concept Experiment

Demonstration of the technological potential of our approach demands a proof of concept experiment. The proposed proof of concept experiment focuses on determining bonding speed – the key parameter limiting winding velocity. Figure 124 shows a block diagram schematic of the calorimeter designed for a proof of concept test apparatus. This design represents the simplest way to make measurements of a high-speed process without the measuring instrument limiting how fast the process can occur. Its approach relies on detecting the heat being evolved by a tape bonding process to find out how fast that process is occurring, without interfering with the mechanical phenomena that ought to be changing as a bond is forming (as might be the case with

speed of sound, ultrasonic impedance, or opacity measurements), or further restricting the choice of experimental gas environment.

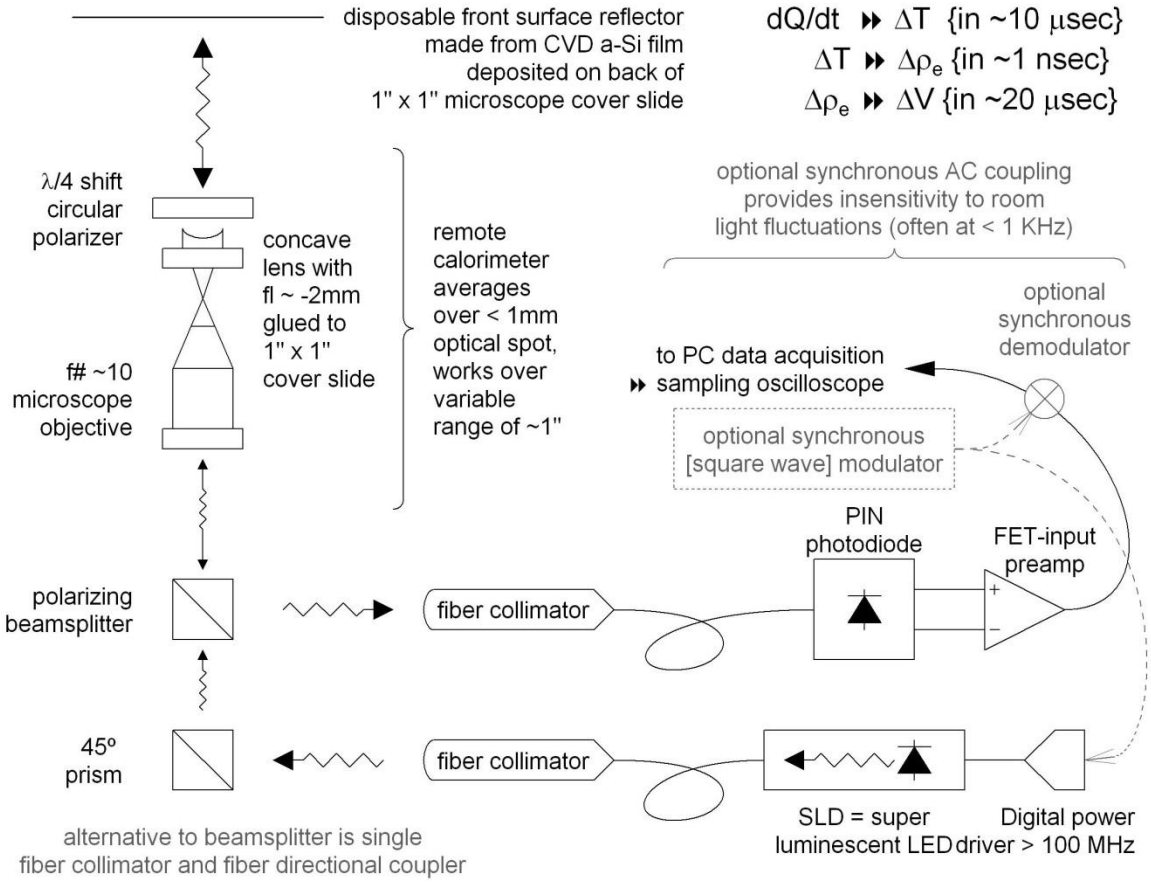

Figure 124. Schematic diagram of calorimeter to determine tape bonding speed by capturing temperature rise due to bonding with a digital oscilloscope. This hardware diagram mixes physical components, optical beam paths including captured photons in fibers, and electronics.

Figure 125 shows the key components of the high-speed calorimeter necessary to measure the heat being evolved during the adhesion process. Thermal isolation trusses in the calorimeter retain their dynamic calibration as stuck-together tape test specimens are bonded and taken out of the instrument.

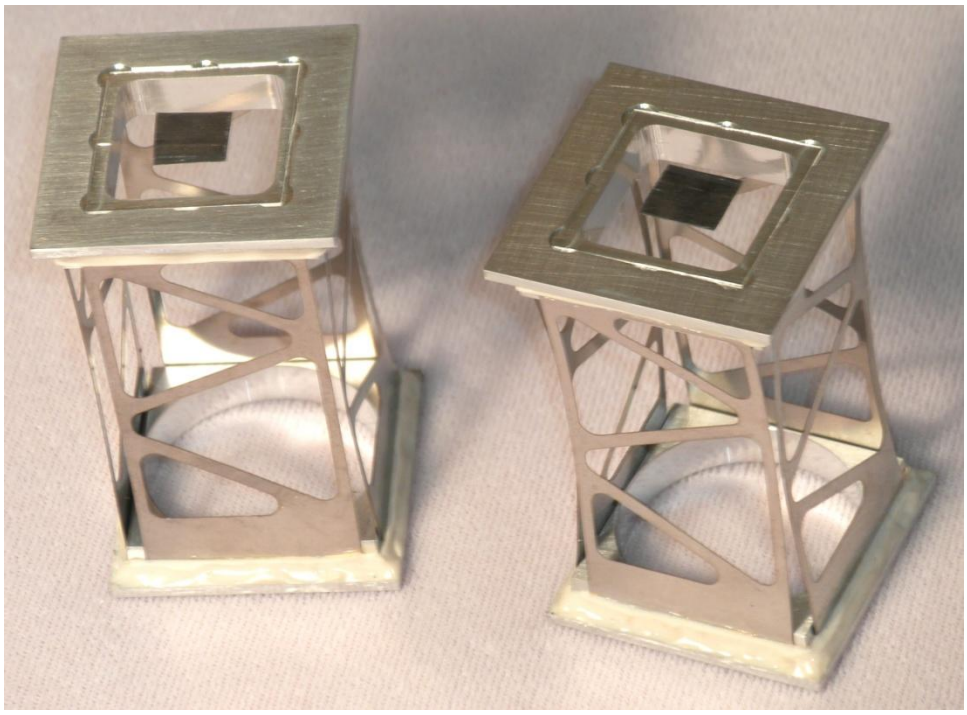

Figure 125. Thermal isolation truss components for proof of concept experiment. These truss stages mount tape specimens (black squares in the center of clear microscope cover slides, glued atop these trusses). One of these trusses is inverted and its tape specimen placed in abrupt contact with the other tape specimen to determine bonding speed with the calorimeter apparatus of Figure 124.

6.5 Conclusions

We propose a methodology for reducing manufacturing time and cost of composite overwrapped pressure vessels (COPVs). Dry winding methodology promises to increase bonding speed enabling rapid vessel winding (10 minute vs. 3 hours with today´s wet winding approach) with no need for oven curing. The proposed approach has been documented and submitted as a patent application [17].

Cost reduction is likely due to higher throughput enabling increased productivity from expensive winding machines as well as reduced labor cost per vessel. Tape manufacture in large scale in a central facility minimizes tape handling and distribution costs. Finally, high ratio of fiber to resin reduces resin cost as well as the wall thickness for any necessary strength, increasing the packaging efficiency of the vessel and reducing weight.

A proof of concept experiment is necessary for demonstrating fast (sub millisecond) bonding – the key parameter enabling rapid vessel manufacture. The approach selected demands construction of a calorimeter to detect heat evolved during the adhesion process.

6.6 Acknowledgments

This project was funded by DOE, Office of Fuel Cell Technologies, Monterey Gardiner,

Technology Development Manager. This work performed under the auspices of the U.S. Department of Energy by Lawrence Livermore National Laboratory under Contract DE-AC52-07NA27344.

7.0 Project Conclusions

The project successful showed the innovative hybrid process of optimizing composite usage by combining traditional filament winding and advanced fiber placement techniques is a viable solution to reduce fiber usage, thus driving down the cost of fuel storage vessels. With PNNL's assistance, based on DOE's baseline vessel size of 147.3L and 91kg, the 129L vessel (scaled to DOE baseline) in this project shows a 32% composite savings and 20% cost savings when comparing the latest hybrid design and Quantum baseline all filament wound vessel.

A number of vessels were built based on the latest hybrid design. It passed burst test, cycle test, accelerated stress rupture test and drop test per European Commission (EC) 79-2009 standard. The design did not pass the remaining test – extreme temperature cycle test – that is critical to the hybrid design. It was discovered the location where AFP and FW overlap for load transfer could be weakened during hydraulic cycling at 85°C.

Due to project timing, there was no additional time available to fine tune the design to improve the load transfer between AFP and FW. Further design modifications will likely help pass the extreme temperature cycle test.

To successfully design this latest hybrid vessel, the in-house modeling software was updated to add capability to start and stop fiber layers to simulate the AFP process. The original in-house software was developed for continuous filament winding only.

To provide Quantum with the highest quality AFP end caps to build hybrid vessels, Boeing improved and refined their manufacturing process significantly to produce parts per design consistently.

Alternative fibers were investigated in this project as another channel to drive down the cost of pressure vessels, but the added mass impacted the vessel cost negatively due to the lower performance from the alternative fiber.

The update software for hybrid vessel design played a critical part to the success of this project. There are opportunities for further improvements. The model taper subroutine is not following the actual geometry and should be updated and modified to better model the actual geometry. The model can also be improved to detect bridging and gaps at the end of a fiber layer.

Without the funding and support from DOE, this project would not have been possible. Quantum and its partners would like to take this opportunity to thank you for all the support DOE has provided to make this project a success.

8.0 References

1. Valery V. Vasiliev and Evgeny V. Morozov, Advanced Mechanics of Composite Materials, 2nd Edition, 2007

2. Valery V. Vasiliev and Robert Jones, Mechanics of Composite Structures, 1993

3. Sotiris Koussios, Filament Winding: A Unified Approach, PhD thesis, Delft University of Technology, 2004

4. Stephen Timoshenko, Elements of Strength of Materials, 4th Edition, 1962

5. Stephen Timoshenko, Theory of plates and shells, 2nd Edition, 1964

6. Henry H. Bednar, Pressure Vessel Design Handbook, 2nd Edition, 1986

7. S. T. Peters, W. D. Humphrey and R. F. Foral, Filament Winding, Composite Structure Fabrication, 1991

8. Lasher, S. 2009. Analysis of Hydrogen Storage Materials and On-Board Systems: Compressed and Liquid Hydrogen Carrier System Cost Assessments. In the Proceeding of the U.S. DOE Merit Review, May 19, 2009. Washington, D.C.

9. James, B.D., J.M. Molton, and W.G. Colella. 2013. "Hydrogen Storage Cost Analysis." Project ID: ST100. 2013 DOE Hydrogen and Fuel Cell Technologies Annual Merit Review and Peer Evaluation Meeting, Arlington. VA, May 13-16, 2013.

10. Ahluwalia, R.K., T.Q. Hue, J-K Peng, and H.S. Roh. 2013. "System Level Analysis of Hydrogen Storage Options." Project ID: ST001. 2013 DOE Hydrogen and Fuel Cell Technologies Annual Merit Review and Peer Evaluation Meeting. Arlington, VA, May 13-16, 2013.

11. Berry GD, Aceves SM. The case for hydrogen in a carbon constrained world. Journal of Energy Resources Technology, 2005;127:89-94.

12. Berry GD, Martinez-Frias, J, Espinosa-Loza, F, Aceves SM. Hydrogen Storage and Transportation. Encyclopedia of Energy, 2005;3:267-281.

13. Ciancia A, Pede G, Brighigna M, Perrone V. Compressed hydrogen fuelled vehicles: reasons of a choice and developments in ENEA. International Journal of Hydrogen Energy 1996;21:397-406.

14. Aceves SM, Espinosa-Loza F, Ledesma-Orozco E, Ross TO, Weisberg AH, Brunner TC, et al. High-density automotive hydrogen storage with cryogenic capable pressure vessels. International Journal of Hydrogen Energy, 2010;35:1219-26.

15. Aceves SM, Petitpas G, Espinosa-Loza F, Matthews MJ, Ledesma-Orozco E. Safe, long range, inexpensive and rapidly refuelable hydrogen vehicles with cryogenic pressure vessels. International Journal of Hydrogen Energy, 2013;38:2480-89.

16. Leavitt M. Development of advanced manufacturing technologies for low cost hydrogen storage vessels. FY2013 Annual Progress Report, DOE Hydrogen and Fuel Cells Program, 2013;VI: 30-34.

17. Weisberg AH. Methods for tape fabrication of continuous filament composite parts and articles of manufacture thereof. United States Patent US 8545657 B2, 2013.

9.0 Patents

"High Pressure Storage Device and Method" was filed and U.S. Patent application No. 12/468736 was assigned.

10.0 Publications/Presentations

- Presentation for 700 Bar Vehicle Tank Design and Manufacturing, USCAR Conference, May 18, 2009.
- Presentation for Development of Advanced Manufacturing Technologies for Low Cost Hydrogen Storage Vessel, Annual Merit Review, Department of Energy, May 18-22, 2009, Arlington, Virginia.
- Presentation for Development of Advanced Manufacturing Technologies for Low Cost Hydrogen Storage Vessel, Annual Merit Review, Department of Energy, June 7-11, 2010, Washington D.C.
- Presentation for Development of Advanced Manufacturing Technologies for Low Cost Hydrogen Storage Vessels, Hydrogen Storage Tech Team, June 30, 2011, Oak Ridge, Tennessee.
- Poster Session for Development of Advanced Manufacturing Technologies for Low Cost Hydrogen Storage Vessel, Annual Merit Review, Department of Energy, June 9-13, 2011, Arlington, Virginia.
- Teleconference Presentation for Development of Advanced Manufacturing Technologies for Low Cost Hydrogen Storage Vessels, Hydrogen Storage Tech Team, June 21, 2012, Oak Ridge, Tennessee.
- Presentation for Development of Advanced Manufacturing Technologies for Low Cost Hydrogen Storage Vessel, Annual Merit Review, Department of Energy, May 14-18, 2012, Arlington, Virginia.
- Poster Session for Development of Advanced Manufacturing Technologies for Low Cost Hydrogen Storage Vessel, Annual Merit Review, Department of Energy, May 13-17, 2013, Arlington, Virginia.
- Alvine KJ, TA Kafentzis, SG Pitman, KI Johnson, DC Skorski, JC Tucker, TJ Roosendaal, and ME Dahl. 2014. "An In-situ Tensile Test Apparatus for Polymers in High Pressure Hydrogen." Submitted to the Review of Scientific Instruments.
- Presentation for Development of Advanced Manufacturing Technologies for Low Cost Hydrogen Storage Vessel, Annual Merit Review, Department of Energy, June 16-20, 2014, Washington D.C.

11.0 Acronyms

AFP	Advanced fiber placement
CMM	Coordinate measuring machine
COPV	Composite overwrapped pressure vessel
CT	Computed tomography
DSC	Differential scanning calorimetry
EC	European Commission
ENF	Edge Notch Flexure
FEA	Finite element analysis
FEP	Fluorinated ethylene propylene
FW	Filament winding
HDPE	High density poly-ethylene
IR	Infrared
LVDT	Linear variable differential transformer
MSV	Mid stage valve
NDI	Non destructive inspection
UD	Unidirectional
UTS	Ultimate tensile strength